AURODICYANIDE DESORPTION FROM ACTIVATED CARBON

by

Dhiman Bhattacharyya

A thesis submitted to the faculty of
The University of Utah
in partial fulfillment of the requirements for the degree of

Master of Science

Department of Metallurgical Engineering

The University of Utah

December 2013

The University of Utah Graduate School

STATEMENT OF THESIS APPROVAL

The thesis of **Dhiman Bhattacharyya**

has been approved by the following supervisory committee members:

Jan D. Miller	, Chair	**Oct. 10, 2013** Date Approved
Michael L. Free	, Member	**Oct. 10, 2013** Date Approved
Sivaraman Guruswamy	, Member	**Oct. 10, 2013** Date Approved

and by **Manoranjan Misra** , Chair of

the Department of **Metallurgical Engineering**

and by David B. Kieda, Dean of The Graduate School.

ABSTRACT

The industrial use of activated carbon for gold adsorption from alkaline cyanide leach solutions has been a major development in gold hydrometallurgy which was commercialized during the last part of the 20^{th} century. In the gold industry, activated carbon is most often used to adsorb gold from dilute alkaline cyanide solutions. The gold is dissolved as the $Au(CN)_2^-$ complex and is recovered from the solution by Carbon-in-Pulp (CIP) or Carbon-in-Leach (CIL) processes.

Activated carbon loaded with gold must be treated by an elution step to desorb the gold for subsequent recovery. In this way, a smaller volume of higher grade gold solution is produced, suitable for final gold recovery by electrowinning. The gold elution efficiency can be increased by the use of hydro-alcoholic solution and high temperature. The effect of particle size on gold elution has not been studied. In this regard, experiments have been performed with different size fractions of activated carbon to study the stripping characteristics of activated carbon for gold elution. It has been observed that it is difficult to elute gold from fine activated carbon which is quite contrary to fundamental expectations. From a technological point of view, it is necessary to develop improved methods of stripping for enhanced gold recovery from alkaline cyanide solutions. As part of this work, to overcome the problem of gold elution from fine carbon, alternative elution procedures have been developed and discussed. These

include, use of hydro-alcoholic solutions, use of vacuum degassing prior to stripping, and application of external pressure.

Research on this topic is carried out to enhance the understanding of the science involved in the elution of gold from fine activated carbon. Hence, current research focuses on finding a plausible explanation to explain the difficulty of eluting gold from fine activated carbon. The emphasis of this research is to address the stripping by experimentation and with the aid of computational chemistry tools.

Since activated carbon consists of a cryptocrystalline graphitic structure which contributes significantly to gold adsorption, research on HOPG (highly oriented pyrolytic graphite) is in progress to determine the nature of graphite surfaces, their wetting characteristics, and their significance in gold adsorption / desorption from alkaline cyanide solutions. Computational chemistry analysis of adsorbed aurodicyanide anions at graphite surfaces are being done to understand the nature of gold adsorption/desorption from alkaline cyanide solutions by activated carbon. Current results from these surface chemistry studies are used to discuss the state of gold cyanide at activated carbon surfaces and the anomalous elution dependence on particle size.

“FEAR GOD AND WORK HARD”

- *David Livingstone*

I dedicate this thesis to my family. A special feeling of gratitude towards my beloved parents, **Kalyan Kumar Bhattacharyya** and **Gargi Bhattacharyya,** who have always encouraged me to stay motivated. My brother **Anirban** and my girlfriend **Sreya** have been very special and have always stood there beside me.

TABLE OF CONTENTS

LIST OF TABLES

ACKNOWLEDGEMENTS

I would sincerely like to express my heartfelt gratitude to Prof. Jan D. Miller for providing me with such a wonderful opportunity to work on this project. His guidance, persistence, and words of encouragement have been a constant source of inspiration for me, throughout my thesis research. I have always been in awe of his vast knowledge on the subject matter and have tried to imbibe some of it through his course lectures and the scientific research discussions.

I would also like to express my sincerest thanks and gratitude to members of my supervisory committee, Prof. Michael L. Free and Prof. Sivaraman Guruswamy, for their valuable inputs and suggestions and for their precious time reviewing my thesis.

Special thanks to Dr. Tolga Depci (visiting researcher from Turkey), without whose help and guidance this thesis would not have been accomplished. Dr. Depci's expertise and guidance on activated carbon adsorption and desorption is greatly acknowledged. His help with graphite surface chemistry is also appreciated and I cherish the time spent with him here at the University of Utah.

Also, I would like to thank Prof. Keith Prisbrey and Dr. Hao Du (China) for helping me with molecular dynamics simulations and Dr. Shoeleh Assemi for helping me with AFM.

Thanks are extended to Newmont Mining Corporation for providing financial support to sustain this research project.

I would like to thank the entire faculty, staff, and my colleagues and friends in the Department of Metallurgical Engineering at the University of Utah for helping me in some way or other during my thesis research.

Last but not the least, I would like to express my love and appreciation towards my parents, brother, my girlfriend, and all those who had indubitable faith in my abilities, and for the endless support I received from them throughout my research work.

CHAPTER 1

INTRODUCTION

Activated carbon has been an indispensable component in the extractive metallurgy of gold. Carbon adsorption is a common method of removing many dissolved species from solution. In particular, activated carbon adsorption has been used extensively in removing gold from the leach solution and hence is considered as a major solution concentration and purification step in gold hydrometallurgy. The introduction of cyanide leaching almost a hundred years ago revolutionized the treatment of gold ores and allowed gold to be recovered from ores that could not be amalgamated or concentrated by gravity.

Activated carbon is used to selectively concentrate dilute (1 to 20 g Au/t) (Marsden and House, 2006) gold bearing solutions to produce a higher grade solution from which gold can be efficiently extracted. Gold is first adsorbed from leach solutions onto activated carbon and then the loaded carbon is separated from the process stream to facilitate desorption of gold into smaller volume of solution suitable for metal recovery. The stripped activated carbon can be reused as an extractant. For this purpose, the stripped activated carbon has to be regenerated to restore its activity and then recycled into the process stream. Activated carbon can be used to treat leach slurries directly by

carbon-in-pulp (CIP) or carbon-in-leach (CIL) processes. Gold after being stripped of the activated carbon is sent for recovery through electrowinning, after which the pure metal is smelted to form ‘dore’.

Primarily coarse, granular activated carbon particles are used in the CIP or CIL processes to facilitate better separation from the slurry by mechanical screening. In contrast, fine activated carbon particles have higher adsorption kinetics as opposed to coarser particles. However, fine activated carbon poses a serious challenge of separation from the slurry stream. This problem has been overcome by the use of fine magnetic activated carbon particles (Miller et al., 2001; Munoz et al., 2002; Miller et al., 2004; Munoz, 2006), which can be used without compromising the adsorption capacity and at the same time, can be separated from the slurry by the application of wet high intensity magnetic separator.

This thesis will focus on the particle size effect of activated carbon on adsorption and desorption of gold cyanide and development of process alternatives for efficient gold elution from fine activated carbon. In addition, the significance of graphitic carbon structures in gold elution will be discussed from a fundamental point of view using surface chemistry results including molecular dynamics simulations.

1.1 Activated Carbon

Activated carbon (AC) is an organic material which essentially has a cryptocrystalline graphitic structure (Adams, 1989). Activated carbon has found diverse industrial applications due to a highly developed internal pore structure, which contributes primarily to an extremely large specific surface area. Typical values for

specific surface area of activated carbon are well in excess of 1000 m^2/g and are comparable to that of a soccer field (in perspective).

Thermal decomposition followed by partial combustion of various carbonaceous materials such as bituminous and anthracite coal, coconut shells, sugar, and apricot stone (Bansal et al., 1988; Depci, 2012) results in the formation of activated carbon particles with a high degree of porosity and extended intraparticulate surface area. Commercial grade activated carbon is manufactured by a two stage process: carbonization or pyrolysis of the carbon source material in the absence of oxygen at temperatures below 700°C followed by activation or gasification of the carbonized product with high temperature steam. Activation of carbon involves removal of hydrogen or hydrogen rich fractions from the carbonaceous matrix, leading to the formation of open, porous residue. The type of source material has a significant influence on the physical structure of the product, in particular, the pore volume and pore area, and particle size distribution. For instance, activated carbon derived from wood is used for decolorization, whereas coal-based, coconut shell, and apricot stone-based carbons are generally used for gas phase adsorption and gold recovery applications [Adams, 1989; Marsden and House, 2006]. Activated carbon with different activation levels can be produced on a pilot plant scale by direct activation of carbonized material with steam at 840–860 °C in a rotary kiln to different burn-off levels (Muller, 2010).Muller (2010) also showed that the different burnoff levels of 50%, 65%, and 80% significantly affect the micropore volume and surface area.

Activated carbon has a high carbon content (87-97 %) with other elements such as hydrogen, oxygen, sulfur, and nitrogen contributed primarily by functional groups

(carboxylic, phenolic hydroxyl, quinine type carbonyl, peroxides, etc.) originating from the raw materials or generated during production. Other inorganic mineral components in quantities of around 1 – 20 % may be present in activated carbon. These mineral substances are often removed as ash. The ash content of commercial activated carbon is between 0.1 – 0.2 % (Bansal et al., 1988; Jankowska et al., 1991).

Activated carbons may be granular or in powdered form depending on its usage. AC has found wide industrial applications in both gas and liquid separation processes although almost 80% of the total activated carbon usage in the U.S. is for liquid phase applications (Marsden and House, 2006). They are excellent adsorbents and are used for purification, decolorization, detoxification, filtration, and concentration of substances. Other diverse areas of interest which use activated carbon in processing include petroleum, mining and metallurgy, nuclear, automobile, pharmaceuticals, and food and beverages industry. Wastewater treatment and drinking water purification are notable applications of activated carbon.

However, its use in the gold recovery industry has only been widespread since about 1980. The most important properties of activated carbon for use in gold extraction are: adsorption capacity, adsorption rate, mechanical strength and wear resistance, reactivation characteristics, and particle size distribution. Other factors such as cost and availability also affect carbon selection.

1.2 Structure and Properties of Activated Carbon

Activated carbons are characterized by their cryptocrystalline graphitic structure (Adams, 1989). They have a similar, though less ordered, structure to that of graphite.

Riley (Marsden and House, 2006) suggested that activated carbon has two basic structures as revealed by x-ray studies: small regions of elementary crystallites, composed of roughly parallel layers of hexagonally ordered atoms; disordered cross-linked, space lattice of carbon hexagons, which is more pronounced in chars formed from materials of high oxygen content. Activated carbon has a disordered microcrystalline structure quite similar to graphite, as shown in Figure 1.1 and 1.2.

Commonly reported dimensions for elementary crystallites are temperature dependent, but typically vary from 9 to 12 Å high and 20 to 23 Å wide. Activated carbon is composed of stacked sheets of aromatic carbon rings cross-linked in a random manner, with a d-spacing value of 3.5-3.7 Å. From these values it has been estimated that the crystallite structures are approximately three layers high, and widths equivalent to the diameter of nine carbon hexagons. Activated carbon is highly porous and has only a weak diffraction pattern. During the activation process, an extremely large internal surface area is generated which is much greater as compared to the outer surface of a carbon granule. The random organization of graphite micro crystals and oxidation during activation creates the microporous structure, which accounts for their high surface area and its notable adsorptive capacity (McDougall and Fleming, 1987; Bansal et al., 1988; Adams, 1989). Accurate determination of the shape of pores poses a challenge and this leads to some difficulty in expressing pore size.

Most commercial activated carbon has a specific surface area of 800-1200 m^2/gm, which is predominantly contained within micropores less than 2 nm in diameter. The complex pore network of activated carbon was classified by Dubinin (1979) on the basis of changes in vapor adsorption mechanism with pore size and is the widely accepted one.

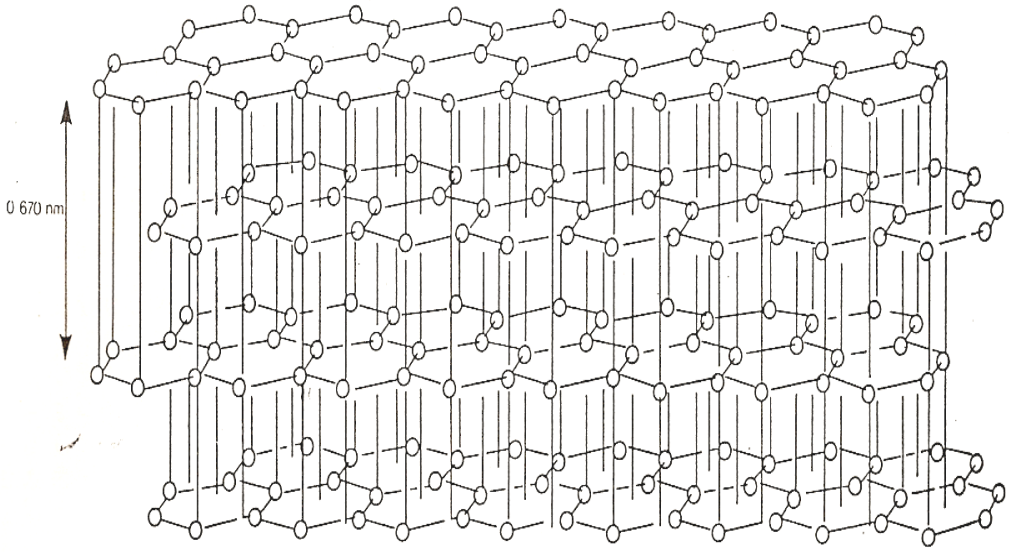

Figure 1.1.Schematic representation of the structure of graphite. The circles denote the position of the carbon atom and the horizontal lines represent the C-C bond.

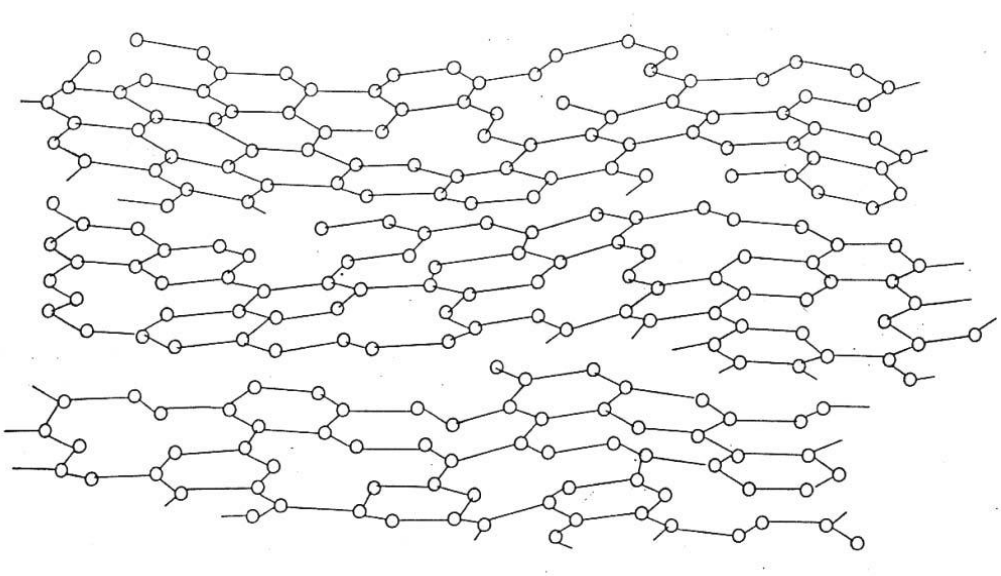

Figure 1.2.Schematic representation of the structure of activated carbon

Macropores: D_p> 100 to 200 nm

Transitional pores or mesopores: 1.6<D_p< 100 to 200 nm

Micropores: D_p< 1.6 nm

where, $D_p$is the pore diameter. The term supermicropore has been used to describe the range 0.6 to 1.6 nm [Marsden and House, 2006].

Micropores constitute the largest part of the internal surface area of an activated carbon and most of the adsorption occurs in micropores. In contrast, mesopores exhibit low surface area contribution and they are important because they serve as passages for the transport to the micropores of the activated carbon. The contribution of the macropores to the total surface area is low; however, due to the large pore size and hence larger volume, they are important for their liquid retention capacity. Figure 1.3 shows a typical schematic representation of activated carbon comprising distorted graphitic sheets with exposed face and edge surfaces. Hence, further study has been accomplished in this thesis to facilitate better understanding of gold adsorption on the graphite face and edge surface. A TEM micrograph of activated carbon has also been presented in Figure 1.4. This figure illustrates the abundant presence of typical slit-shaped micropores around a cylindrical mesopore. Further studies encompassing the discussion of gold adsorption in slit pores have been presented in this thesis.

The edges of the micro-crystallites formed during the activation of char contain unfilled carbon valences which react with the oxidizing gas to form a wide variety of oxygen containing functional group. Also, the surface of activated carbon is heterogeneous in nature, having both hydrophobic and hydrophilic domain, which explains the ability of activated carbon to adsorb a wide variety of compounds.

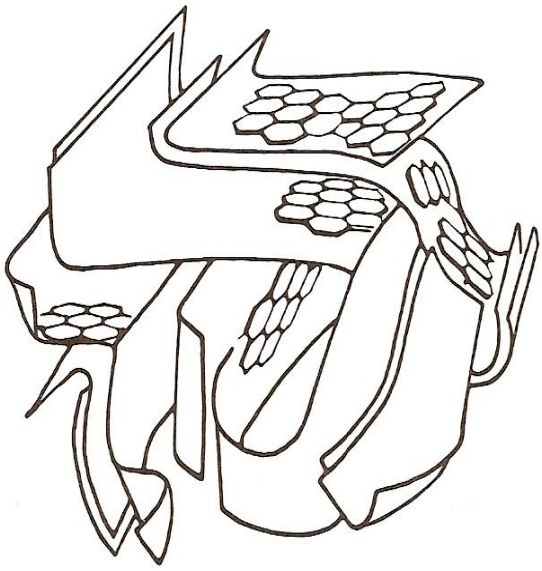

Figure 1.3. A typical schematic representation of activated carbon comprising distorted graphitic sheets. (Rodriguez-Reinoso and Molina Sabio, 1998)

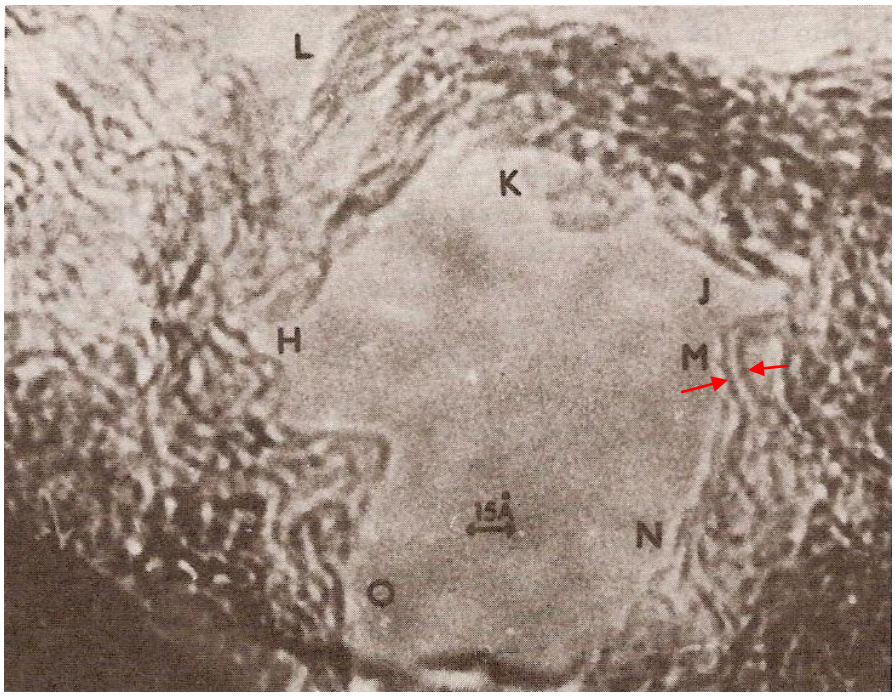

Figure 1.4. TEM micrograph of activated carbon, with a typical slit-shaped micropore M (0.5 nm), at the edge of a cylindrical mesopore.

In many other applications, including gold cyanide adsorption, transportation of the adsorbate within the pores can be rate determining. Consequently, decreasing the particle size of granular activated carbon has a large effect on the rate of adsorption, despite only a small change in net surface area.

Typical coconut shell activated carbon used in the gold industry has an ash content of 2% to 4%, an apparent density of 420 to 450 kg/m^3, and BET surface area 900 to 1000 m^2/g.

The adsorptive properties of activated carbon are not only determined by surface area but also by its chemical properties. Although these characteristics are less well understood, the activity of carbon is attributed to the following factors.

- The presence of edge dislocations might cause disturbances in the microcrystallite structure. This may lead to the presence of residual carbon valencies and might affect adsorption of polar and polarizable species.
- The nature of chemically bound oxygen and hydrogen is dependent upon the type of source material and the activation conditions and this might determine the activity of the resultant activated carbon.
- The presence of inorganic matter such as ash components or other fouling agents from flotation chemicals might be detrimental to adsorption or might facilitate specific adsorption.

The interaction between these factors might further be detrimental for the activated carbon product. For instance, disturbance in the carbon lattice can be created by inorganic impurities and can cause preferential adsorption of oxygen in the defects during activation.

Activated carbons can be broadly classified into two types based on their activation temperature: H-carbons and L-carbons (Marsden and House, 2006). Typically, H-carbons are formed at temperatures > 700°C (usually around 1000°C) and are characterized by their ability to reduce the pH of the bulk solution by adsorbing hydrogen ions. On the other hand, L-carbons are activated at temperatures < 700°C (usually between 300 and 400°C) and preferentially adsorb hydroxyl ions. Activated carbon used for gold recovery is steam activated at about 1000°C is predominantly of the H-type.

Surface reactions, wettability, and electrical and catalytic properties of the carbon can be influenced by the C-O complexes that are formed due to the greater tendency of chemisorption of oxygen onto carbon than other elements. Functional groups contribute almost 90% of oxygen present in activated carbon while the remainder exists as neutral bonds in ether bridges (Marsden and House, 2006). Analytical techniques such as FTIR, etc. have identified carboxyl, phenol, quinine, and hydroxyl, as well as ester groups as the major functional groups present on the surface. Oxide groups such as carboxylates are formed at lower temperatures whereas phenolic groups are formed at higher temperatures. These functional groups affect the acid-base characteristics of the surface.

Depci et al. (2012) investigated the zeta potential variation of virgin activated carbon with change in pH of the solution and found the iso-electric point (IEP) as approximately pH 2.4. They also said that the zeta potential of virgin activated carbon increases in the negative direction with increase in pH due to ionization of the acidic oxygen surface groups.

Having understood the structure and properties of activated carbon, the adsorption and desorption mechanisms of gold cyanide will be reviewed in the next section.

1.3 Review of Activated Carbon Adsorption and Desorption of Gold from Alkaline Cyanide Solutions

The process of leaching gold by cyanide solutions (also known as gold cyanidation) brought about a revolution in the treatment of gold ores and is the most imperative and the primary metallurgical process used for gold extraction and has been present for over a century (de Andrade Lima and Hodouin, 2006).

Activated carbon has found increased application in the field of hydrometallurgy, especially in the recovery of gold and silver from cyanide solutions (Davidson, 1974; Adams and Fleming, 1989).The phenomena of adsorption and desorption of gold cyanide complex onto and from activated carbon, the most prolific and widely used adsorbent, has been observed and studied with utmost success (Adams and Flemings, 1989; Ibrado and Fuerstenau, 1995; Jones et al, 1989; McDougall et al, 1980; Rees and van Deventer, 2000).

The cyanidation process comprises two stages, namely extraction and recovery. The extraction stage of the process involves the dissolution of gold present in the finely disseminated ore by cyanide in an aqueous solution and the recovery stage involves the use of activated carbon to adsorb the complex ion ($Au(CN)_2^-$)followed by desorption, gold electrowinning

Continuous processes like the Carbon–In-Pulp (CIP) process and the Carbon-In-Leach (CIL) processes have been primarily dominant in the area of gold recovery and have been used worldwide, accounting for nearly 44% of net world production (Marsden and House, 2006). Carbon adsorption processes are comparatively important and are significantly used more than other processes as they eliminate the need for solid-liquid

separation stages, like thickening and filtration. Hence, operating costs are greatly reduced (Marsden and House, 2006).

The perfect or exact mechanism of gold adsorption from cyanide solutions is still a paradox and has been difficult to decipher. Numerous mechanisms have been put forth by various investigators, as illustrated in the subsequent section.

The process of adsorption of gold cyanide onto activated carbon is directly dependent on many chemical and physical factors which affect the adsorption kinetics considerably. The initial rate of adsorption of gold cyanide is pretty rapid, and occurs at the most accessible sites in macro-pores and meso-pores. However, the kinetics of this process is reduced as equilibrium is approached. Under the prevalence of such conditions, the rate of the reaction is controlled by the mass transport of gold cyanide species to the activated carbon surfaces. However, when this adsorption capacity has been utilized and exhausted, a pseudo-equilibrium state is established beyond which the adsorption takes places in the micro-pores (Fleming and Nicol, 1984). This requires gold cyanide species diffusion along the pores within the carbon structure. This is a relatively slower process as compared to the process of boundary layer diffusion, attributing to the length and tortuosity of the pores. Studies have revealed that the film transfer controls the adsorption rate of aurodicyanide onto the activated carbon during the preliminary stages of gold recovery (Coetzee and Gray, 1999).

Loaded activated carbon has to be treated by an elution step to recover the gold. Suggested mechanisms for gold desorption have been discussed in the subsequent section of this chapter. Desorption/elution systems have primarily been categorized into two types:

- Processes that operate at atmospheric pressure and at temperatures less than $100^{o}C$
- Processes that are functional and operate at augmented and elevated pressures to allow for stripping at temperatures greater than $100^{o}C$, thereby achieving comparatively faster elution rates.

The various stripping procedures are discussed as follows:

- Atmospheric and Pressurized Zadra: The predominantly used elution process is the Zadra process, which recycles and reuses hot solutions of 1% w/v NaOH, 0.5% w/v NaCN through a gold cyanide-loaded carbon bed for up to 72hours at $95–100^{o}C$ to desorb $Au(CN)_2^-$ (Zadra, 1950; Zadra et al., 1952). Atmospheric elution of gold from loaded activated carbon by using caustic soda is better known as the Atmospheric Zadra process. A modified version of this process has been adopted by some plants and used, wherein the operating temperature and pressure are $140^{o}C$ and 600kPa respectively, thereby reducing elution times by 10-12 hours.
- Davidson: This is an Anglo elution procedure (Davidson and Duncanson, 1977; Davidson and Veronese, 1979), which elutes gold in 8-12 hours using de-ionized water at $100\text{-}120^{o}C$. For this process, carbon is presoaked with 5% w/v NaCN and 1% w/v NaOH solution. This process is pretty sensitive to the quality of water used. Optimized conditions for the maximum recovery of gold from the carbon surface were found to be obtained by pretreatment with a solution containing 5% potassium carbonate and 10% potassium hydroxide, thereby followed by elution with hot water at $90^{o}C$. This process was observed to recover 99% of loaded gold

in 12 bed volumes and almost all of it in 22 bed volumes (Bansal et al., 1988; Davidson et al., 1974).

- Anglo American Research Laboratory [AARL]: The AARL method requires carbon loaded with gold to be washed in a dilute mineral acid, and thereafter washed in de-ionized water. Thereafter, the process includes soaking the gold-loaded carbon in 3% NaCN and 2% NaOH solution for about 30 minutes. This is followed by stripping the gold-loaded carbon with de-ionized water at elevated temperatures (McArthur et al., 1987; Marsden and House 2006).
- Alcohol Stripping: Precious metals adsorbed onto the surface of activated carbon are extracted by various processes such as hot elution or pressure desorption with hydro-alcoholic solutions, before final recovery is effected by electrochemical methods(Muir et al., 1985; Espiell et al., 1988; Ubaldini et al., 1998). However, the rate of elution was significantly elevated and increased by the addition of ethanol to the Zadra elutant.

  Gold stripping from activated carbon using a range of different alcohols (isopropanol, ethanol and ethylene glycol) has been reported. The most rapid elutant was isopropanol with 98% Au eluted after 1 hour at 80^{o}C. Ethylene glycol had a similar extraction and recovery after 2 hours, and ethanol was the least effective of all with 5 hours required for 95% extraction.
- Vacuum Elution Process: The desorption process is the reverse of adsorption, and hence the chemical and physical properties that inhibit adsorption will favor the process of desorption. Similarly, the converse is also applicable in a sense that the factors that augment adsorption will inhibit desorption. Consequentially, the

depletion of dissolved oxygen in the elutant will benefit the desorption of gold from activated carbon (Feng et al., 2003). Vacuum degassing the loaded activated carbon can result in depletion of the dissolved air.

Also vacuum driven cavitation can cause chemical and physical variations in a liquid medium. Vacuum driven cavitation refers to the growth and violent collapse of microbubbles in a liquid medium as a consequence of physical vibrations and perturbations. A hotspot effect is also induced due to cavitation, which produces localized high temperatures and pressures. This hotspot effect has the potential to directly occur at the surfaces of carbon. This may lead to a weakening of the physical and chemical bonds between gold cyanide and the surfaces of carbon, due to generation of high temperatures and elevated pressures. This, in turn, may lead to faster and more rapid kinetics of elution. This also indicates notable reasons as to why elution is possible at lower temperatures and pressures in the presence of vacuum degassing. Cavitation effects are usually accompanied by the formation of radicals, which may induce and generate further reactions.

Alcohol also reduces the threshold for cavitation, and captures the radicals to form secondary radicals beneficial for desorption of gold. Hence, alcohol coupled with vacuum degassing can prove to be an effective process alternative for gold stripping from loaded activated carbon.

With a firm understanding of the fundamentals of elution processes obtained from this review, several experiments were performed using various traditional and alternative techniques for gold elution and the results are reported and discussed in this thesis.

1.4 Mechanism of Gold Adsorption / Desorption

Several mechanisms of gold adsorption from cyanide solutions had been proposed in the literature prior to 1980 (McDougall and Fleming, 1987) but only recently, evidences have been provided.

Gold cyanide adsorption is a reversible process with generally faster kinetics for desorption under modified conditions. Researchers have also stated that under most conditions, the molar ratio of loaded gold to nitrogen is 0.5:1, which is consistent with the presence of $Au(CN)_2^-$ group. There was a consensus that the adsorption of aurocyanide ion $Au(CN)_2^-$onto carbon occurs without chemical change, and that the graphitic structure of carbon was of great importance (Cashion et al., 1988; Ibrado and Fuerstenau, 1995; Jones et al, 1989; Klauber 1991; Sibrell and Miller 1992). The primary factors that determine gold adsorption by carbon seem to be the graphitic structure and surface area (Sibrell, 1991; Miller and Sibrell, 1991).

Detailed experimental evidences and investigations using spectroscopic techniques such as Mossbauer spectroscopy, XPS, and model extractants on high ionic strength solutions, typical of those obtained in actual gold leaching systems, indicate that gold cyanide complex is adsorbed on the carbon surface predominantly as a neutral ion pair $M^{n+}[Au(CN)_2^-]_n$ [Marsden and House, 2006]. Surface chemical analyses have established that the oxidation state of gold on carbon is +1 and this is consistent with the ion pair concept. The adsorption mechanism is best described by the following reversible equation:

$$M^{n+} + nAu(CN)_2^- \leftrightarrow M^{n+}[Au(CN)_2^-]_n \quad \ldots\ldots\ldots\ldots (1.1)$$

where, the ion pair $M^{n+}[Au(CN)_2^-]_n$ is the adsorbed gold species.

Currently, the most accepted theory regarding the mechanism of gold adsorption is the adsorption of ion pairs onto active sites of activated carbon. This ion-pair adsorption process is somewhat selective due to the structure of the aurocyanide anion, which is considered to be less hydrated than other cyanoanions. On this basis, the selective solvent extraction of gold from alkaline cyanide solutions had been previously explained (Mooiman and Miller, 1984). In addition, some adsorption of the unpaired anion $Au(CN)_2^-$ occurs through electrostatic interactions at highly active sites of activated carbons that have appropriate polarity (Lagerge et al., 1997, 1999).

To understand the adsorption sites of gold cyanide on carbon, the most accepted theory suggests that gold is adsorbed at the edge or defect sites rather than at sites on the basal planes of carbon (Sibrell and Miller, 1991, 1992; Lagerge et al., 1999). Sibrell and Miller (1992) clearly showed that adsorption occurs at the edges (defects) of graphite (HOPG) crystals and that adsorption on the basal surface of the crystal was insignificant by comparison. This was demonstrated through autoradiographs of radiolabelled gold cyanide on HOPG crystals, which clearly showed much higher adsorption intensity at the edge surface and through XPS study HOPG edge and face surface. This led Sibrell and Miller to suggest that adsorption of the aurocyanide complex by activated carbon and graphite occurs preferentially at the edges of the aromatic sheets in the carbon structure. The edges of the aromatic sheets are expected to provide localized sites of mild polarity, resulting from defects in the aromatic structure, at which aurocyanide ion pairs undergo physical adsorption. These results were later confirmed by in situ scanning tunneling microscopy in 1998 (Poinen et al., 1998). It is evident that site-specific adsorption is prevalent in the adsorption of gold by graphitic carbons (graphite, carbon black, and

activated carbon), and most of the favored sites are at edge defects in the graphite crystal structure. As mentioned earlier, McDougall et al. (1980) have hypothesized that the adsorption of the gold-cyanide complex is due to ion exchange under conditions of low ionic strength, and to ion-pair adsorption at high ionic strengths. It is likely that both of these mechanisms take place at edge defects in the graphite structure. Ion exchange would take place with functional groups that would be found at graphitic carbon edges. For adsorption of ion pairs, van der Waals forces would be involved, and the unsymmetrical distribution of charge at edge defects in the graphite structure could well play a role in the adsorption process. These graphite edge-sites or defects in activated carbons and in natural carbonaceous matter are expected to form at high temperatures and a suitable oxidizing potential. For example, defect pits, or nanocorrals, form spontaneously on graphite surfaces (Zhu et al., 2001; Paruchuri et al., 2003). These pits vary from 2 nm to several microns in size and it seems that such cages could easily accommodate the aurocyanide ion-pair adsorption reaction.

Regarding the role of surface functional groups on adsorption by activated carbon, researchers suggest that the presence of basic surface functional groups, specifically the pyrone type, favors the adsorption of gold onto activated carbon (Papirer et al., 1987, 1991, 1995; Polonia-Leo´ n et al., 1993). Ofori-Sarpong et al. (2010) inferred that the gold cyanide adsorption on activated carbon is facilitated by high carbon-to-oxygen ratio. Adams (1989) examined commercial activated carbons by heating to various temperatures under nitrogen, air, and steam atmospheres and showed through FTIR analysis that carbons heated above 750°C were rich in carboxylic and phenolic functional groups whereas the one heated below 750°C indicated ether functionality and C=C

stretching. He also concluded that carbons heated above 750°C showed high gold cyanide complex adsorption activities whereas those heated to less than 750°C showed only mild cyanide complex uptake, and this was observed regardless of the atmosphere under which heating occurred.

Thus, it is clear from the evidences presented above that functional groups play a significant role in gold cyanide adsorption. Also, it can be inferred that gold cyanide is adsorbed as a neutral ion pair at the graphitic edge surfaces.

Having reviewed the gold cyanide adsorption mechanism onto activated carbon, it is only appropriate in perspective of this thesis that some light is also thrown on the desorption mechanism.

Van Deventer et al. (1994) said that the most important subprocesses constituting the elution of aurodicyanide are the decomposition or adsorption of cyanide on the surface of the carbon followed by the elution of cyanide, concomitant removal of spectator cations and the subsequent elution of aurocyanide. Spectator cations depress the desorption of aurodicyanide by the formation of the neutral ion pair species on the carbon, which is promoted by the presence of high concentration of cations in the solution. This follows that very little desorption of gold is observed when the cation concentration in the eluant is high and no cyanide is present in the solution or on the carbon. Hence, it can be concluded that pretreatment of loaded carbon with cyanide and reduced concentration of cations in the eluant will facilitate rapid and enhanced elution of gold cyanide. They also said that during cyanide treatment, CN^- reacts with the functional groups on the carbon surface and passivates the carbon disabling the adsorption of anionic gold cyanide. Passivation of the active sites causes gold elution during Zadra or

AARL method rather than the free cyanide carried over from the pretreatment. Degree of passivation is determined by the temperature of the eluant. Higher temperatures, which inhibit adsorption, favors gold cyanide desorption.

Therefore, for most industrial practices, activated carbon stripping to obtain a concentrated solution of gold cyanide takes place at near boiling temperatures at atmospheric pressure and higher temperatures under pressure and sufficient amount of cyanide is used in the eluant and pretreatment step.

1.5 Review of the Nature of Graphite (HOPG) Surfaces

Activated carbon essentially has a cryptocrystalline graphitic structure (Adams, 1989) which plays a significant role in gold adsorption and desorption. In this regard, many researchers have used highly oriented pyrolytic graphite (HOPG) as a model carbonaceous surface for their fundamental experimental studies. The major surfaces of interest in HOPG for most practical applications are the face surface and the edge surface, as illustrated in Figure 1.5.

HOPG is a highly anisotropic material, exhibiting quite different properties on its face and edge planes. For example, these surfaces exhibit contrasting electrochemical behavior, where electrochemical reactions at the edge surface have been shown to be anomalously faster than reactions at the face surface (Davies et al., 2004 and 2005; Banks and Compton, 2006;McCreery, 2008; Dale et al., 2012). Physical properties of HOPG, such as resistivity, thermal conductivity, thermal expansion, and Young's modulus, display an anisotropy dependence on these surfaces (McCreery, 1991). Some researchers reported anisotropy in the double-layer capacitance (Robinson et al., 1991; Rice and

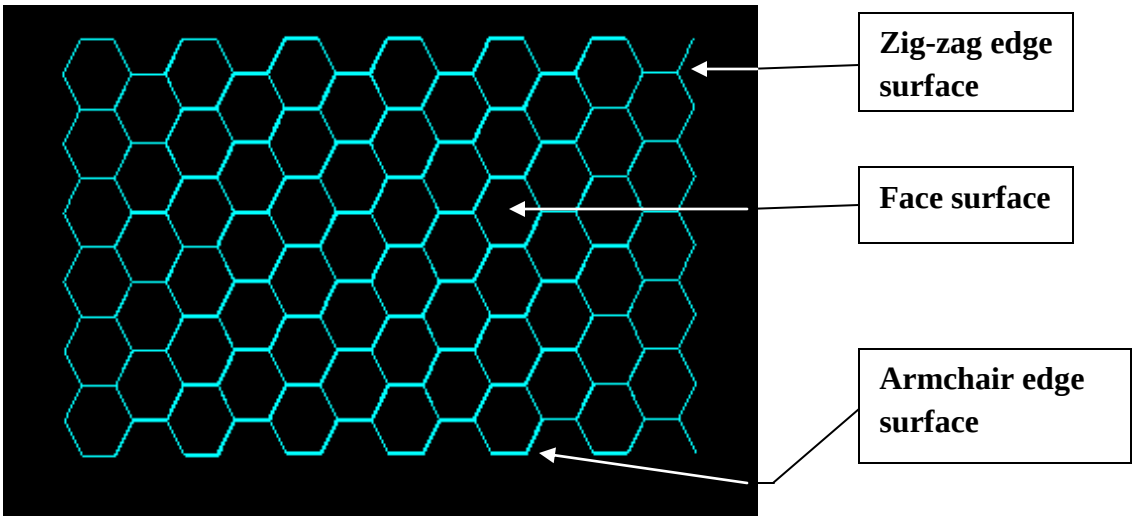

Figure 1.5. HOPG surfaces of interest: face and edge surface

McCreery 1989; Morcos and Yeager 1970; Randin and Yeager 1975) and heterogeneous electron-transfer rate constant (k°) (Robinson et al., 1991; Rice and McCreery 1989; Wightman et al., 1978; 1984) for some benchmark redox systems, with both C° and k° being higher for edge vs face plane HOPG (Mark et al., 1992). As understood, the face and edge surfaces and edge steps of HOPG surface are well documented in physics and nuclear research areas.

In order to explain the adsorption mechanism of some chemicals (quinones and some aromatic molecules, nonpolar organic compounds) on carbonaceous materials, the well-ordered face surface of HOPG was used as a reference point by some researchers (McDermott and McCreery, 1992). In addition, some researchers directly investigated the adsorption of some chemicals and compounds at the HOPG face surface including potassium, deoxyribonucleic acid (DNA), polyelectrolytes, calcium carbonate. All researchers considered only the face surface as being well-ordered with a certain degree

of hydrophobicity. None of the researchers considered the less hydrophobic edge defects / steps or the edge surface in their experiments.

Molecular simulations have been done for the HOPG face surface to understand the underlying molecular-level phenomena and the adsorption mechanism for methane/water vapor mixtures (Muller and Gubbins, 1998), water (Muller et al., 1996), nonpolar organics (Kwon et al., 2002), and gold atoms (Jensen et al., 2004).These researchers selected a perfect/pristine face surface of HOPG to explain activated carbon adsorption phenomena and have ignored the edge surface. The perfect/pristine face surface of HOPG has no edge plane (in theory), no location for surface functional groups, and there are no dangling bonds since the carbon atoms have satisfied valances (McCreery, 2008).

Researchers have evaluated both the face and edge surface of HOPG for adsorption of some compounds as stated in this paragraph. McDermott and McCreery (1994) thought that the defects on the face plane of HOPG might affect the adsorption of quinines due to the partial electronic charges. Sibrell and Miller (1992), Adams (1993) and Poinen et al., (1998) used HOPG to explain the adsorption of gold cyanide at the surface of activated carbon. They mentioned that the gold cyanide ion pair was adsorbed at the edge surface of HOPG. The adsorption of propane and acetone (Kwon et al., 2003) on the HOPG surface was studied following heat treatment. They mentioned that oxygen-containing functional groups exist on air cleaved HOPG and they would result in higher adsorption capacity of carbonaceous surfaces for polar organic molecules (acetone) than for the nonpolar (propane). Wildgoose et al. (2006) mentioned that the edge steps on the face plane surface should be chemically more active and often lead to the presence of a

variety of chemical sites, including oxo, acid, and hydroxyl terminations. Domi et al. (2012) investigated the formation of a solid electrolyte interphase (SEI) and the thickness of surface films on HOPG. They mentioned that the edge plane was more effectively covered than the face plane. Their experimental results showed that graphitic edge plane, as compared to the carbon paste, glassy carbon, and screen-printed carbon electrodes, are the most suitable carbon material for investigating conformational changes in proteins. However, none of them discuss the differences in wetting characteristics between the edge and face surfaces of HOPG.

The essential aim of this work is to provide wetting information for HOPG surfaces that are not currently available, in order to facilitate future research on adsorption phenomena for carbonaceous surfaces. This has been achieved in this thesis through experimentation, spectroscopic analysis, and molecular dynamics simulations.

1.6 Research Objectives

This thesis research was stimulated by the desire to provide an explanation for unsatisfactory gold elution from fine activated carbon and to develop process alternatives for improved elution. It has been reported that traditional atmospheric Zadra and Mintek methods for gold elution show that the amount of gold eluted increases initially with a decrease in particle size but falls drastically with further decrease in particle size. This problem might be attributed to the difference in pore size of the activated carbon of different particle size and the wetting characteristics of the eluting solution.

In this regard, two research objectives were identified. The first research objective is to investigate process alternatives for gold elution from activated carbon, including the

following: isopropanol and ethanol for alcohol elution; vacuum degassing activated carbon prior to its stripping by Zadra and alcoholic solutions; and pressure treatment with a syringe pump method. It is expected that the results from the above experiments will help to clarify the activated carbon particle size effect in stripping of gold cyanide and provide alternative process strategies for enhanced gold elution at shorter retention times.

Since the graphitic structure of activated carbon seems to be an essential feature for effective gold adsorption / desorption, fundamental surface chemistry studies of graphite surfaces are included as the second research objective in order to provide further insight into the nature of graphite surfaces and their significance in gold adsorption.

1.7 Thesis Organization

Chapter 1 reviews the two major topics that the thesis deals with: activated carbon adsorption / desorption of gold from alkaline cyanide solutions and the nature of graphite (HOPG) surfaces. The first part of this chapter reviews the traditional gold elution processes such as the Mintek, atmospheric Zadra, AARL, etc. and also gives an idea of alternative eluants that have been tried, including use of hydro-alcoholic solutions. The latter part of the chapter reviews the importance of the two major graphite surfaces of interest: the face surface and the edge surface. It summarizes the work that has already been done by previous researchers on these surfaces and presents the scope of work that needs to be done in order to obtain a better understanding of these surfaces.

Chapter 2 gives details of the characterization of activated carbon relevant to the study of the adsorption and desorption properties in this thesis. The BET surface area and pore volume analysis has been done for ten different size fractions. This has been done to

support or provide logical explanations for the variations in gold adsorption capacity, adsorption rate, and desorption with particle size. Further, SEM and X-ray CT micrographs of activated carbon particles of different sizes have been given for better understanding of the pore structure.

Chapter 3 shows study of the activated carbon adsorption of gold cyanide from alkaline cyanide solutions. It is necessary to understand the adsorption phenomena prior to desorption. Hence, the effect of activated carbon particle size on adsorption capacity and adsorption rate has been investigated here.

In Chapter 4, following adsorption, the effect of particle size on the stripping of loaded activated carbon was studied in-depth. Traditional elution processes such as Mintek and atmospheric Zadra were investigated for all the particle size fractions. To provide a plausible explanation for unsatisfactory gold elution from the finer particles, alternative processes were tried and the results discussed. Hydro-alcoholic solutions were tried for gold elution at room temperature and 65°C, then Zadra coupled with alcoholic solution was tried for gold stripping at 98°C. In another method, loaded activated carbon was vacuum degassed prior to stripping by the above solutions. To see the influence of pressure on gold elution from the different size fractions, syringe pump and filter press method was used.

After studying the activated carbon adsorption and desorption kinetics with respect to particle size, the focus was shifted in Chapter 5 towards the study of the significance of graphitic surfaces in gold adsorption. Some fundamental wettability studies on the HOPG face and edge surfaces were performed through contact angle measurements of the as-received and oxidized HOPG surfaces. The face and the edge

surfaces were also characterized with Raman spectroscopy. The iso-electric point of graphite powder was determined through electrokinetic measurements. Also, the iso-electric point of the HOPG surfaces was determined using AFM surface force measurements. Also, previous results are reviewed in relation to the XPS spectra of gold adsorbed on the face and edge surface and micrographs of radiolabelled gold cyanide on HOPG surfaces. Molecular dynamics simulations (MDS) were performed to visualize the accommodation of gold cyanide on graphite face and edge surfaces and pores. Further, water and isopropanol were also used to study the effect of pore size on water accommodation.

In the final chapter of the thesis, the results from all the above chapters have been summarized and conclusions stated.

CHAPTER 2

CHARACTERIZATION OF ACTIVATED CARBON

Activated carbon was characterized to enhance our understanding of the effect of particle size on gold cyanide adsorption and desorption form alkaline cyanide solutions. The morphology, structure, and properties of the activated carbon were determined by BET, SEM, and X-ray CT. Physical properties of activated carbon such as particle size, specific surface area, and pore volume analysis were determined using BET. Other microscopy techniques such as Scanning Electron Microscope (SEM) and X-ray CT were used to further characterize the activated carbon samples.

2.1 Source of Activated Carbon

The activated carbon particles used in this thesis research were procured from Calgon Corporation, and were coconut shell-based activated carbon from Thailand. For robust applications such as recovery of gold cyanide from alkaline cyanide solutions, coconut shell activated carbon is preferred over carbon derived from other sources as it offers higher resistance to shear, attrition, and abrasion. In addition, a larger distribution of micropore area over other carbons renders it as the preferred choice in gold industry. Predominantly, all the activated carbon particles had a monosize distribution with an

average particle size of 2.8 x 1.4 mm. These carbon particles were crushed and screened to obtain finer particles of different size fractions.

2.2 Particle Size Distribution

Classification of activated carbons on the basis of their behavior, surface characteristics, and preparation methods is a difficult task. However, some general classification based on their physical characteristics is possible. In this regard, particle size distribution is one of the most important physical properties of activated carbon.

Generally, granular activated carbon is categorized and designated by sizes, for instance, a 20x40 carbon comprised of particles that will pass through a U.S. Standard Mesh Size No. 20 sieve (0.84 mm) (generally specified as 85% passing) but be retained on a U.S. Standard Mesh Size No. 40 sieve (0.42 mm) (generally specified as 95%retained). Carbon particles such as 8x20, 20x40, or 8x30 are predominantly used for liquid phase applications while particles in the size fraction 4x6, 4x8, or 4x10 find use in vapor phase applications. The most popular aqueous phase carbons are the 12x40 and 8x30 sizes because they have a good balance of size, surface area, and head loss characteristics.

Conventional activated carbon circuits for gold recovery applications use granular (7 x 12 mesh) activated carbon particles. These particle sizes are significantly coarser than the ground ore to facilitate effective separation of gold-loaded activated carbon from the slurry phase by mechanical screening (Marsden and House, 2006).

In the current study, granular [2.8 x 1.4mm] activated carbons as-received were usually washed several times with deionized water and dried overnight at 110^{o}C in an

oven. Dried coarse activated carbons were then crushed using a mortar and pestle. Crushed samples were then wet-screened to different particle size fractions using a bank of test sieves in series, ranging in size from 2.8 mm to 0.037 mm, as shown in Table 2.1. After wet screening, the different size fractions collected from the respective sieves were again dried overnight at 110^{o}C in an oven and stored in clearly labeled dry glass bottles in a desiccator.

For the adsorption capacity and rate experiments and traditional Zadra and Mintek elution methods, all the particle size fractions were used. Based on the results obtained

Table 2.1. Activated carbon particle size fractions with designated nomenclature

Code	**Particle size mesh**	**Particle size, mm**
S1	7 x 12	2.83 x 1.41
S2	12 x 20	1.41 x 0.841
S3	20 x 28	0.841 x 0.595
S4	28 x 35	0.595 x 0.420
S5	35 x 48	0.420 x 0.297
S6	48 x 65	0.297 x 0.210
S7	65 x 100	0.210 x 0.149
S8	100 x 150	0.149 x 0.105
S9	150 x 200	0.105 x 0.074
S10	200 x 400	0.074 x 0.037

from traditional stripping processes, only 7 x 12 mesh and 48 x 65 mesh size fractions were used for the alternative stripping methods.

2.3 BET Surface Area and Pore Volume Analysis

Surface area is the most prominent property of activated carbon which contributes to its widespread usage in the industry. Likewise, the most important property of activated carbon which highly affects the gold adsorption properties of activated carbon is its extremely large surface area and highly developed pore structure. In this study, the effect of particle size of activated carbon on its properties such as specific surface area and pore volume was investigated. In order to investigate these properties, virgin activated carbon was ground and sieved to obtain desired particle size fractions, as described in Table 2.1. In addition, surface areas of the different size fractions of the Calgon virgin activated carbon were also investigated. A Tri Star 3000 (Micromeritics, USA) surface analyzer was used to measure nitrogen adsorption isotherm at 77K in the range of relative pressures from 0 to 1. The pore structures of active carbon were investigated by using the standard Micromeritics DFT plus software. Before measurement, the sample was degassed at 300ºC for 3h.

Brunauer–Emmett–Teller (BET) theory serves as the basis for an important analysis technique for the measurement of the specific surface area of a material and is explained by the physical adsorption of gas molecules on a solid surface.

The BET equation was used to calculate the specific surface area (S_{BET}).The BET surface area, total pore volume, average pore radius (4V/A by BET), and micropore area

were obtained from the adsorption isotherms and are given in Table 2.2. Mesopore volume was determined by subtracting the micropore volume from total pore volume.

Table 2.2 contains the BET surface area (S_{BET}), external surface area (including mesopores and macropores area S_{ext}), micropores surface area (S_{mic}), total pore volume (V_t), and average pore diameter (Dp) results for all the size fractions. The pore diameter was obtained by applying the BET equation for N_2 adsorption at 77K. It was found that the activated carbon had a remarkable BET surface area, which was primarily contributed by micropores. The average pore diameters were between 2.15 nm and 2.20 nm, indicative of its microporous character. It appears that activated carbons were predominantly microporous. As can be understood from table, there is no significant effect of activated carbon particle size on micropore structure as determined by this method.

The nitrogen adsorption isotherms for two size fractions 7 x 12 mesh and 48 x 65 mesh as illustrated in Figure 2.1 and Figure 2.2 do not reveal any significant difference.

Table 2.2. Surface area and porosity of activated carbon of different size fractions

Particle Size	**S_{BET}**	**S_{mic}**	**S_{ext}**	**Vt**	**Vmic**	**Vmeso**	**Dp**
mesh	**(m^2/g)**	**(m^2/g)**	**(m^2/g)**	**(cm^3/g)**	**(cm^3/g)**	**(cm^3/g)**	**(nm)**
7 x 12	923	802	121	0.504	0.413	0.091	2.18
12 x 20	913	801	112	0.492	0.42	0.072	2.16
20 x 28	903	798	105	0.488	0.41	0.078	2.16
28 x 35	925	795	130	0.502	0.416	0.086	2.17
35 x 48	950	805	145	0.523	0.44	0.083	2.20
48 x 65	918	813	105	0.494	0.421	0.073	2.15
65 x 100	906	794	112	0.49	0.42	0.07	2.16
100 x 150	902	780	122	0.487	0.406	0.081	2.16
150 x 200	916	809	107	0.493	0.42	0.073	2.15
200 x 400	928	807	121	0.504	0.44	0.064	2.17

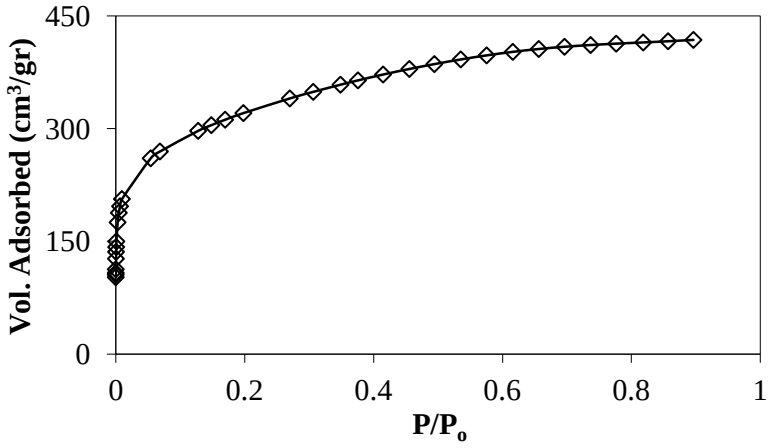

Figure 2.1.The nitrogen adsorption isotherm for coarse size fraction7 x 12 mesh.

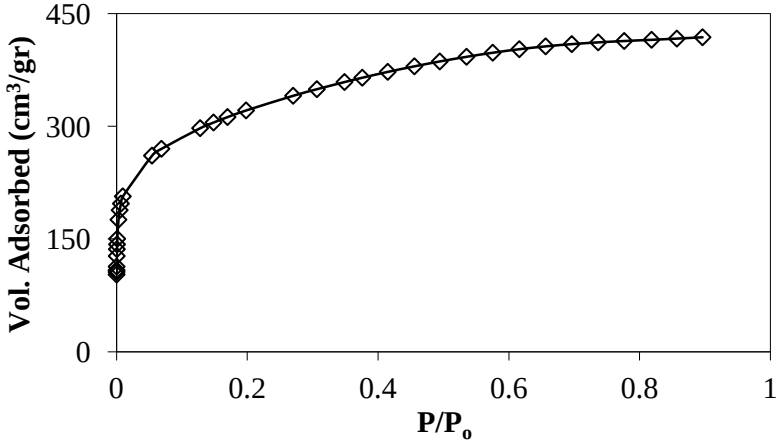

Figure 2.2. The nitrogen adsorption isotherm for fine size fraction 48 x 65 mesh

.

Hence, as evident from Table 2.2 and pore size distribution of coarse (Figure 2.3) and fine (Figure 2.4) particle size activated carbon, particle size hardly has any effect on the surface area. This is an important point to note as this is the basis to explain the adsorption reactions. Also, it is clear that the micropore and the mesopore area do not change much with the particle size.

2.4 SEM Images of Activated Carbon Particles

In order to investigate the morphology of the activated carbon samples, a LeO EVO 40 scanning electron microscope (SEM) was used.

The SEM images the sample surface by scanning it with a high-energy beam of electrons produced by an electron gun at the top of the microscope. The electron beam follows a vertical path through electromagnetic fields and lenses held within a vacuum chamber. Once the beam hits the sample, the ejected x-rays, backscattered electrons, and secondary electrons are collected by detectors and converted into a signal that is sent to the computer screen. SEM has found diverse applicability due to its ability to image samples at high magnification and resolution.

Imaging of activated carbon particles of all the different size fractions were done in a tightly closed vacuum chamber at 30 kV voltage and 1000x magnification. The SEM images are presented in Figure 2.5 (a) through (j).From the SEM images it is somewhat evident that the morphological features of activated carbon particles vary slightly with size. Since the SEM gives a picture of the surface features and does not provide much information of the internal pore network, it is difficult to comment on the pore size distribution of activated carbon particles of different size fractions based on these images.

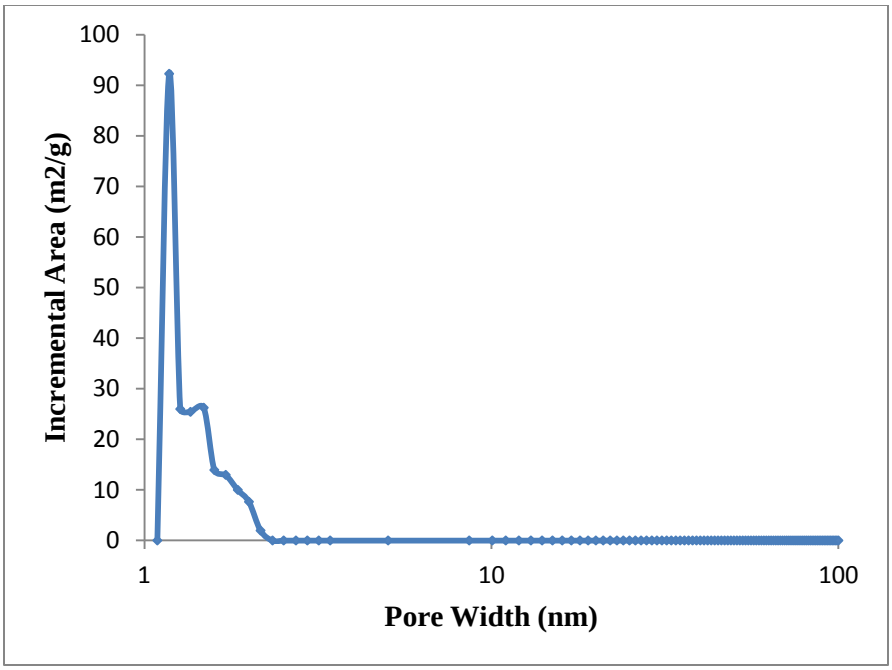

Figure 2.3. Pore size distribution for coarse size 7 x 12 mesh activated carbon.

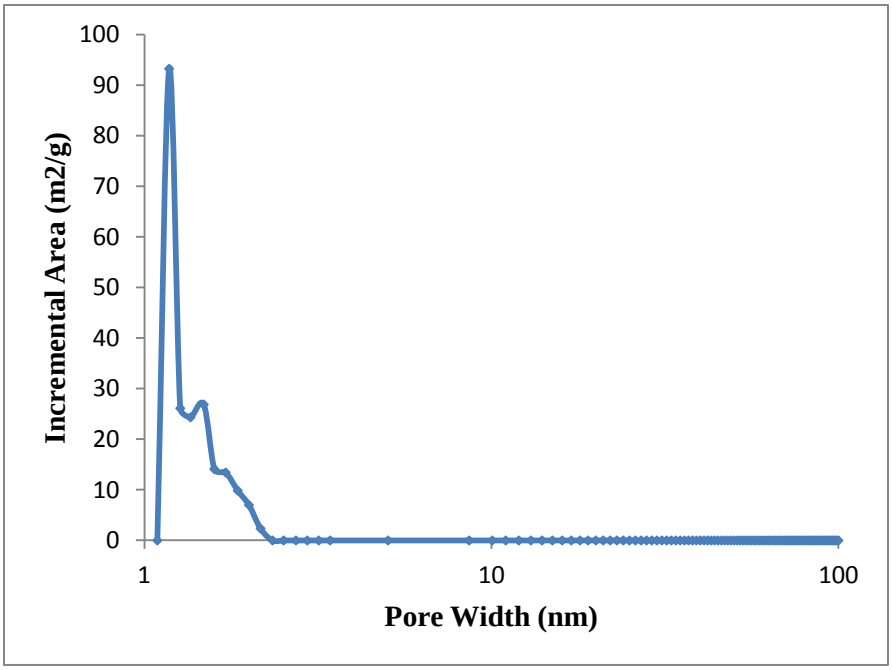

Figure 2.4. Pore size distribution for fine size 48 x 65 mesh activated carbon

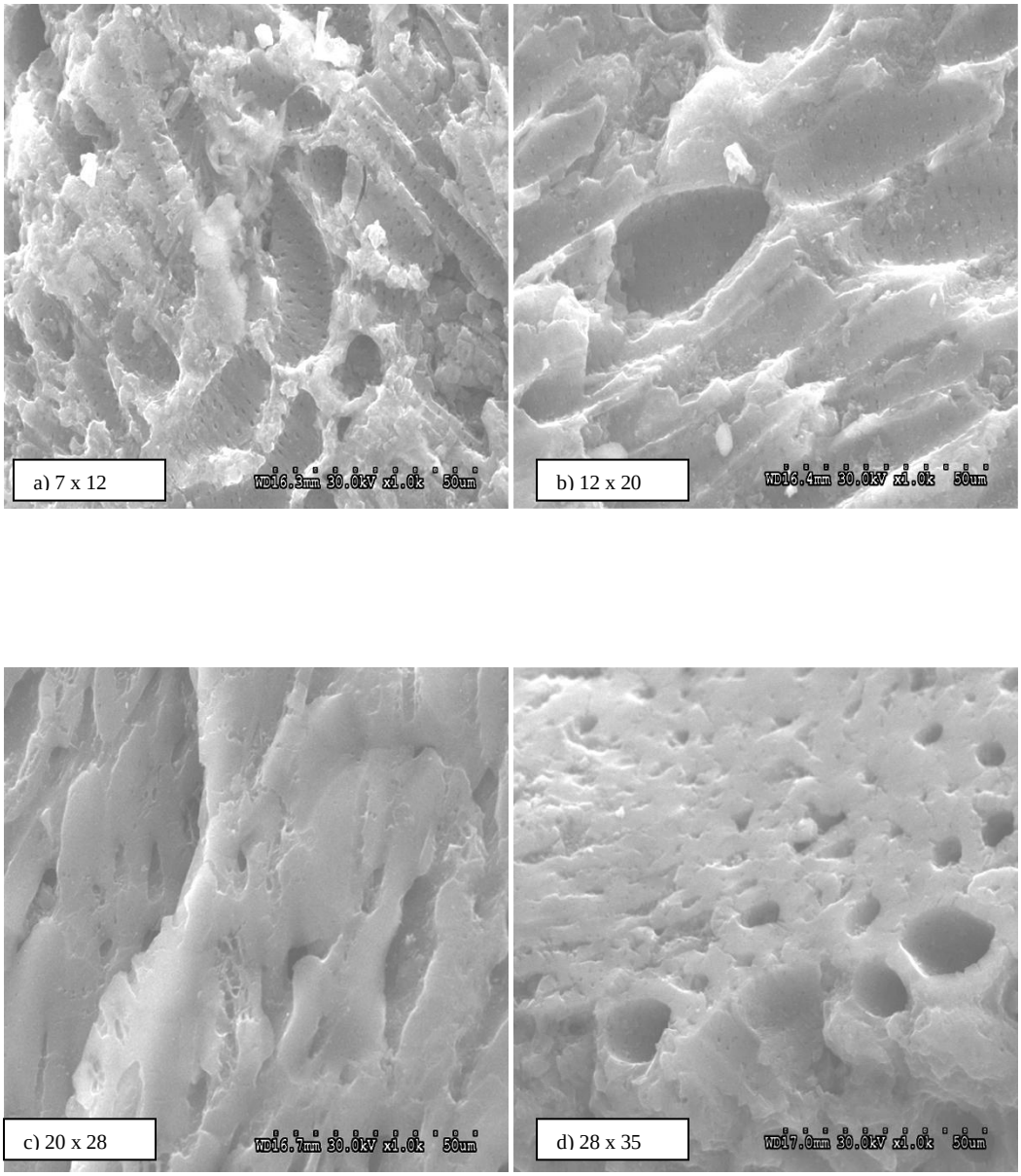

Figure 2.5. SEM images of activated carbon particles of different size fractions a) 7 x 12 mesh b) 12 x 20 mesh c) 20 x 28 mesh d) 28 x 35 mesh e) 35 x 48 mesh f) 48 x 65 mesh g) 65 x 100 mesh h) 100 x 150 mesh i) 150 x 200 mesh j) 200 x 400 mesh at 1000X magnification and 30kV power.

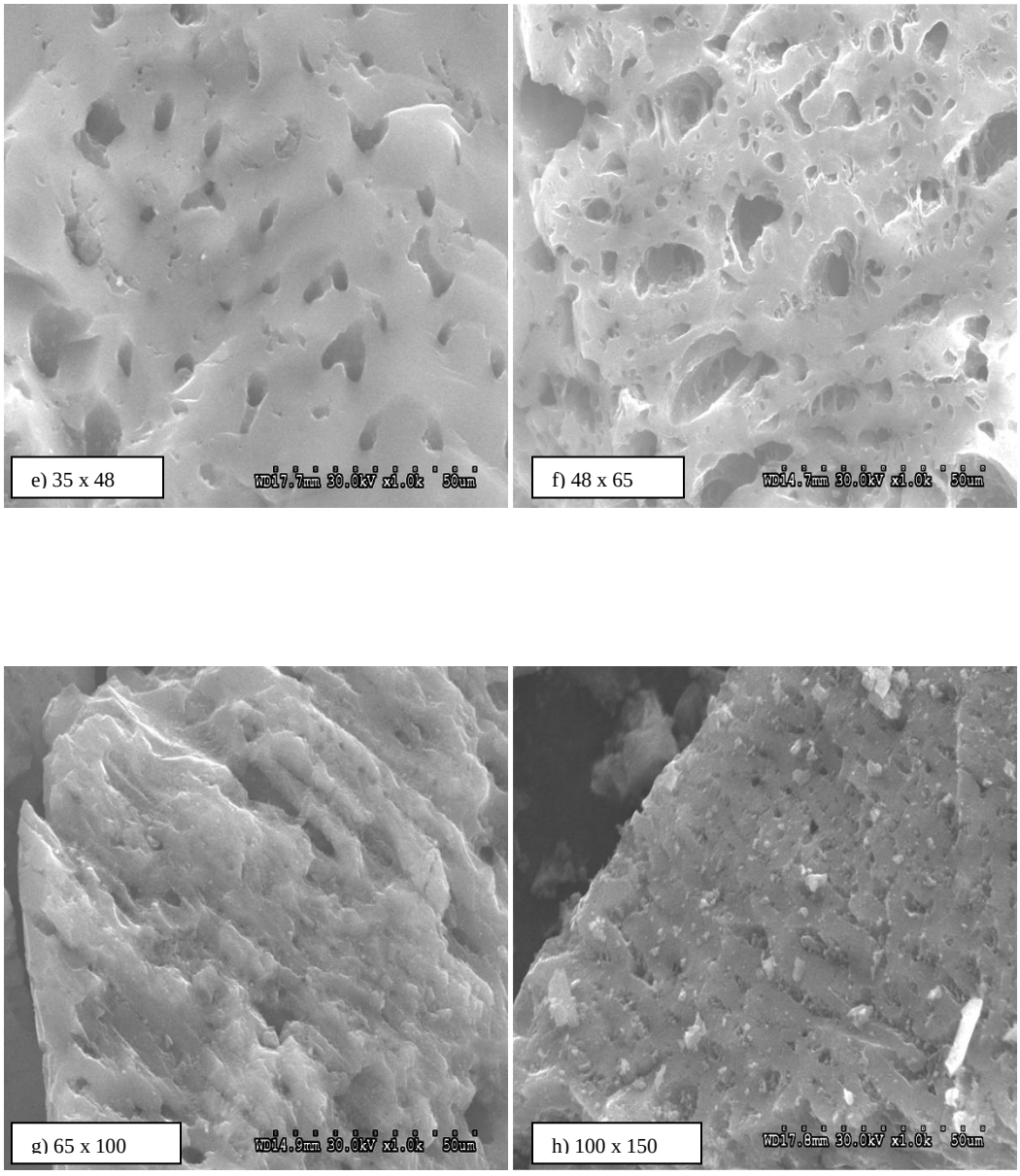

Figure 2.5 continued.

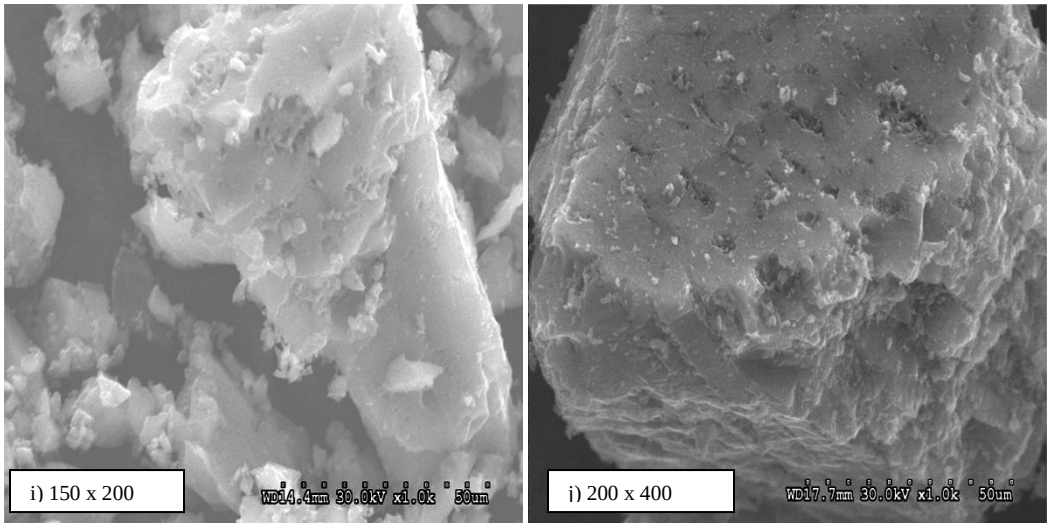

Figure 2.5.continued.

The SEM images do not reveal many differences with variation in particle size. Though the ultimate specific surface area might be similar for all the particle size fractions due to the extended network of micropores contributing to the large internal surface area, the actual pore diameter might not be correctly revealed simply by BET analysis which involves nitrogen adsorption, as the van-der-Waals diameter of nitrogen atom is only 0.31 nm. The macropores are several orders of magnitude greater than the diameter of the nitrogen atom. However, for most practical applications and in the scope of this thesis research, the BET results will be considered acceptable.

To analyze the pore structures better, high-resolution x-ray micro computer tomography studies of the activated carbon particles of different size fractions have been performed and these images provide more information of the pore size. Details on this characterization technique have been presented in the following section.

3.5 X-ray Micro CT Images of Activated Carbon

X-ray computer tomography was used as a tool to further study the highly developed internal pore structures of activated carbon through analysis of reconstructed 3D images. High Resolution X-ray Microtomography (HRXMT) is a powerful tool for the 3Dcharacterization of multiphase particles. This HRXMT scan and subsequent analysis with special software generates a three-dimensional reconstruction of packed particle beds and gives information of quantitative composition of individual particles in the particle bed. The High Resolution X-ray Microtomography is a nondestructive technique that has the capability to scan particles with a density up to 8 g/cm3 (Miller and Lin, 2004). The particles do not require any special preparation. The sized particles from

the sample are placed inside a plastic cylinder of up to 40 mm in diameter. The sample is placed between the x-ray source and the detector, photons pass through the sample, and the projected image is collected by the detector. The sample is rotated and projections at different angles are collected for 3D reconstruction. In previous research (Miller and Lin, 2004), HRXMT applications have been reported for 3D analysis of coal washability, mineral exposure/liberation, the pore network structure of packed particle beds, and geometric features of the particles, including size, shape, and texture.

A high resolution x-ray microtomography system MicroXCT-400 from Xradia was used for imaging. Cone beam x-ray geometry was used for scanning a packed bed of particles in a thin syringe. X-rays generated at 40 kV was used to image samples. Lenses are mounted in a rotary turret for different resolution analysis. A 4X magnification lens for the coarser size fraction 7 x 12 mesh and 10X magnification lens for the finer size fraction 48 x 65 mesh was used for scanning for a duration of 4 hours and 10 hours, respectively. The 10X and 4X magnification corresponds to a voxel resolution of 5μm and 2μm, respectively. The detector has a pixel resolution of 2048 x 2048 for imaging the projections of the sample. 1000 images were collected by rotating the sample stage 360°. Image slices were reconstructed in 3D using Image J software and further analyzed to study the pore structure. It should be noted that even in a particular size fraction, not all activated carbon particles are the same as some may have more pores than other. Hence, computer tomography analysis of particles will only give an approximate idea of the pore structure.

It is fairly evident from the CT micrographs that a large number of macropores having dimensions of the order of 260 μm are present in the activated carbon particles of

the coarser size fraction (Figure 2.6). In addition, micropores were also present in the coarser size fraction. In comparison, pores having dimensions of the order of 18 μm and smaller were present on the surface of the fine activated carbon particles (Figure 2.7).

Only one among many slices of the CT image has been analyzed and it reveals mostly the macropores. The micropores typically have dimensions in angstroms. The micro CT images do not provide much information about the internal pore structure. For most practical purposes and in context of this thesis research, the BET analysis will be considered adequate and be used for most explanations.

2.6 Summary

Activated carbon was crushed and sieved to obtain ten different particle size fractions ranging from 7 x 12 mesh to 200 x 400 mesh. These size fractions were prepared to perform an extensive study to observe the effect of particle size on gold adsorption capacity, adsorption rate, and with more emphasis on desorption characteristics with an aim to develop alternative processes with shorter retention times for efficient gold elution. In this way, the research objective would be satisfied.

To understand the adsorption and desorption phenomena, the activated carbon was characterized for its surface area and pore volume. BET surface area analysis shows that the specific surface area of activated carbon particles is virtually independent of particle size with an average area of approximately 920 m^2/g and average pore diameter of 2.18 nm for one gram of particles. Given the small size of the particles, specific surface area is considered to be massive and most of it is contributed by the micropore surface area. The large surface area is the reason for its wide usage in the gold industry

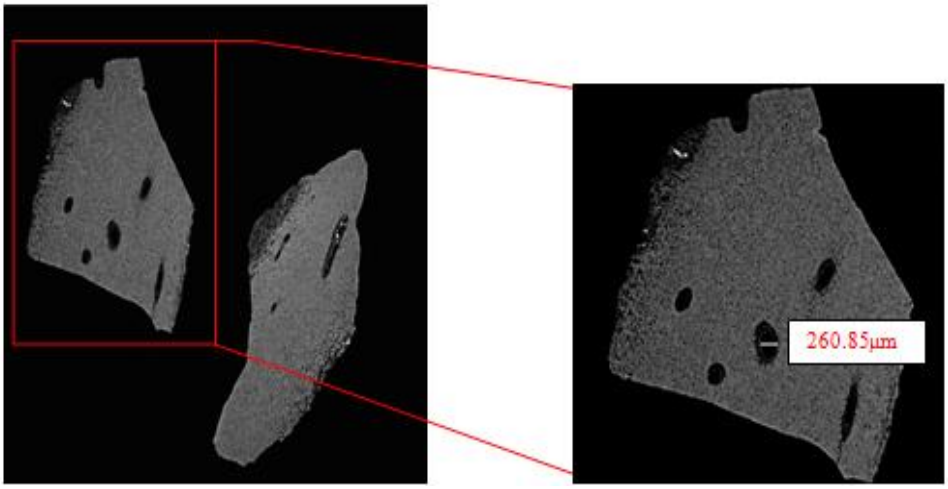

Figure 2.6. HRXMT image of coarse activated carbon particles 7 x 12 mesh with a 4x lens at 40kV power, indicating a pore diameter of 260.85 µm.

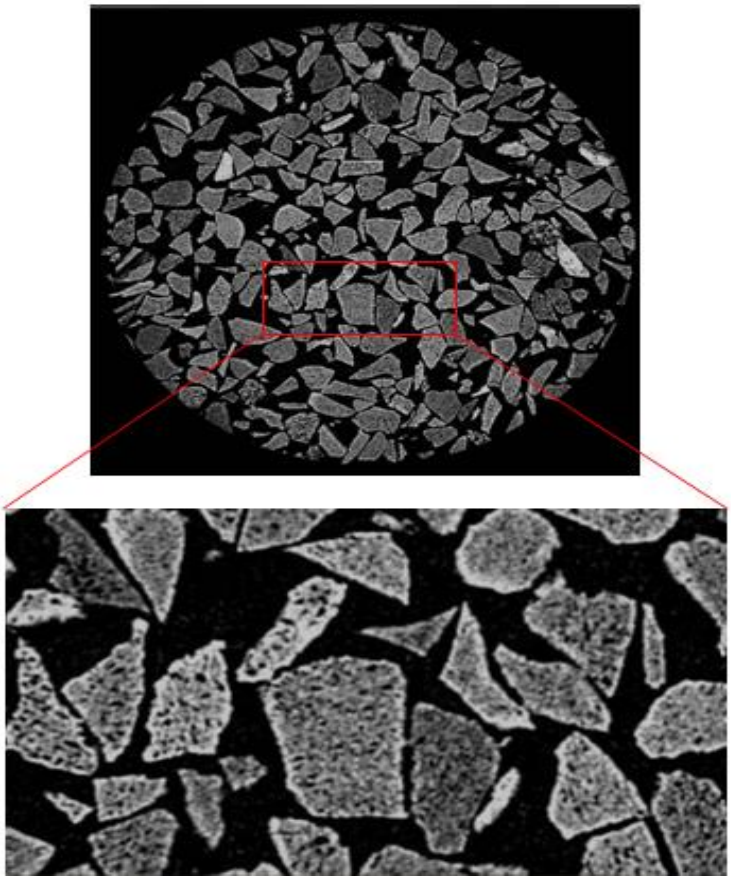

Figure 2.7. HRXMT image of fine activated carbon particles 48 x 65 mesh with a 10x lens at 40kV power.

and for other applications. The SEM micrographs provide surface morphological information and do not reveal much information about the extended internal pore network.

The computer tomography images provide some more information about the pore size of activated carbon of two different particle sizes. Also, it should be noted from X-ray CT images that all particles are not the same as some activated carbon particles are more porous than others.

The characterization results might help to provide plausible explanations for the variation in adsorption and desorption properties of activated carbon with particle size.

CHAPTER 3

ACTIVATED CARBON ADSORPTION OF GOLD CYANIDE

3.1 Adsorption Experiments

Experiments were done to determine the adsorption characteristics of all the size fractions of activated carbon. Freundlich adsorption isotherms were used to determine the adsorption capacities. Chemicals used for the adsorption experiments were all of reagent or analytical grade and deionized [DI] water was used for the solution phase in the experiments. Deionized water was obtained from a Milli-Q system and the resistivity of the water was above 18 MΩ in all experiments. The adsorption capacities and adsorption rates of all the size fractions of activated carbon used in the research were determined by procedures described in the following sections, and have been the standard procedures for all subsequent adsorption tests conducted during the course of this research. Figure 3.1shows the experimental set-up for all adsorption experiments.

3.1.1 Adsorption Capacity

The gold adsorption capacities [K- value] for all the particle sizes of activated carbon were determined. Gold adsorption capacity gives the gold loading on the carbon in equilibrium with 1 ppm residual gold solution after 24 hours contact time and

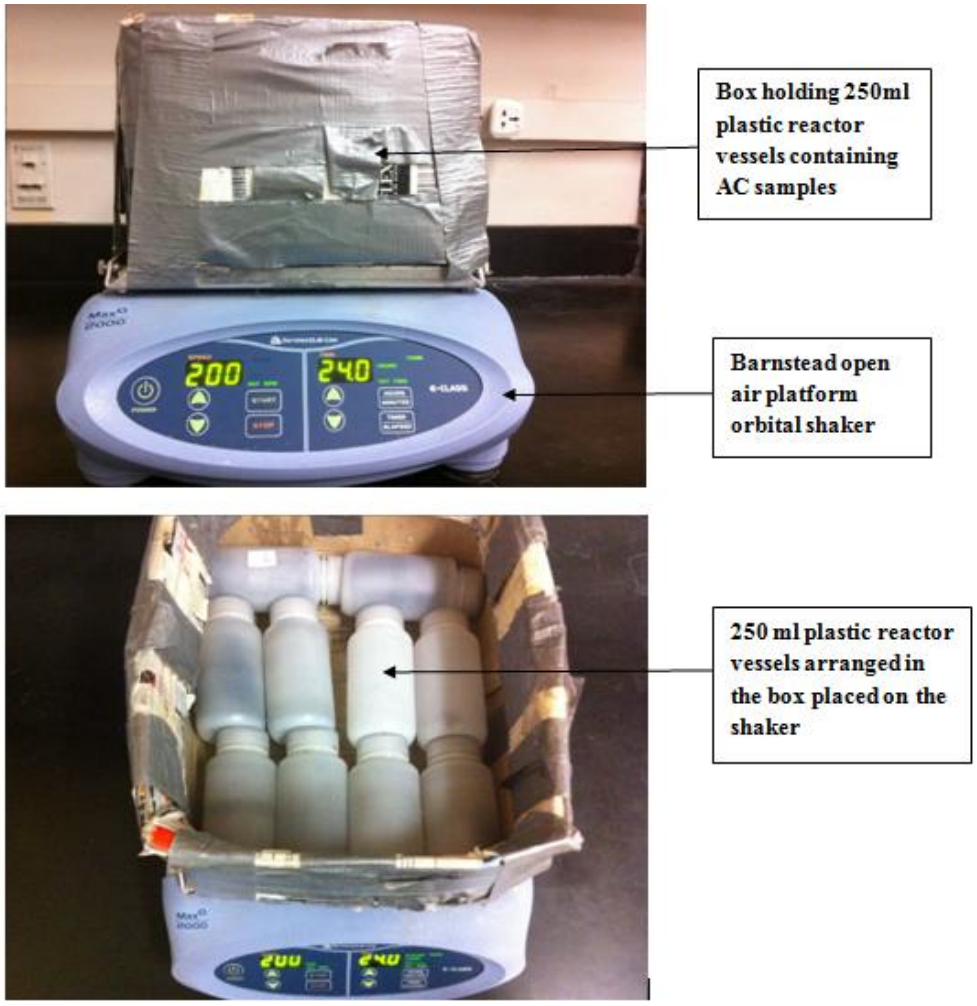

Figure 3.1 Adsorption Capacity and Adsorption Rate Experimental Set-up.

activated carbon samples effective for gold loading should have a K-value greater than 25kg Au/t C (McArthur et al., 1987; Shipman and Jativa, 1987).

The activated carbon particles of different particle size used were washed thoroughly to remove all fines and dried overnight at 110^{o}C in a Stabil-Therm Gravity oven. The samples were then removed and cooled to room temperature and stored in clearly marked glass bottles, until ready to be used. Subsequently, these bottle were placed in a desiccator.

100 mg per liter of gold solution was used in the adsorption capacity experiments. In the preparation of 100 mg Au per liter of solution, 1L borate buffer solution was first prepared, in which 3.09 g of boric acid and 3.73 g of potassium chloride were weighed into a 1L beaker. About 500 ml of DI-water was added to the beaker and stirred. A mass of 2 g of NaOH was added to the contents of the beaker to adjust the pH to between 10 and 11. Then 0.1462 g of $KAu(CN)_2$ was added to the borate buffer and stirred thoroughly to obtain homogenous mixture. The content of the beaker was then transferred to a 1L volumetric flask and more DI-water was added to make 1L of 100 mg/L Au solution required for the adsorption capacity test. A mass of 200 mg of NaCN was dissolved in the solution prior to use. A sample of this solution was taken for gold analysis to determine the initial concentration of the stock solution.

Masses of 0.1, 0.2, 0.3, 0.4, 0.5 g from each of the cooled activated carbon samples were weighed into 250 ml plastic reactors. Each sample in the plastic reactor was contacted with 100 ml of the 100 mg/L Au solution on a Barnstead Laboratory shaker for 24 hours at 25^{o}C while the shaker speed was set at 200 revolutions per minute. After the shaking cycle was completed, the carbon in each vessel was filtered off under vacuum using a Whatman filter paper. 20-30ml sample of the filtrate from each reactor vessel was stored in sample vials for gold analysis by a Spectro Genesis ICP-OES [inductively-coupled plasma (ICP) - optical emission spectrometer (AES)] instrument. From the ICP solution analysis, the gold adsorbed by the carbon in each case was determined by the difference in gold concentration before and after adsorption multiplied by the volume of gold cyanide solution used. A five point isotherm [from the five carbon masses] plotting gold adsorbed versus the residual equilibrium concentration was then prepared.

From the isotherm, the gold equilibrium constant [K-value] was determined, using the Freundlich isotherm:

$$C_c = KC_s^{1/n} \qquad \text{..... (3.1)}$$

where Cc and Cs represent the gold concentrations on the carbon and in solution, respectively, and K and n are constants (n = 1 for linear adsorption isotherm).

Therefore, the loading capacity, K-value is defined as the carbon-loading [mg Au / g C] in equilibrium with a residual gold concentration of 1 ppm, as determined from a plot of the isotherm (McArthur et al., 1987; Shipman and Jativa, 1987).

3.1.2 Adsorption Rate

The carbon activity plays an important role in the determination of the plant efficiency in CIP processes but it is the kinetic activity which determines the quantity of carbon required and the size of the adsorption stages (La Brooy et al., 1986). This kinetic activity can be evaluated in terms of the rate constant k. It has been seen experimentally that the k value of fresh carbon is 1200/hour while it goes as low as 200/hour after aging for24 hours in a typical plant conditions. When the k value goes below 50/hour it becomes necessary to either increase the amount of carbon or increase the residence time of carbon to maintain same plant throughput and gold recovery (La Brooy et al., 1986).

Gold adsorption rates of different particle sizes of AC were also determined. Usually, the percentage gold adsorbed by 1g of carbon from 10 mg/L gold solution in 1 hour should be greater than 60 % (McArthur et al., 1987; Shipman et al., 1987).

Activated carbons of all particle sizes used were washed thoroughly to remove dust and fine particles. Carbon samples were then dried at 110^{o}C overnight in an oven to

remove any residual moisture. Samples were removed from the oven and stored in a desiccator to cool. A lower concentration of gold solution, 10 mg Au per liter of solution was used for the test. 0.2769 g amount of $CaCl_2$ and 0.2503 g amount of KCN were measured into a 1L beaker containing about 0.5L of DI-water and stirred thoroughly to ensure complete dissolution of the reagents. 0.015 g amount of $KAu(CN)_2$ was further dissolved in the beaker and the contents transferred into a 1L volumetric flask and more DI-water was added to the flask to make up the 1L gold solution required for each test. A mass of 1 g of each pretreated carbon sample was measured into 1.2 L stoppered plastic containers for the rate test. One liter of 10 mg gold solution at a pH between 10 and 11 was measured into each plastic reactor [standing upright on the shaker shown in Figure 3.1] containing carbon samples and the starting time was noted.

The plastic containers holding the carbon samples in contact with gold cyanide solution were then shaken for 6 hours. The gold concentrations of the solutions of all particle sizes activated carbon particles were determined periodically over the 6 hours exposure. Periodically during the shaking cycle, 10ml samples were withdrawn and filtered into vials from each plastic container at 0, 15, 30, 45, 60, 120, 180, 240, 300, and 360 minutes for gold analysis by ICP-OES.

To find out the equilibrium time, % gold adsorbed was plotted against time. From the results of the ICP solution analysis, the quantity of gold adsorbed by the carbon was calculated at each time interval.

The results were treated with a rate equation in which it is assumed that the rate is proportional to the concentration of gold in solution but independent of the concentration of gold on the carbon, as found for the initial stages of loading when the reaction is far

from equilibrium. To investigate it even further, the rate constant was determined using equation 3.2 suggested by Fleming et al. in 1980. This equation gives linear plot only within the first few hours of adsorption. Hence, only the first few data points were taken for all the experiments.

$$\Delta[Au]_c^t = k\,[Au]_s^t\;t \qquad \ldots\ldots\ldots \quad (3.2)$$

where $\Delta[Au]_c^t$ is the amount of gold adsorbed by carbon, $[Au]_s^t$ is the concentration of gold in solution, and k is the rate constant. To determine the value of k from this equation, $\log(\Delta\,[Au]_c^t / [Au]_s^t)$ was plotted against log(t) for the first few hours of adsorption and the k-value was calculated by taking the antilog of the intercept.

To further investigate the effect of particle size on the rate of gold adsorption by activated carbon, R-value was determined which is the reciprocal of intercept at zero time in the plot of time divided by loading on carbon versus time when contacting 10 mg/L gold cyanide solution with a closely sized active carbon fraction. The data obtained in such adsorption experiments yield a straight line that can be expressed by equation 3.3(Urbanic et al., 1985; Anonymous, 1983b)

$$\frac{t}{X/_M} = \left(\frac{1}{M}\right)t + \frac{1}{R} \qquad \ldots\ldots\ldots \quad (3.3)$$

where, X/M represents the carbon loading in mg Au/g of carbon, t is the time, and M and R are reciprocal of the slope and intercept at zero time, respectively. The R-value for each carbon is relative, i.e., a higher value indicates faster adsorption.

3.2 Results and Discussion

3.2.1 Effect of Particle Size on Adsorption Capacity

The degree of gold adsorption occurring at equilibrium is measured using the empirical Freundlich Isotherm. The Freundlich constant, K, is an important parameter to determine the gold adsorption capacity in mg Au/ g C and is illustrated in equation 3.1(Urbanic et al., 1985):

The isotherm curve obtained by plotting the amount of solute adsorbed per unit mass of adsorbent against residual solute concentration at a given temperature results in an isotherm equilibrium curve. The Freundlich isotherms for each activated carbon size fraction are given in Figure 3.2 and K-values obtained from the isotherms are given in Table 3.1.

The data of the table indicate, as was expected, that the adsorption capacity (K values) is essentially independent of the particle size. Also all K –values are well in the range of K-values of activated carbons used in the industry (Shipman and Jativa, 1987). The adsorption capacity values correlates well with the BET surface area which also showed that the surface area was independent of the particle size of activated carbon.

3.2.2 Effect of Particle Size on Adsorption Rate

The rate of gold adsorption from alkaline cyanide solutions for activated carbon particles of different size was determined. The purpose of the rate experiments was to study the effect of the particle size of activated carbon on rate of adsorption. Usually, for activated carbons to be considered as having an effective rate of adsorption, the percentage gold adsorbed by 1g of carbon from 10 mg/L gold solution in 1 hour should

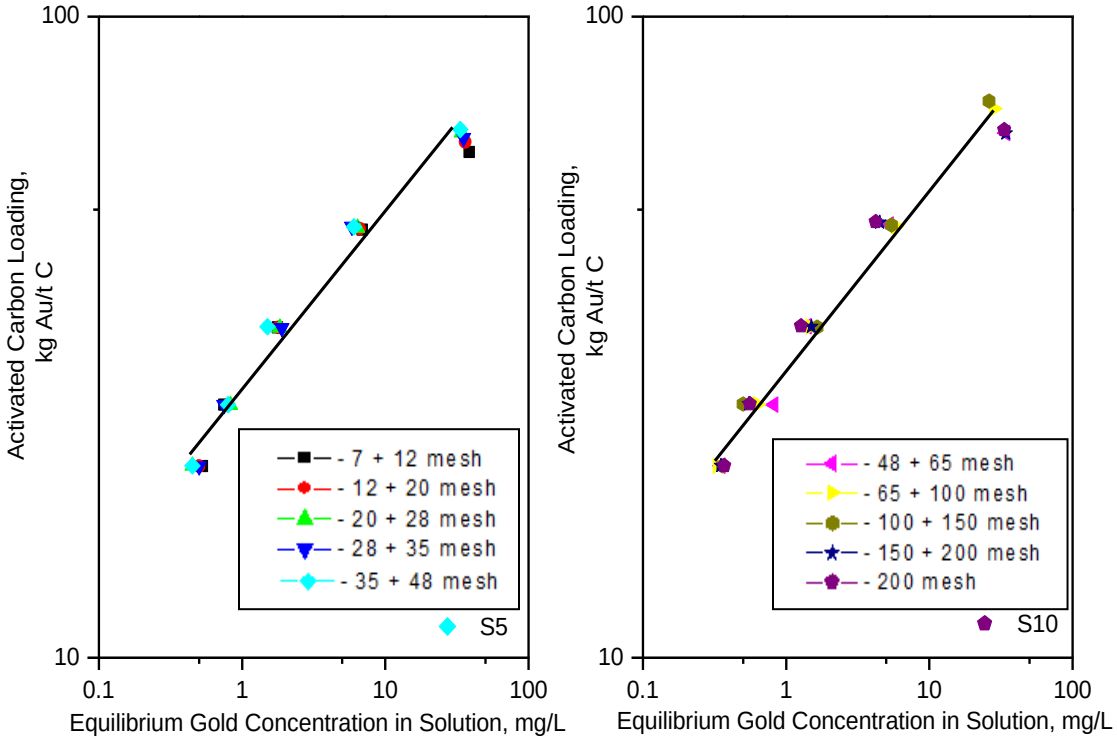

Figure 3.2.Particle size effect of activated carbons on gold adsorption capacity. Adsorption conditions: 1-5 g/L activated carbon, 100 mg/L Au, 200 ppm NaCN, pH 11, 200 rpm, 25°C, 24 hours of adsorption time.

Table 3.1. Result of gold loading capacity experiments showing the effect of particle size on equilibrium loading capacity (K).

particle size mesh	**average particle diameter, mm**	**K –value, mg Au/g C**
7 x 12	2.12	26.14
12 x 20	1.13	26.11
20 x 28	0.72	26.24
28 x 35	0.51	26.30
35 x 48	0.36	26.81
48 x 65	0.25	27.69
65 x 100	0.18	28.26
100 x 150	0.13	28.53
150 x 200	0.09	28.61
200 x 400	0.06	28.88

be greater than 60 %(McArthur et al., 1987; Shipman and Jativa, 1987).

The rate of adsorption is measured by the R-value which is the reciprocal of intercept at zero time in the plot of time divided by loading on carbon versus time when contacting 10 mg/L gold cyanide solution with a closely sized active carbon fraction. The data obtained in such adsorption experiments yield a straight line that can be expressed by equation (3.3) (Urbanic et al., 1985).

In the equation, X/M represents the carbon loading in mg Au/g of carbon, t is the time and M and R are reciprocal of the slope and intercept at zero time, respectively. The R-value for each carbon is relative, i.e., a higher value indicates faster adsorption.

The gold adsorption rate data for the different particle sizes are then plotted in Figure 3.3. The plots of time divided by carbon loading as a function of time for the different activated carbon particle sizes are plotted in Figure 3.4 and 3.5. The R-values, calculated from the same plots, as a function of the average particle diameter (characteristic of each size fraction) are then plotted in Figure 3.6. The R-values are summarized in Table 3.2.

The results from the adsorption rate experiments for the different particle sizes of activated carbon used are shown in Figures 3.3 to 3.6 and Table 3.2. Figure 3.3 shows the relationship between rate of gold adsorption and activated carbon particle size while Figures 3.4 to 3.6 present results for initial rate of gold adsorption with variation in particle size. It is evident from the results presented that rate of adsorption increases as the particle size decreases. In particular, Figure 3.6 and Table 3.2 clearly reveal this trend; as the activated carbon particles decrease in size from 2.8 x 1.4 mm to 212 x 45 µm and minus 45 µm, the rate of adsorption increases quite significantly. The results also show that while the finer carbons adsorbed 70 % of the gold in the first 15 minutes and nearly 100 % after 1 hour, the coarser carbons were consistently below 20 % in the first 15 minutes and also below 50 % after 1 hour. This further shows that according to McArthur et al. (1987) and Shipman and Jativa (1987), finer activated carbon are more effective adsorbents.

These results are in line with traditional beliefs that smaller particles present better kinetics due to shorter diffusion paths. Thus, the inverse dependence of adsorption rate on the activated carbon particle size is further confirmed and validated through these results.

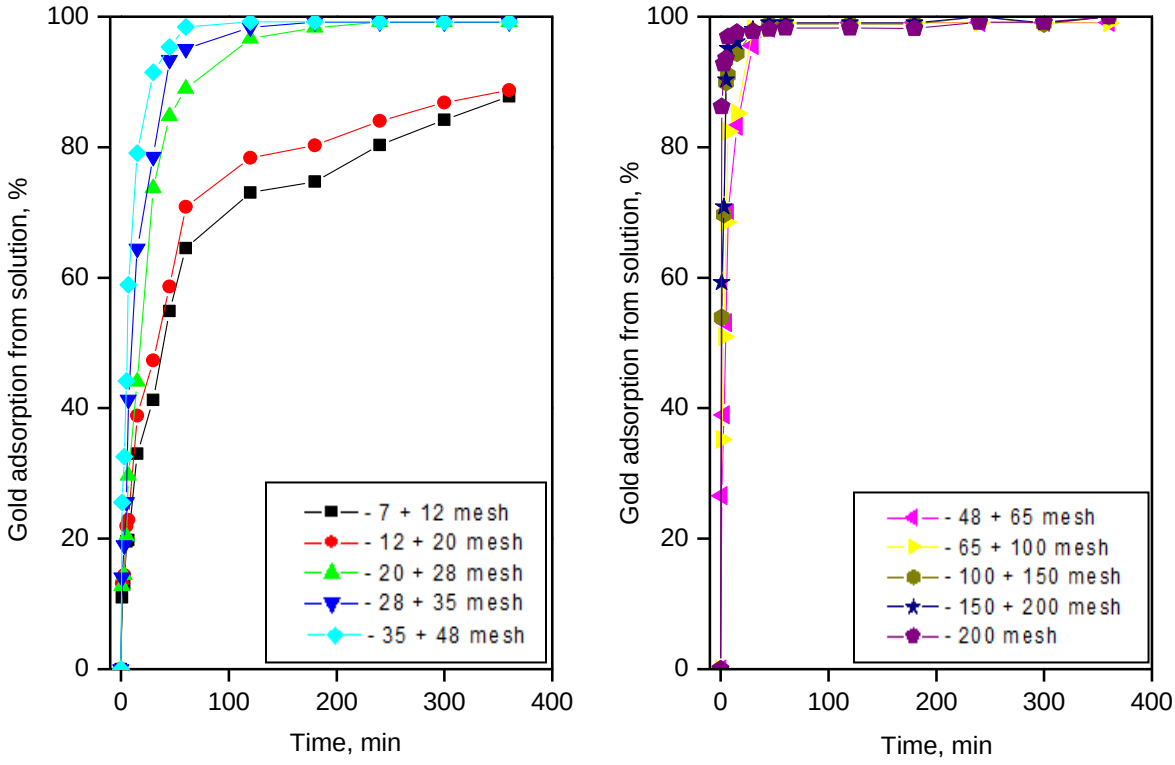

Figure 3.3.Particle size effect of AC on gold adsorption kinetics. Adsorption conditions: 1g/L activated carbon, 10mg/L Au, pH11, 200 prm, 25 °C

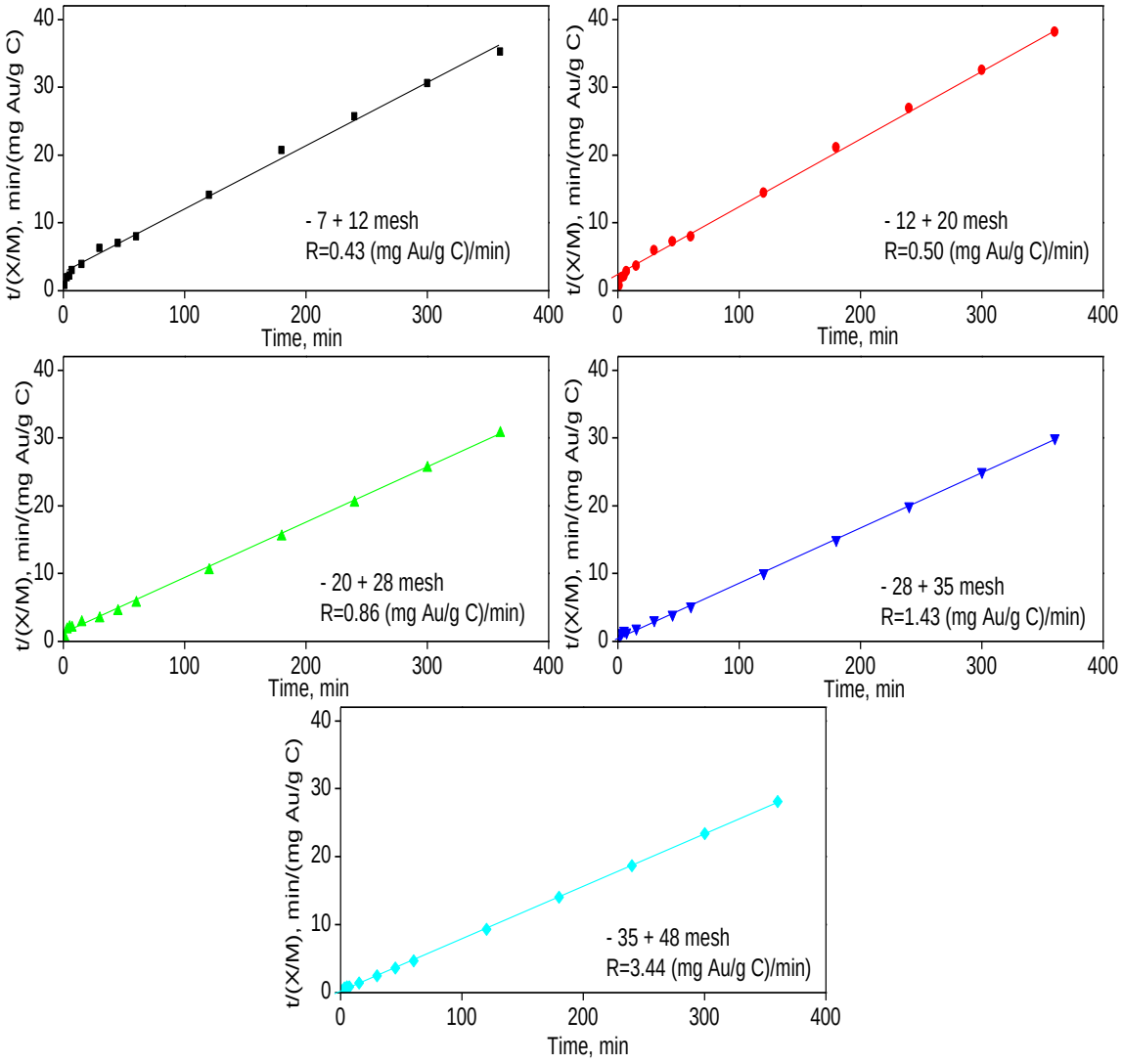

Figure 3.4.Rate of gold adsorption for activated carbons of particle size greater than 48 mesh. Adsorption conditions: 1g/L activated carbon, 10mg/L Au, pH 11, 200 rpm, 25 °C

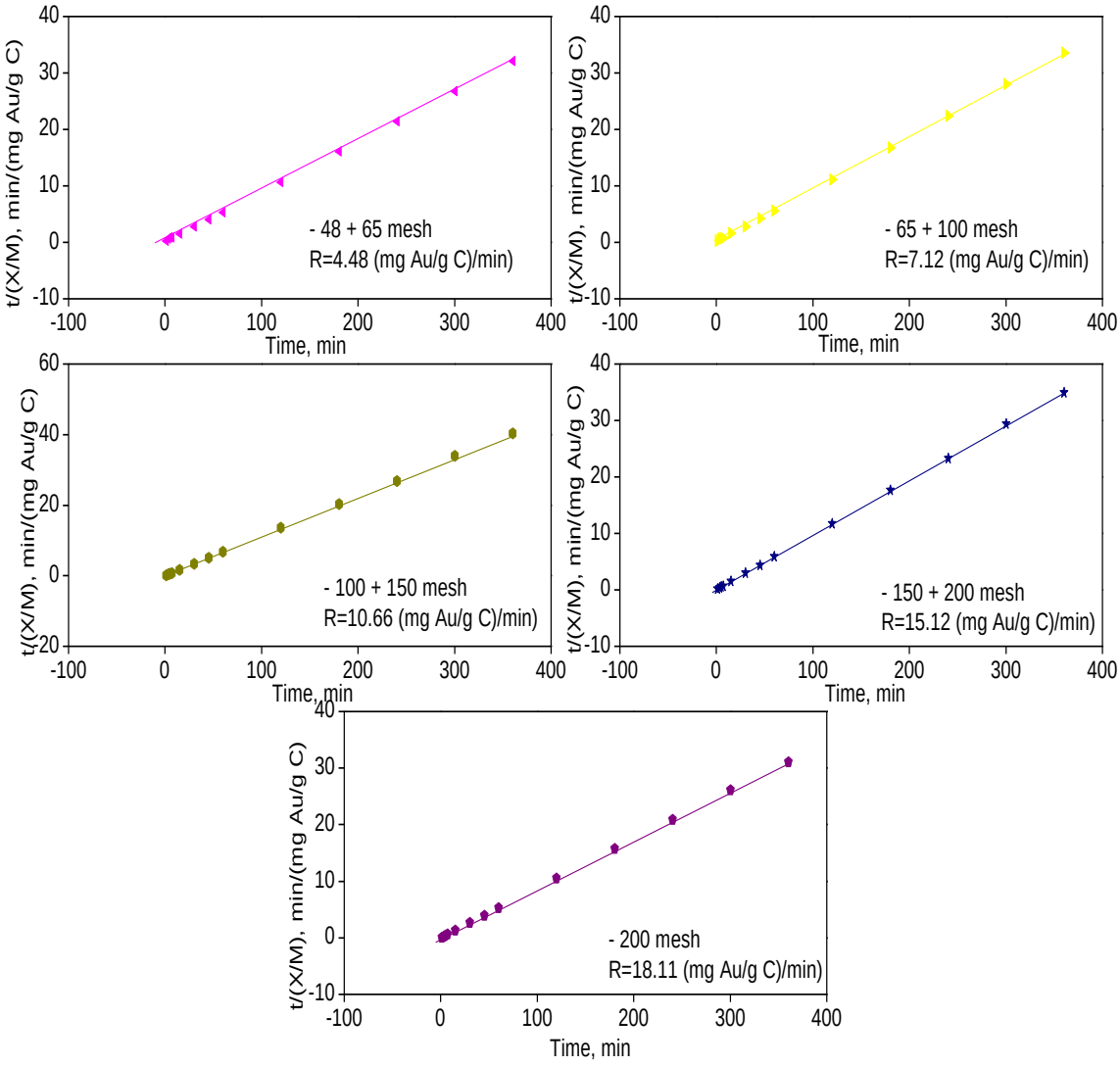

Figure 3.5. Rate of gold adsorption for activated carbons of particle size below 48mesh. Adsorption conditions: 1g/L activated carbon, 10mg/L Au, pH 11, 200 rpm, 25 °C

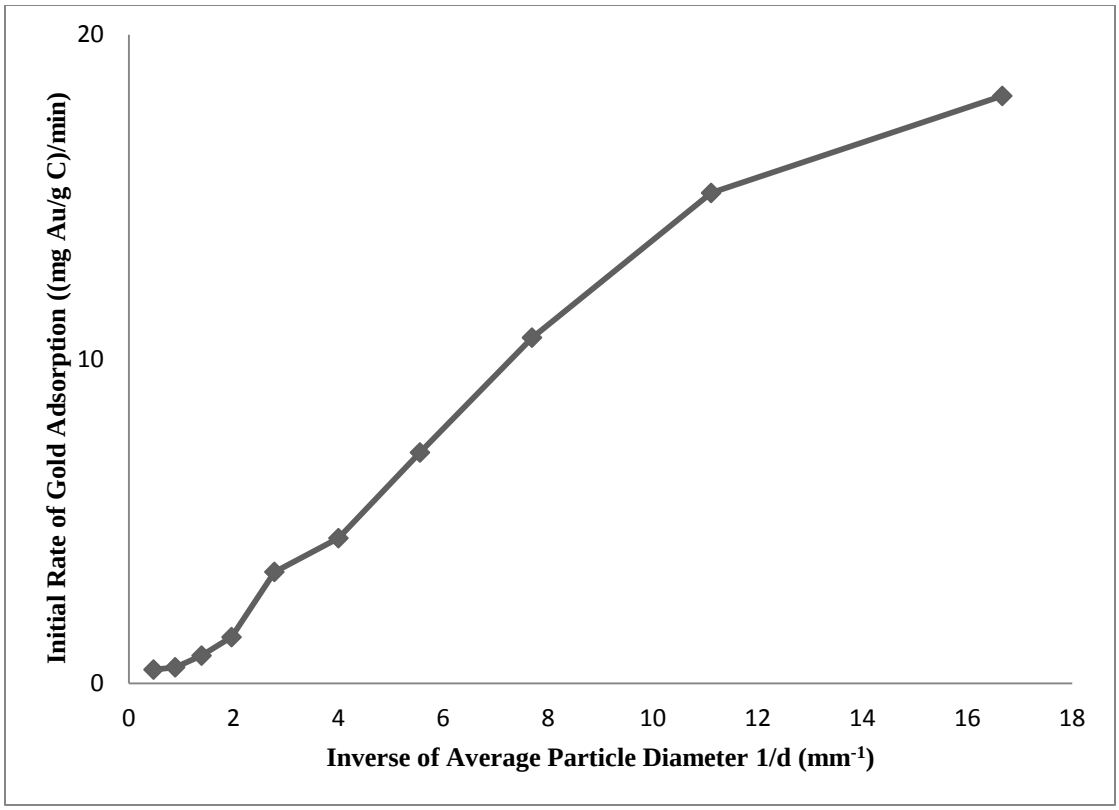

Figure 3.6.The effect of average particle size of activated carbon on the initial rate of gold adsorption.

Further, to validate equation 3.2 and to determine the reaction rate constants, the plots of $\log(\Delta[Au]_c^t/[Au]_s^t)$against log(t) for all the size fractions are given in Figure 3.7 (a) to (j). These figures will yield the reaction rate constant *k* by taking the antilogarithm of the intercept value from the linear equation obtained from the plots. The reaction rate constant is then plotted against the inverse of the average particle diameter to observe the variation of the rate constant with particle size (Figure 3.8). Subsequently, the rate constant values are summarized in Table 3.2 to compare with the initial rate values in order to observe the trend with variation in particle size.

Table 3.2.Summary of the variation of the initial rate and the reaction rate constant with particle size.

Particle Size, mesh	**Average Particle Diameter mm**	**R –value Initial Rate (mg Au/g C)/min**	**Reaction Rate Constant, x 10^3 h^{-1}**
7 x 12	2.12	0.43	1.53
12 x 20	1.13	0.50	1.90
20 x 28	0.72	0.86	10.37
28 x 35	0.51	1.43	16.02
35 x 48	0.36	3.44	26.37
48 x 65	0.25	4.48	31.92
65 x 100	0.18	7.12	37.26
100 x 150	0.13	10.66	43.34
150 x 200	0.09	15.12	52.49
200 x 400	0.06	18.11	52.89

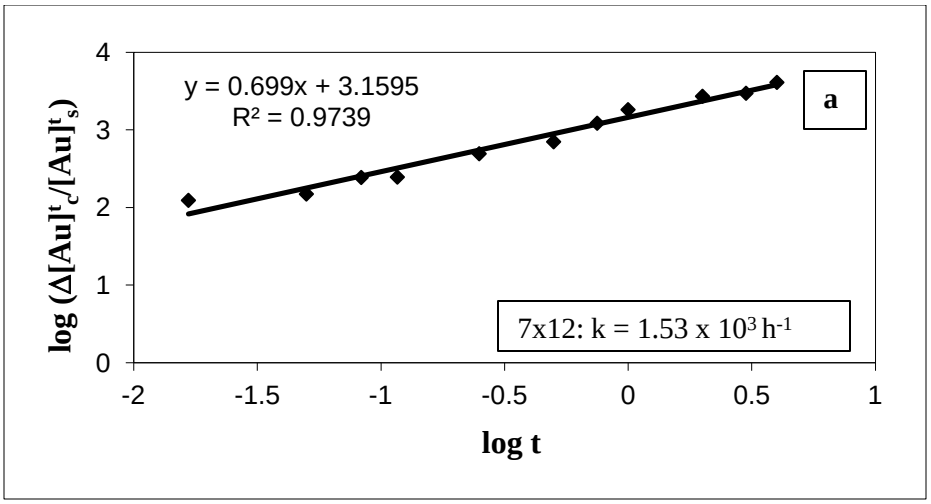

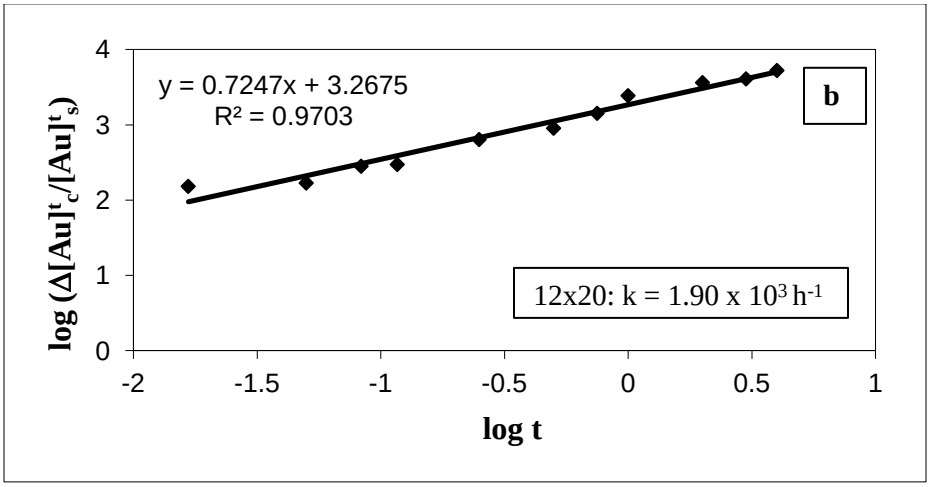

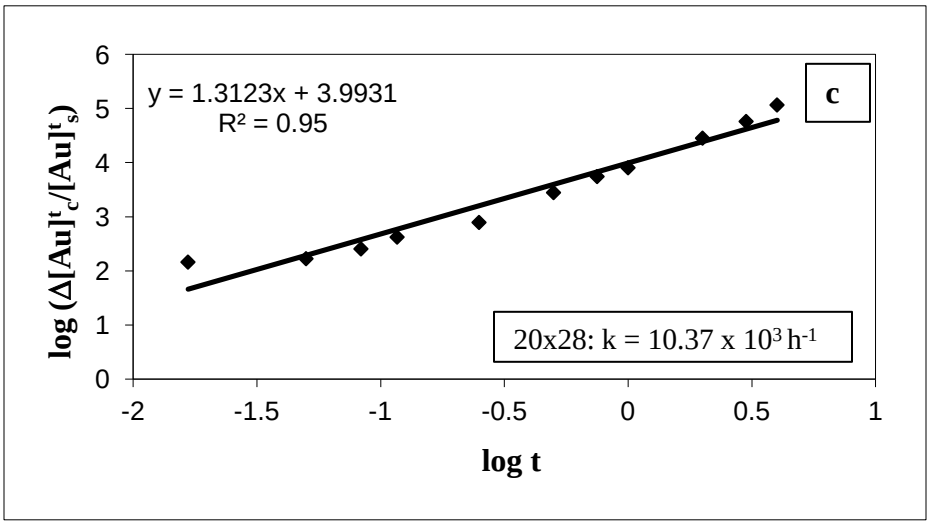

Figure 3.7. Plots of $\log(\Delta[Au]_c^t/[Au]_s^t)$against log(t) for all the size fractions as shown in figures (a) to (j)

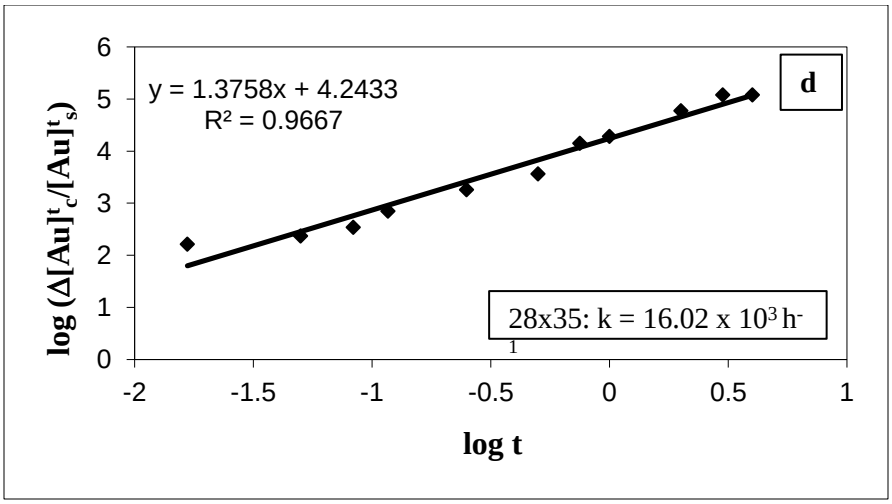

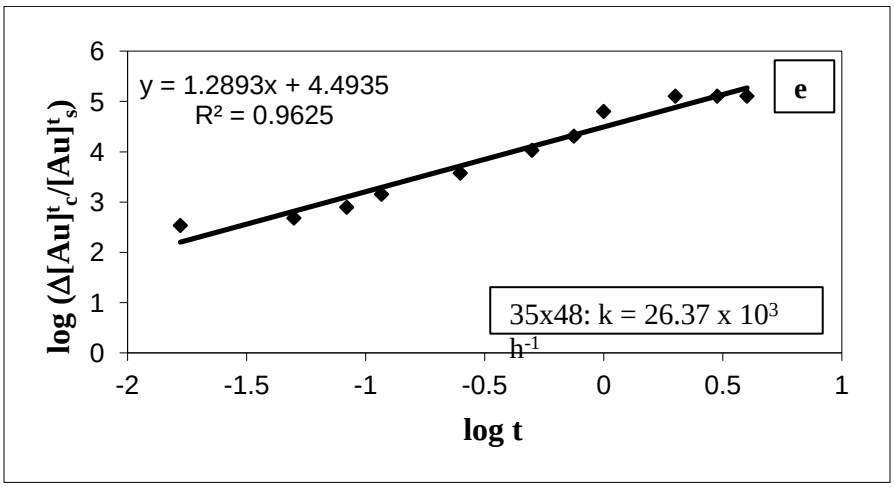

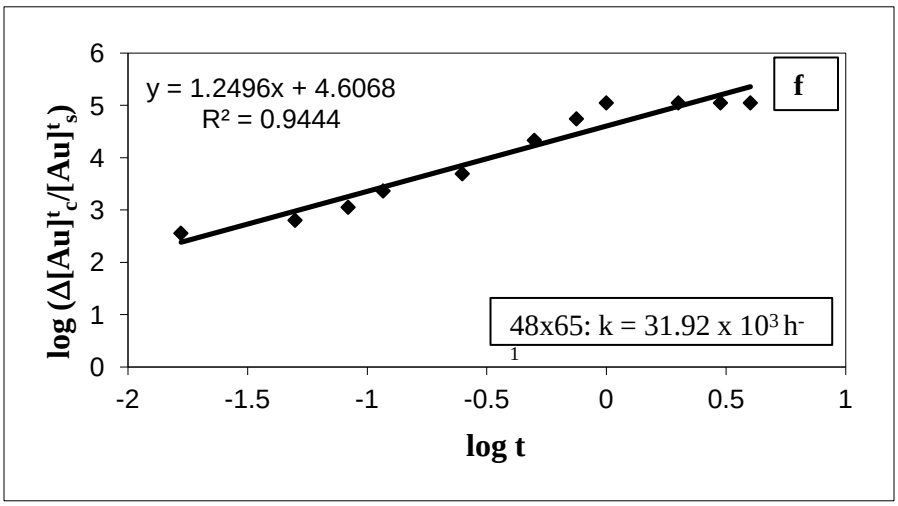

Figure 3.7.continued.

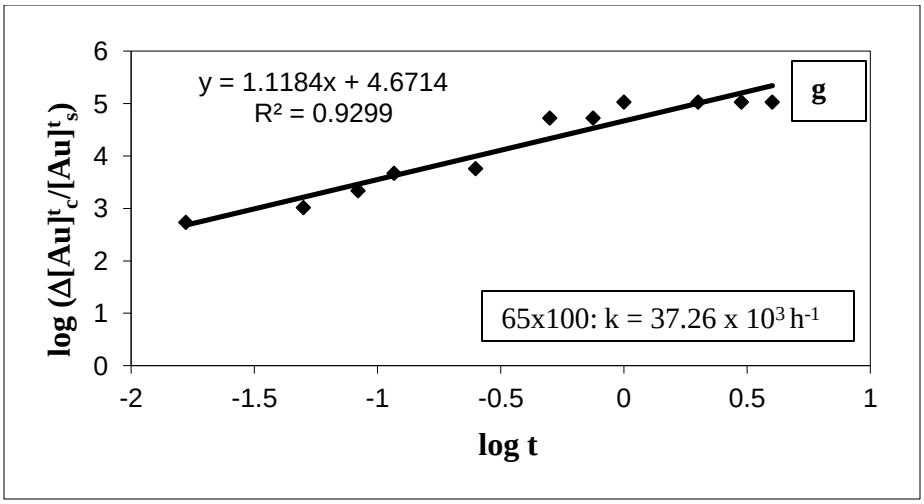

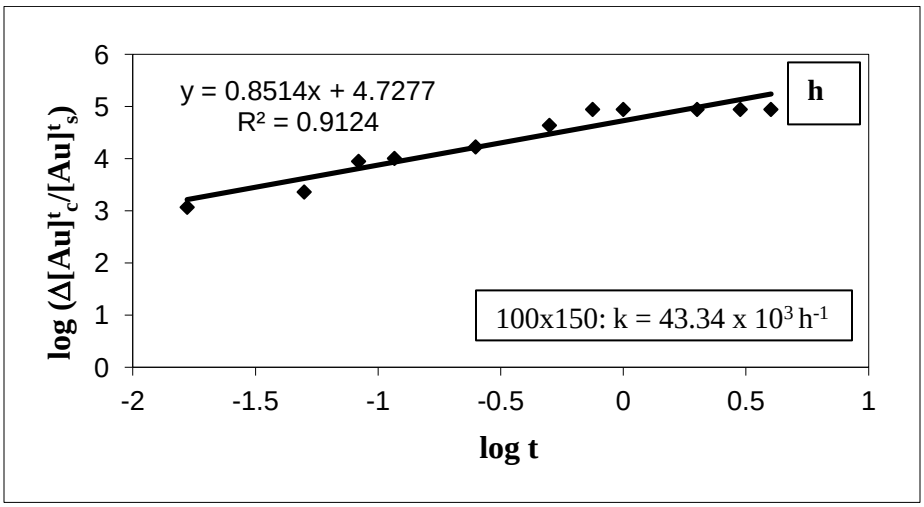

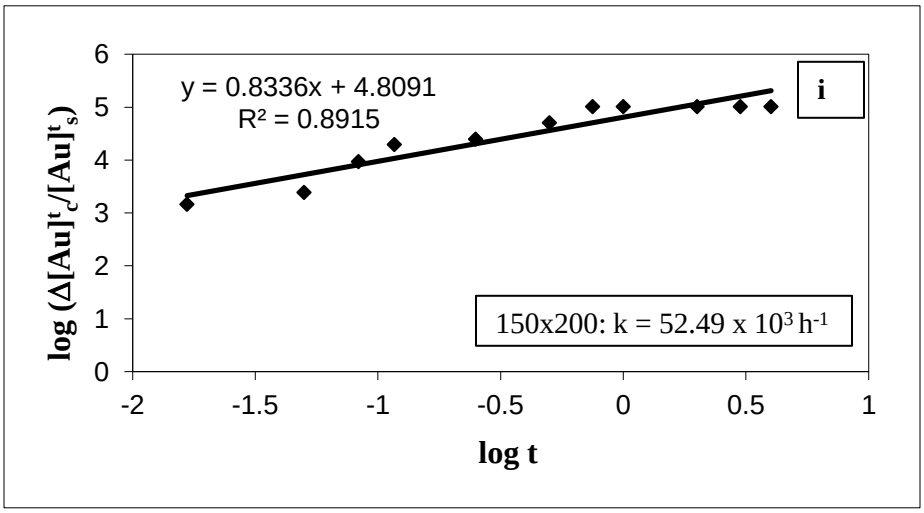

Figure 3.7.continued.

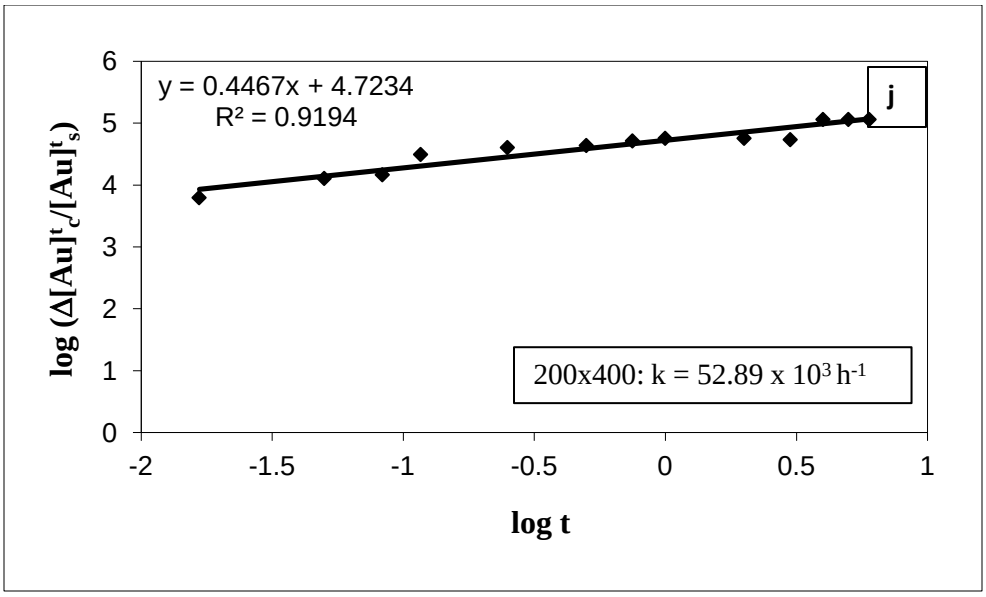

Figure 3.7.continued.

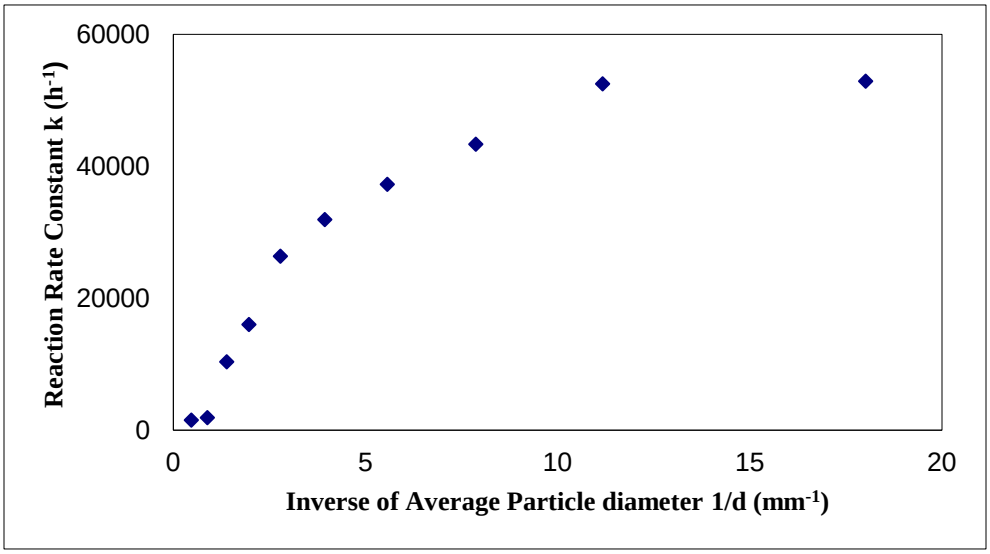

Figure 3.8. The effect of particle size (average particle diameter) on reaction rate constant

Figure 3.3 shows the gold adsorption kinetics of activated carbon particles. As can be seen, the percent of gold adsorption onto activated carbon particles shows different trends according to particle size. The initial rate of adsorption of gold cyanide is rapid, with adsorption occurring at the most accessible sites in macrospores, and possibly mesopores, but the kinetics decrease as equilibrium is approached. Under these conditions, the rate is controlled by the mass transport of gold cyanide species to the activated carbon surfaces. However, once this adsorption capacity has been utilized, a pseudo-equilibrium is established beyond which adsorption must take place in the micropores. This requires diffusion of gold cyanide species along pores within the carbon structure, typically a much slower process then boundary layer diffusion due to the length and tortuosity of the pores [Marsden and House, 1986].

It is also seen from Table 3.2 that rate of adsorption increases with decrease in particle size and initial adsorption rate in small particle size is nearly 42 times greater than that of big size (Figure 3.6). The reaction rate constants calculated for all the size fractions and as shown in Figure 3.7 and 3.8 also show a similar trend with the reaction rate constant much higher for the fine particles in comparison to the coarse particles. The particle size has a large effect on the mean pore length within the carbon particles. Hence, the particle size of granular activated carbon has a large effect on the rate of adsorption, despite only a small increase in net surface area (Marsden and House, 1986).

3.3 Summary

The gold adsorption experiments give a good insight into the adsorptive properties of activated carbon. Adsorption experiments were carried out with different

size fractions of activated carbon. These experiments reveal that the adsorption capacity of activated carbon is independent of the particle size. This can be explained on the basis of results from the BET surface area characterization which also shows that the specific surface area of activated carbon is independent of the activated carbon particle size. The reported activated carbon loading capacity (K-value) of 26 to 28 mg Au/g C or kg Au /t C for all the size fractions is well in agreement to the values reported in literature for industrial-scale operations.

The adsorption rate experiments were also critical in understanding the kinetics of gold adsorption on activated carbon for both coarse and fine sizes. Experiments clearly reveal the dependence of adsorption rate on the activated carbon particle size. As was expected, finer activated carbon showed faster adsorption kinetics with close to 90% of the gold being adsorbed from alkaline cyanide solutions within the first hour. Whereas, for coarser activated carbon particles, only 40 to 50% of the gold was adsorbed in the first hour. The tabulated results also depict that the initial rate of gold adsorption by fine activated carbon particles is almost 42 times greater than that of coarse activated carbon particles. This was further supported by the calculated values of the reaction rate constants, which also showed a similar trend as the initial rates, with variation in particle size. Further, the adsorption rate experiments can serve as a basis for understanding the elution experiments and the anomalies associated with it as revealed in the next chapter.

CHAPTER 4

ACTIVATED CARBON DESORPTION OF GOLD CYANIDE

4.1 Elution Experiments

The gold industry incurs substantial losses due to generation of activated carbon fines which are difficult to process. Mostly these fines are stockpiled or shipped offsite for processing. These activated carbon fines still contain significant gold. This chapter focuses on the investigation of the effect of particle size of activated carbon on the elution of gold cyanide from loaded activated carbon particles; and whether a cost-effective way of eluting such loaded fine carbons is possible. In this regard, traditional and alternative procedures for gold elution have been studied, including:

Traditional Procedures:

- Mintek
- Atmospheric Zadra

Alternative Procedures:

- Elution using hydro-alcoholic solutions
- Elution involving vacuum degassing of loaded activated carbon
- Filter press stripping method
- Syringe pump elution method

The carbon preparation and loading procedures as well as the stripping methods used are described in the following sections. It is worth mentioning here that this research is an extension of previous research by Francis Elnathan (Elnathan, 2007)and Tolga Depci.

4.1.1 Activated Carbon Preparation and Loading

The procedure used to load the different particle size classes of activated carbons with gold cyanide for subsequent elution experiments is described in this section. Carbon loadings were carried out using the experimental set-up in Figure 3.1. Coarse granular (2.8 x 1.4mm) activated carbons as-received were usually washed several times with DI-water and dried overnight at 110^{o}C in an oven. Dried coarse activated carbons were then crushed using a mortar and pestle. Crushed samples were then wet-screened to different particle size fractions, as shown in Table 4.1. After wet screening, the different size fractions were again dried overnight at 110^{o}C in an oven.

Dried activated carbons were then stored in a desiccator until ready to be loaded with gold cyanide solution for further experiments. Dried and cooled activated carbons were loaded with gold cyanide prior to elution experiments. Carbon loading was carried out using 250 mg/L gold concentration solution dissolved as $KAu(CN)_2$ at pH 11 buffered by a borate solution.

Gold cyanide solutions (250 ppm) were prepared first by preparing the specific volume of borate buffer required using 3.09 g of boric acid, 3.73 g of potassium chloride, 2 g of sodium hydroxide, and 1L deionized water. This then was followed by adjusting the borate buffer to the required pH (10-11), and then finally dissolving 411.5 mg of $KAu(CN)_2.2H_2O$ specific to the concentration of 250 ppm required in the buffer solution.

Table 4.1 .Activated carbon particle size fractions

Code	Particle size mesh	Particle size, mm
S1	7 x 12	2.83 x 1.41
S2	12 x 20	1.41 x 0.841
S3	20 x 28	0.841 x 0.595
S4	28 x 35	0.595 x 0.420
S5	35 x 48	0.420 x 0.297
S6	48 x 65	0.297 x 0.210
S7	65 x 100	0.210 x 0.149
S8	100 x 150	0.149 x 0.105
S9	150 x 200	0.105 x 0.074
S10	200 x 400	0.074 x 0.037

A mass of 200mg NaCN was dissolved in the solution prior to use. Activated carbon (1g) was weighed into the plastic reactors and subsequently, 200 ml of 250 ppm gold solution was added to it and shaken for 24 hours at 200 rpm.

Carbon loadings were always carried out at room temperature by contacting the carbons with potassium gold cyanide solution for 24 hours on a Barnstead platform shaker. A sample of the initial gold cyanide stock solution prepared was always taken for gold analysis by ICP-OES.

After the AC-loading cycle was completed (after 24 hours), the mixture of AC and gold-depleted solution was filtered. Samples of each filtrate were stored in vials for gold solution analysis by ICP-OES. The difference between the initial quantity of gold in

solution and the quantity of gold in the filtrate after the loading procedure, multiplied by the volume of gold cyanide solution, was used to determine the amount of gold adsorbed on each sample of AC for any subsequent procedures, such as elution.

Loaded carbons were then washed thoroughly with deionized water several times while on the filter paper and allowed to dry at room temperature under the hood. Loaded, washed, and dried carbon samples were stored in sample bottles and used for the various elution tests conducted as described in the following sections

The loaded activated carbons were eluted using the traditional atmospheric Zadra and Mintek procedures and subsequently using other alternative procedures which are described later in this chapter.

4.1.2 Traditional Activated Carbon Elution Methods

4.1.2.1 Mintek Procedure

In the Mintek elution procedure, loaded activated carbon is stripped with a stripping cycle of 1 hour. In this procedure, the carbon samples of all size fractions were stripped at elevated temperature (98-100^{o}C) by refluxing the strip solution. In the batch-continuous stripping method, a specified volume of strip solution was used for a sample's entire stripping cycle. In the batch-continuous stripping, carbon samples to be eluted were directly submerged in the strip solution in the three-neck distillation flask as was the case with the Zadra method mentioned previously.

200 ml of Mintek solution of 0.5% NaCN solution was prepared. For this, 1 gm of NaCN was mixed with 200 ml of DI water. The solution was heated in a three-neck distillation flask using a heating mantle until the solution started boiling. The loaded

activated carbon was carefully contacted with the boiling solution. The three-neck distillation flask was fitted with a condenser (Figure 4.1) through which cold water was circulated continuously to condense the boiling strip solution. Thus, the solution was refluxed in this closed system for 1 hour. 10 ml of the solution was extracted using a glass syringe and filtered at 15, 30, 45, and 60 minutes and stored in glass vials for gold analysis by ICP-OES. From the ICP-OES results, the percentage gold eluted was calculated as a function of time for all the size fractions of carbon samples. The results for the Mintek procedure are given in later sections of this chapter.

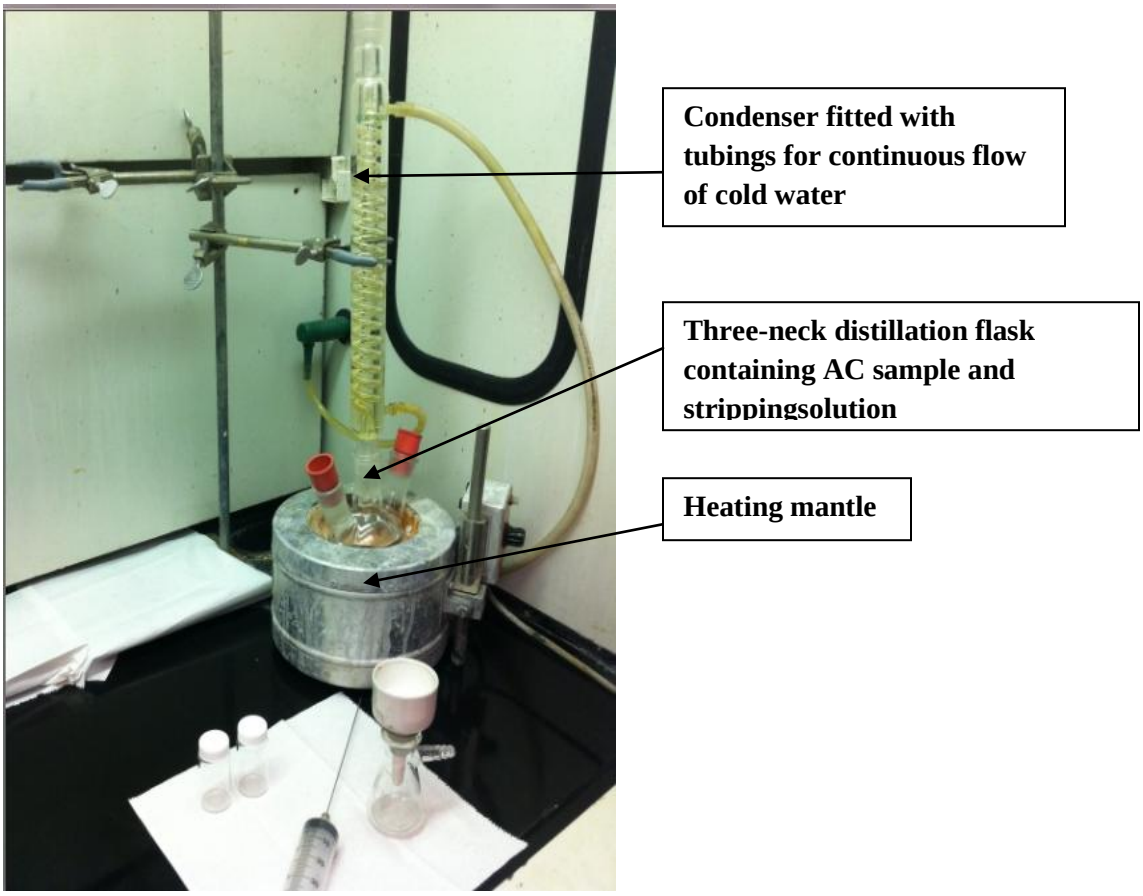

Figure 4.1. Experimental set-up for Mintek and Atmospheric ZadraProcedure

4.1.2.2 Atmospheric Zadra Procedure

The atmospheric Zadra elution method involved stripping the different particle size fractions of loaded activated carbons at atmospheric pressure and elevated temperatures, as shown in Figure 4.1.

Batch stripping with strip solution reflux [or batch-continuous stripping method] was employed. In the batch-continuous stripping method, a specified volume of strip solution was used for a sample's entire stripping cycle. In the batch-continuous stripping, carbon samples to be eluted were directly submerged in the strip solution in the three-neck distillation flask.

200 ml of strip solution used in the batch experiment was enough to submerge the carbon in the three-neck distillation flask during elution. During the stripping procedure, the boiling solution agitated the carbon particles. Stripping time for atmospheric Zadra elution was kept constant at 48 hours.

The Zadra solution was made up of 0.5% NaCN, 1% NaOH, and pH between 11 and 12 [Marsden and House, 2006]. The temperature of the Zadra solution was maintained at boiling point (98-100^{o}C).

Loaded activated carbons to be eluted were contacted with boiling Zadra solution in a three-neck distillation flask fitted with a condenser. The distillation flask was heated by a heating mantle, while the condenser had cold water running continuously through it condensing the strip solution. Solution samples were taken from the atmospheric Zadra elution set-up at certain time intervals over a 48-hour period, using a glass syringe and stored in glass vials for gold solution analysis by ICP-OES. From these results, percentage gold eluted was calculated as a function of time for each size fraction of the

loaded carbons. Results for atmospheric Zadra elution are presented and discussed in the later sections.

4.1.3 Process Alternatives for Gold Elution

The results of the traditional activated carbon elution methods are discussed in section 4.2. On the basis of these results, alternative procedures for gold elution were developed and tried in order to provide a plausible explanation for the reduced gold elution from fine activated carbon.

Several alternative procedures for gold elution were tried, including the following: elution using hydro-alcoholic solutions of different concentrations of isopropanol and ethanol; elution involving vacuum degassing loaded activated carbon prior to its stripping by Zadra and alcoholic solutions; pressure treatment using syringe pump method and filter press method. For these procedures, two particle size fractions (7 x 12 mesh and 48 x 65 mesh) were selected. It is expected that the results from the above experiments will help to clarify the activated carbon particle size effect in stripping of gold cyanide and provide efficient alternative procedure strategies for enhanced gold elution at shorter retention times.

4.1.3.1 Elution Using Hydro-Alcoholic Solutions

Gold adsorbed onto activated carbon are extracted during a subsequent stage using various technologies such as hot water elution as seen in the previous sections, before final recovery by electrolysis. Conventional stripping systems involve the use of relatively high temperatures (90–120°C) and long elution times (12–72 hours). In the

present work, the efficiency of the alcohol use in gold stripping procedure from previously loaded activated carbon was investigated, with the aim to find an interesting alternative for gold stripping, which might be cheaper than conventional systems. In particular, the effects of extraction time and of temperature on the gold desorption rate have been investigated, in the presence of different hydro-alcoholic eluants, containing NaOH but no cyanide.

200 ml of hydro-alcoholic eluant solutions of ethanol and isopropanol were prepared in 20% v/v (40 ml alcohol + 160 ml DI water) and 40% v/v (80 ml alcohol + 120 ml DI water) with 0.2 g NaOH added to the solution to adjust the pH between 10.5 and 11.

The stripping solution was added to 1g of loaded activated carbon in a 500 ml three-neck distillation flask placed on a hot plate with temperature controller and equipped with a magnetic stirrer. The stripping experiments were performed at room temperature and 60°C, respectively. The experimental set-up is presented in Figure 4.2

Figure 4.2. Experimental set-up for elution experiments involving alcoholic solutions.

The solution was gently stirred at 200 rpm using a magnetic bar, to keep the carbon particles in suspension. 10 ml solution sample was collected using a glass syringe at regular intervals over a 48-hour period, and stored in glass vials for gold analysis using ICP-OES.

To simulate industrial conditions, another set of experiments were performed where ethanol and isopropanol were added separately to the boiling Zadra solution in 20% v/v (40 ml alcohol + 160 ml Zadra solution) and 40% v/v (80 ml alcohol + 120 ml Zadra solution) concentration. The Zadra solution was prepared according to the recipe mentioned in section 4.1.2.1. These sets of experiments were conducted at 98°C in a three-neck distillation flask fitted with a condenser and the temperature controlled using a heating mantle. Cold water was circulated through the condenser to reflux the strip solution. The mixture of Zadra solution and alcohol in different concentration was added to 1 g of loaded activated carbon in the three-neck distillation flask. 10 ml solution sample was collected using a glass syringe at regular intervals over a 48-hour period, and stored in glass vials for gold analysis using ICP-OES. Desorption isotherms were calculated for each case.

4.1.3.2 Elution Involving Vacuum Degassing of Loaded Activated Carbon

The effect of vacuum degassing loaded activated carbon prior to stripping using different solutions was investigated with two particle size fractions (7 x 12 mesh and 48 x 65 mesh). The vacuum degassing procedure was employed in an attempt to increase the gold elution rate from fine activated carbon and is demonstrated in Figure 4.3.

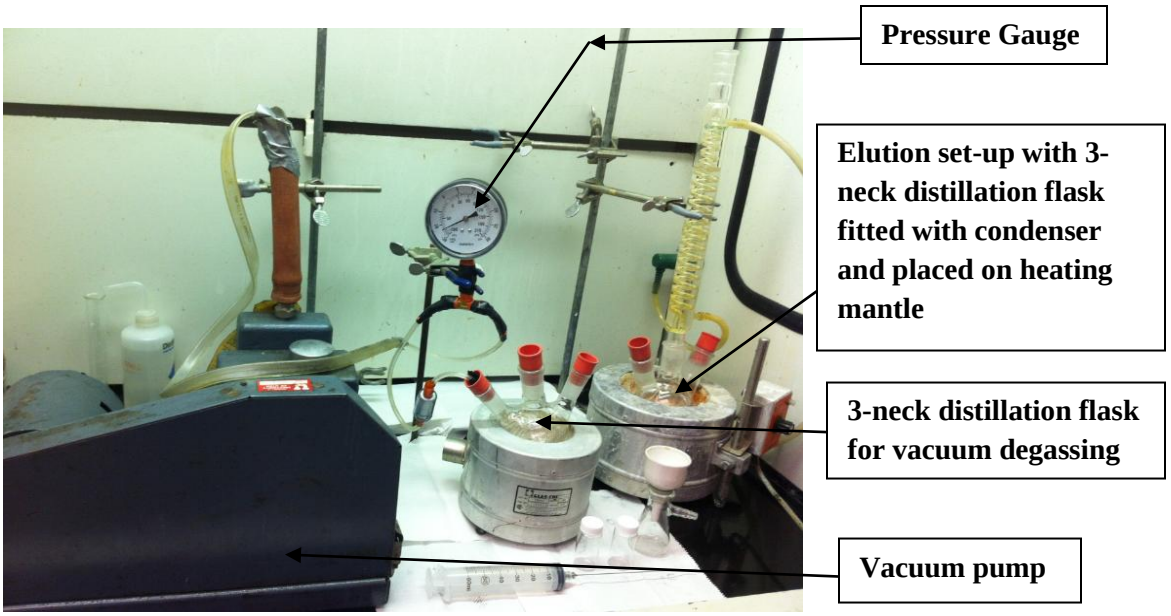

Figure 4.3.Experimental set-up for elution experiments involving vacuum degassing of loaded activated carbon.

For both size fractions, loaded activated carbon was placed in a three-necked distillation flask and subjected to vacuum degassing at -25 psi using a vacuum pump, for different exposures of time such as 0 hr, 0.5 hr, 1 hr, 1.5 hr, 2 hr, 3hr, 4 hr, 5hr, and 6hr. After the stipulated degassing time for each case, the vacuum pump was turned off and 200 ml of Zadra strip solution at around boiling temperature was introduced into the system using a glass syringe. The system was then placed on the heating mantle with the temperature set around 98°C and subsequently, the condenser was fitted to reflux the boiling solution. 10 ml solution sample was collected periodically using a glass syringe over a 48-hour period, and stored in glass vials for gold analysis using ICP-OES.

From the desorption isotherms, it was determined that the percent of gold eluted did not change significantly after 3 hours. Hence, for further experiments, it was decided that the loaded activated carbon particles would be vacuum degassed for 3 hours prior to stripping.

The next set of experiments was aimed to investigate the combined effect of vacuum degassing and stripping with hydro-alcoholic solutions. The investigation was carried out with the same two particle size fractions 7 x 12 mesh and 48 x 65 mesh. The loaded activated carbon particles were subjected to 3 hours of vacuum degassing at -25 psi in a three-neck distillation flask after which 200 ml of alcoholic solution was added to the system using a glass syringe. Alcoholic solutions of ethanol and isopropanol were prepared in 20% v/v. Stripping experiments were carried out at 60°C. 10 ml solution sample was collected periodically using a glass syringe over a 48-hour period, and stored in glass vials for gold analysis using ICP-OES. The results from the ICP analysis was used to plot the desorption isotherms.

Similar stripping experiments were repeated for both the size fractions involving vacuum degassing loaded activated carbon for 3 hours and subsequently stripping with Zadra + 20% alcohol solution (both isopropanol and ethanol). The experiments were conducted at 98°C and samples were collected periodically over 48 hours and analyzed through ICP-OES.

4.1.3.3 Filter Press Stripping Method

Loaded activated carbon of two size fractions, 7 x 12 mesh and 48 x 65 mesh, were used for the filter press stripping experiments. The carbons were loaded with gold cyanide for the stripping experiments as described in section 4.1.1 and the set-up for this stripping method is shown in Figure 4.4. Only Zadra stripping solution was used for this pressure method. The experiment was conducted at room temperature, 60^{o}C, and boiling point (98^{o}C) of the strip solution. 3 g mass of each size fraction of the carbon sample was

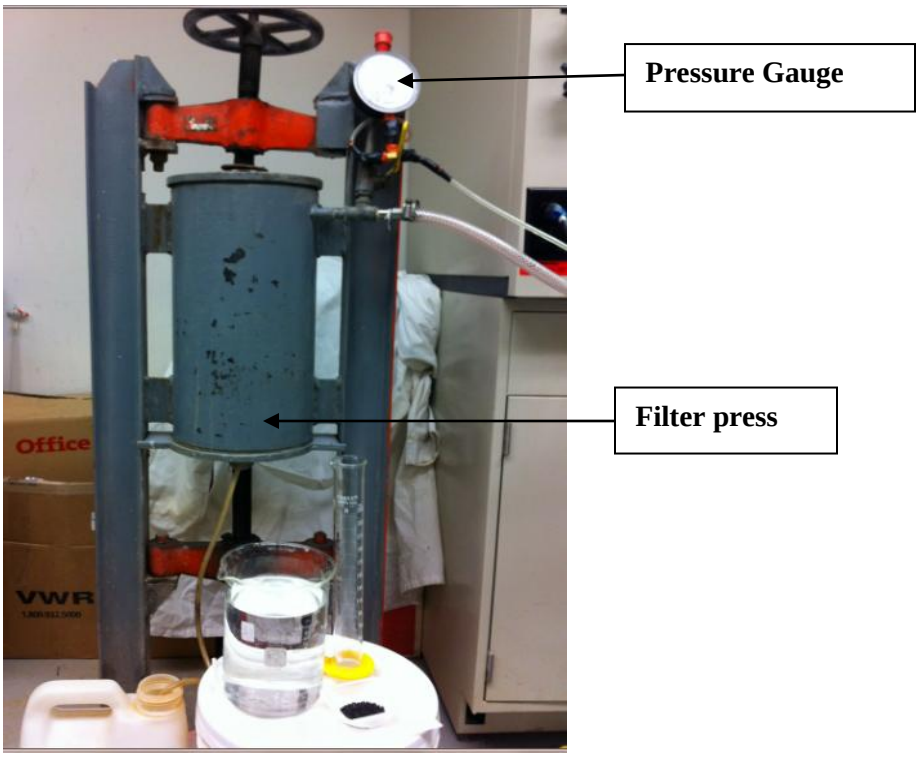

Figure 4.4.The filter press elution experimental set-up.

used for the filter press experiments. The composition and pH of the Zadra strip solutions used was: 1 % NaOH, 0.5 % NaCN pH 11.5

An air pressure of 80 psi was used for stripping all the carbon samples using the Zadra stripping methods. Three grams of each of the carbon samples to be stripped was presoaked for 30 minutes in 100 ml of strip solution in a 1.2L plastic container at room temperature. A liter of stripping solution was considered a sample cycle. After initial presoaking, strip solution was added to the plastic container to make it to the 1L mark and the entire content was poured into the chamber of the filter press. The base of the filter press was lined with filter cloth and Whatman Cat No 1001 240 filter paper. Experiments were conducted at boiling temperature (98^{o}C), at 60^{o}C, and room temperature. Results are presented in subsequent sections.

The sample chamber was closed tightly to prevent strip solution and pressure leaks from the filter press. The air pressure valve preset to 80 psi was opened and this forced the strip solution through the bed of carbon in the filter press. The stripped solution was collected in a five liter plastic bucket placed at the discharge end of the filter press. The stripped solution collected in the bucket was thoroughly mixed and a sample was stored in sample vials for gold analysis though ICP-OES. The temperature of the strip solution in the sample chamber of the filter press and stripped solution in the bucket at the discharge end of the filter press were measured. For stripping at the boiling point, the average temperature of the strip solution in the sample chamber of the filter press and the strip solutions in the buckets were 98^{o}C and 65^{o}C, respectively; and for stripping at 60^{o}C, the corresponding average temperatures measured were 60^{o}C and 35^{o}C, respectively. A total of 4L of strip solution was passed through each activated carbon sample for stripping at the respective temperatures.

4.1.3.4 Syringe Pump Elution Method

The syringe pump stripping method involved using the syringe pumping mechanism to force strip solution through the bed of gold-loaded carbons in the syringe, as shown in Figure 4.5. This method was employed to investigate the effect of moderate pressure on the stripping of loaded activated carbon using Zadra solution, as opposed to the high pressure used in the filter press method. Zadra strip solution was used for stripping gold-loaded carbons using this method. The strip solution flow rate through the bed of carbon in the syringe was varied and the minimum pressure applied to the syringe plunger was calculated from the plunger diameter and force applied to it.

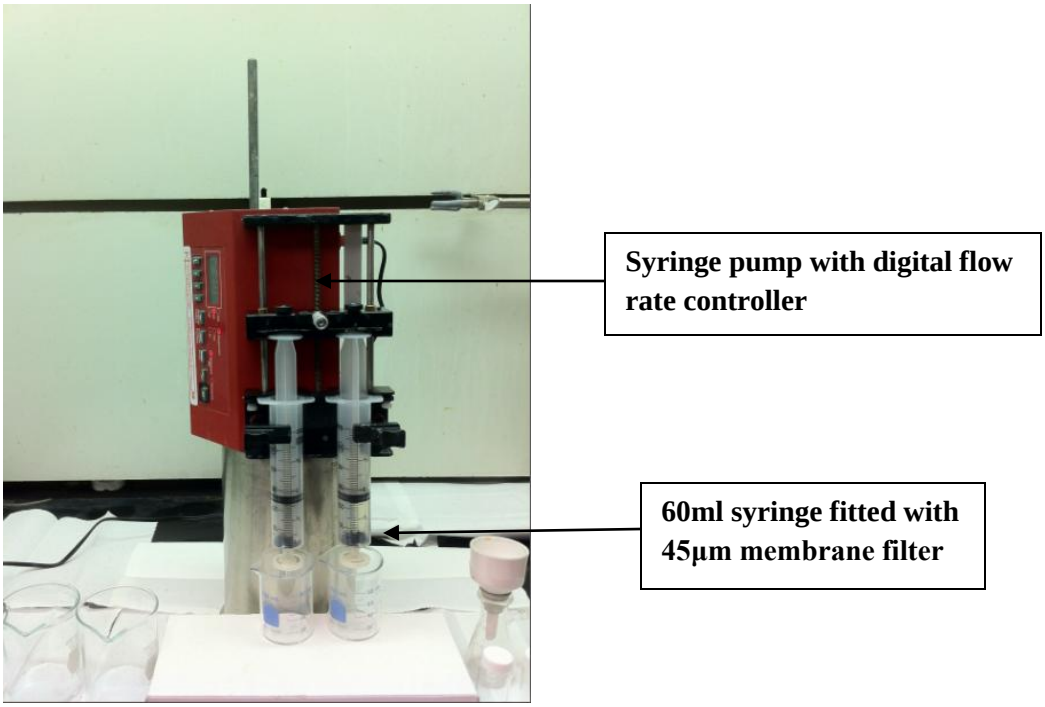

Figure 4.5.Experimental set-up for elution experiment with syringe pump.

1 gram each of the two particle size fractions 7 x 12 mesh and 48 x 65 mesh of gold-loaded carbons was placed on the filter paper, cut out in the diameter of the syringe, in the 60ml syringe. A 0.2/0.45 µm size Millipore membrane filter was fitted to the lower end of the syringe through which the stripped gold solution passed into beakers placed below. This was done to ensure that there was enough pressure build-up in the syringe to facilitate the stripping of the carbon samples and also to prevent carbon particles from falling into the stripped solution underneath. Experiments were conducted with the Zadra strip solution at boiling temperature (98-100^{o}C). The Zadra strip solution had a composition of 1% NaOH, 0.5% NaCN, and a pH around 12. Eluant was pumped through the bed of carbons in the syringe with the flow rate varied between 1, 2.5, 5, and 15 ml/minute

The strip solution retention time in the syringe depended on the flow rates, and so the retention times of the eluant varied from 12- 60 minutes. The carbon samples for experiments were presoaked for a time which varied from 30 minutes with 50 ml of strip solution at room temperature prior to the stripping procedure and the pH of the strip solutions was around 11.5. The calculated pressure at 15 ml/min was around 36 psi, while at 1 ml/min it was around 2.4 psi.

The stripped gold solution was collected in the beakers at the end of the syringe discharge, as shown in Figure 4.5. 1 L of strip solution was passed through the bed of carbon in 50 ml batches. The stripped solution from each batch was thoroughly mixed and a representative sample taken for gold analysis by ICP-OES. A liter of Zadra strip solution was passed through each bed of carbon sample to flush out any residual gold. The percent gold eluted in the stripping cycle was determined for the procedure as a measure of its efficiency.

4.2 Results and Discussion

4.2.1 Activated Carbon Loading

After the carbon loading experiments were completed, solution was filtrated using vacuum filtration with Whatman filter paper. Gold concentration in the solution was analyzed by ICP and the carbon loading was calculated by equation 4.1:

$$CarbonLoading, kg/t = \left([Au]_s^O - [Au]_s^{24}\right) * S_v / (M_c * 1000)$$

(4.1)where, $[Au]_s^0$ and $[Au]_s^{24}$ are initial gold concentration (ppm) at the start of the experiment and final gold concentration (ppm) after 24 hours, respectively. S_v is the solution volume (ml) and M_c is the mass carbon (g).

Carbon loading values are given in Table 4.2. From the tabulated results, it is evident that the ultimate gold loading on activated carbon is independent of particle size. The carbon loading results are well in agreement with the results of the specific surface area for all the size fractions. The specific surface area of all the different particle size fractions of activated carbon is independent of particle size. Hence, it can be concluded that the gold loading on activated carbon is directly related to its specific surface area.

4.2.2 Particle Size Effect on Traditional Gold Elution Procedures

4.2.2.1 Particle Size Effect on Mintek Elution Procedure

In the Mintek elution procedure, 10 ml solution sample was extracted periodically over a 1-hour period at 15, 30, 45, and 60 minutes and stored in clearly labeled glass vial.

Table 4.2. Carbon loading on activated carbon

particle size mesh	**average particle diameter, mm**	**Gold on AC mg Au/g C**
7 x 12	2.12	48.04
12 x 20	1.13	47.98
20 x 28	0.72	48.09
28 x 35	0.51	48.23
35 x 48	0.36	48.50
48 x 65	0.25	48.18
65 x 100	0.18	48.15
100 x 150	0.13	48.33
150 x 200	0.09	48.37
200 x 400	0.06	48.49

Subsequently, the gold concentration in each solution was determined by ICP-OES.

The gold concentration on the carbon (kg/t) at 15, 30, 45, and 60 minutes are calculated using equations 5.2 to 5.5, respectively.

$$15\,\text{min} - kg/t = [Au]_c^0 - 200 * [Au]_s^{15} / 1000 * M_c \quad (4.2)$$

$$30\,\text{min} - kg/t = [Au]_c^0 - (200 * [Au]_s^{30} + 10([Au]_s^{15} - [Au]_s^{30}) / 1000 * M_c \quad (4.3)$$

$$45\,\text{min} - kg/t = [Au]_c^0 - (200 * [Au]_s^{45} + 10([Au]_s^{15} + [Au]_s^{30} - 2 * [Au]_s^{45}) / 1000 * M_c \quad (4.4)$$

$$60\,\text{min} - kg/t = [Au]_c^0 - (200 * [Au]_s^{60} + 10([Au]_s^{15} + [Au]_s^{30} + [Au]_s^{45} - 3 * [Au]_s^{60}) / 1000 * M_c \quad (4.5)$$

where, $[Au]_c^0$ is initial carbon loading (kg/t) and $[Au]_s^{15}, [Au]_s^{30}, [Au]_s^{45}, [Au]_s^{60}$ are solution concentration (ppm) at 15,30,45, and 60 minutes, respectively. M_c is mass of carbon. Figure 4.6, Figure 4.7, and Figure 4.8 show the gold elution rate of the different activated carbon particle size fractions from the Mintek Procedure.

Figure 4.6 illustrates the gold elution rate and the extent of gold elution for all the ten activated carbon particle size fractions. Figure 4.7 and 4.8 separately illustrate the rate of gold elution for the coarse and the fine size fractions, respectively.

These figures clearly illustrate that with a decrease in activated carbon particle size, the rate of gold elution increases as expected. This shows an inverse dependence of the rate of gold elution on the particle size and holds true for the first four coarse size fractions. Further, when the particle size was reduced below 35 mesh, the rate of gold elution decreased with reduction in particle size. This caused some worry as the behavior of the gold elution behavior was contrary to popular belief and the inverse dependence of gold elution on the particle size was not observed.

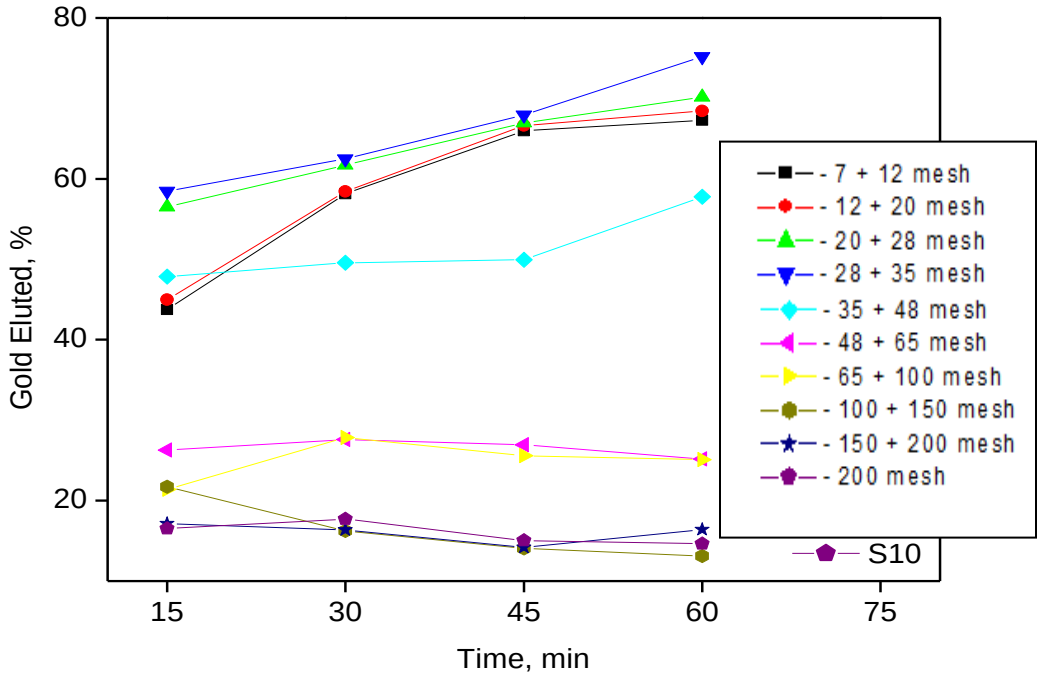

Figure 4.6. Rate of desorption for activated carbon samples of different particle size using the Mintek Procedure.

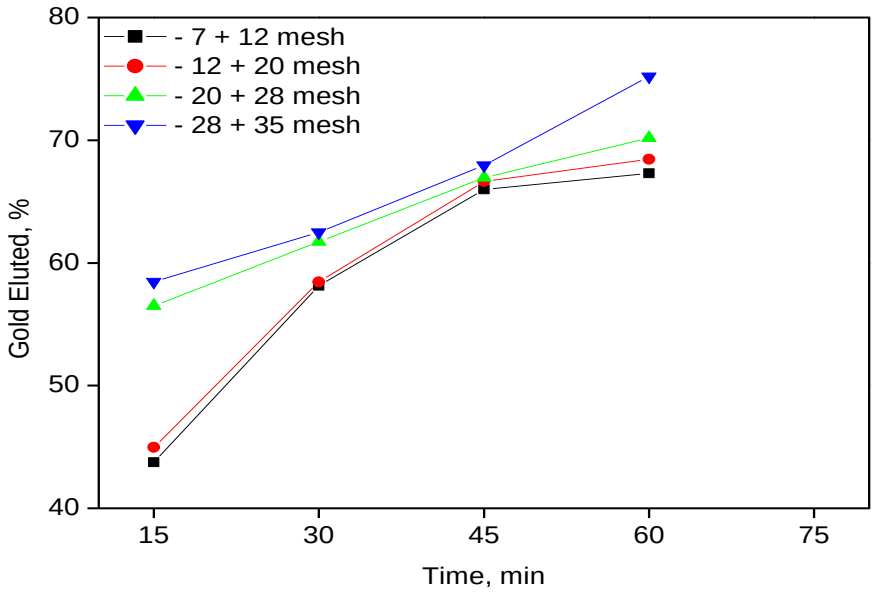

Figure 4.7. Rate of gold desorption from activated carbons of coarse particle size fractions (in the range from 7 mesh to 35 mesh) using Mintek Procedure**.**

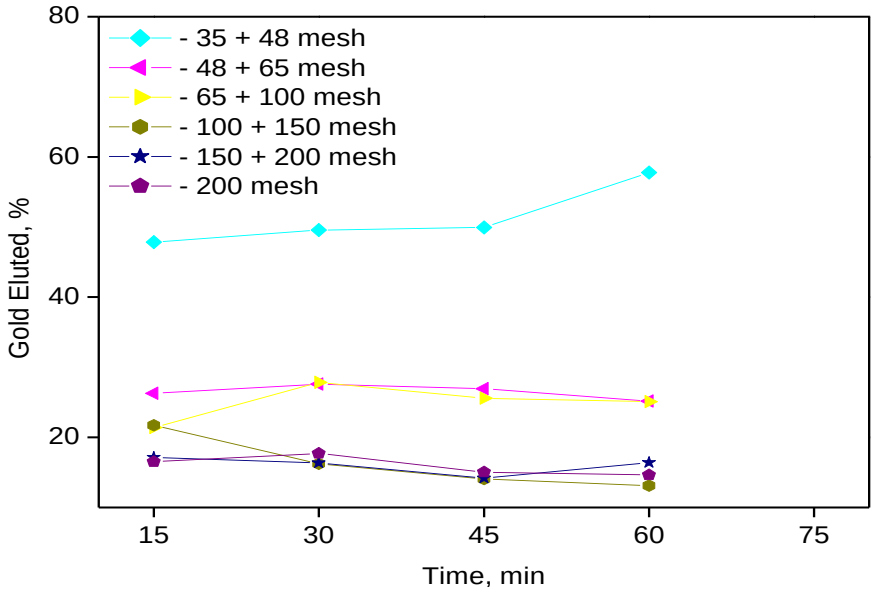

Figure 4.8. Rate of gold desorption from activated carbons of fine particle size fractions (in the range from 35 mesh to 200 mesh) usingMintek Procedure.

As can be seen from the Figure 4.9, gold elution increased with a decrease in particle size for particle size classes greater than 35 mesh in size. With further decrease in particle size below 35 mesh, gold elution dropped significantly. These results were quite contrary to our general expectations. Unlike the adsorption rate results, the results of the stripping reaction by the Mintek procedure are clearly inconsistent with the belief that rate of reaction is inversely dependent on particle size.

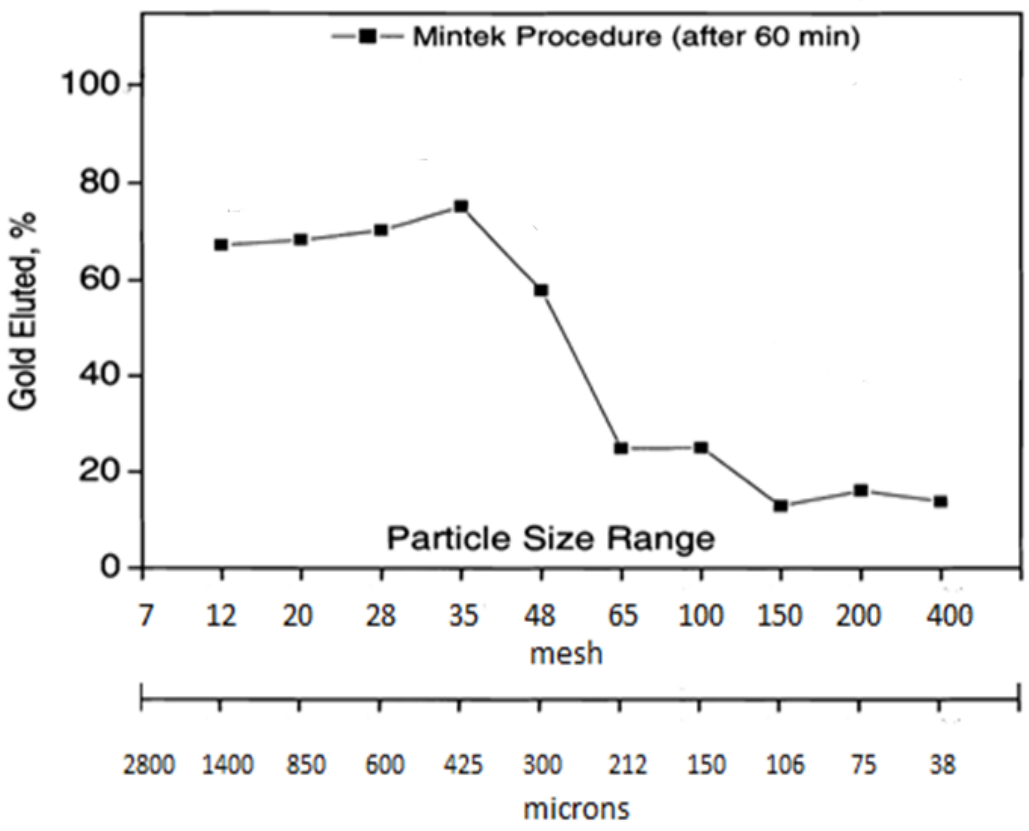

Figure 4.9. The variation of the percent gold eluted as a function of particle size from MintekProcedure, indicating that the percent gold eluted increases initially with decrease in particle size until 35 mesh, and with further decrease in particle size the gold elution decreases.

4.2.2.2 Particle Size Effect on Atmospheric Zadra Elution Procedure

The atmospheric Zadra elution procedure is very similar to the Mintek Procedure and bears a high resemblance to its operating conditions, the only differences being the slight modification in the stripping solution and the procedure time. This method of stripping was studied under batch mode without solution replacement [or batch-continuous stripping] with the solution being refluxed by a condenser. In other words, for the batch-continuous stripping method, a specified volume of strip solution was used for stripping each size fraction of carbon sample in the sample's stripping cycle without replacement of the strip solution.

In atmospheric Zadra procedure, the elution rate of activated carbon particles of all size fractions was determined by collecting samples periodically over a 48-hour period and analyzing for gold concentration through ICP-OES. The gold concentrations on the carbon (kg/t) are calculated from equations similar to the ones used for Mintek procedure.

Figure 4.10 illustrates the gold elution rate and the extent of gold elution for all the ten activated carbon particle size fractions. Figure 4.11 and 4.12 separately illustrate the rate of gold elution for the coarse and the fine size fractions, respectively.

These figures are similar in trend to the elution results presented in the previous section for the Mintek procedure. They clearly show that with a decrease in activated carbon particle size, the rate of gold elution increases as expected and this confirms the inverse dependence of the rate of gold elution on the particle size for the first four coarse size fractions. Further, when the particle size was reduced below 35 mesh, the rate of gold elution decreased with reduction in particle size. The inverse dependence of gold elution on particle size was not observed for the fine particles.

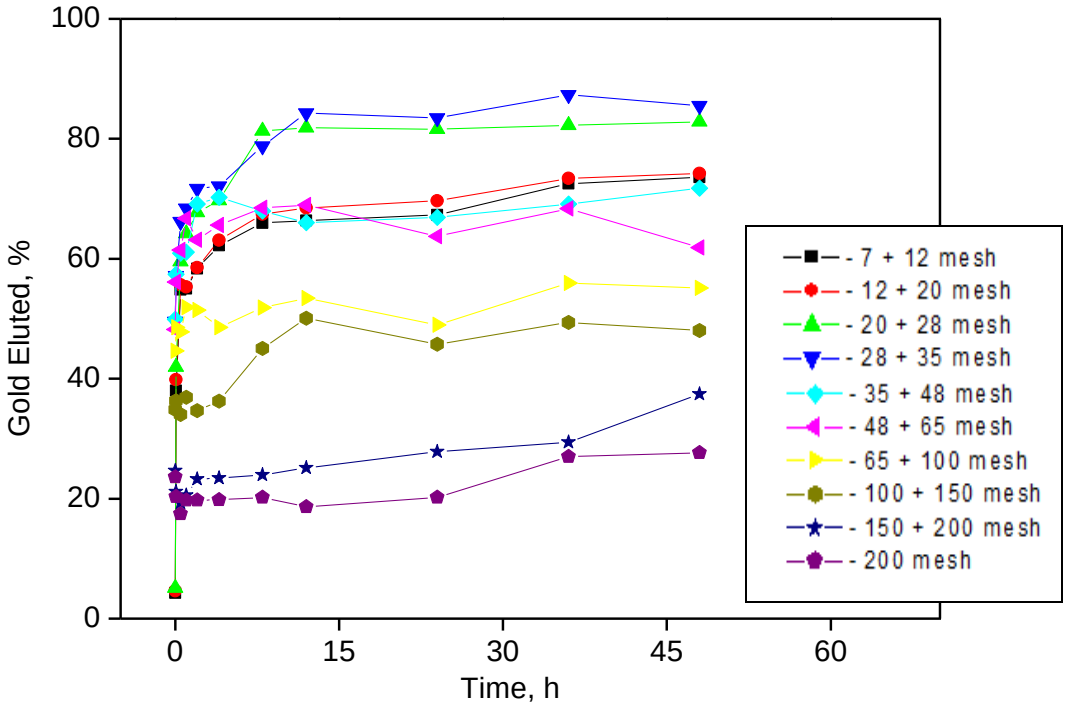

Figure 4.10. Rate of desorption of gold from activated carbon samples of different particle size fractions using the Atmospheric ZadraProcedure.

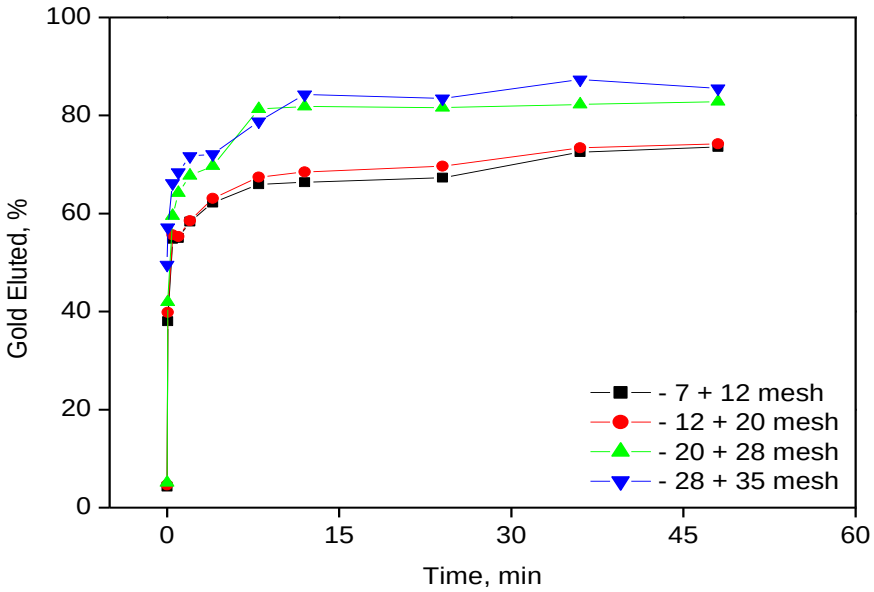

Figure 4.11. Rate of desorption of gold from activated carbon samples of coarse particle size fractions (in the range from 7 mesh to 35 mesh) using the Atmospheric ZadraProcedure.

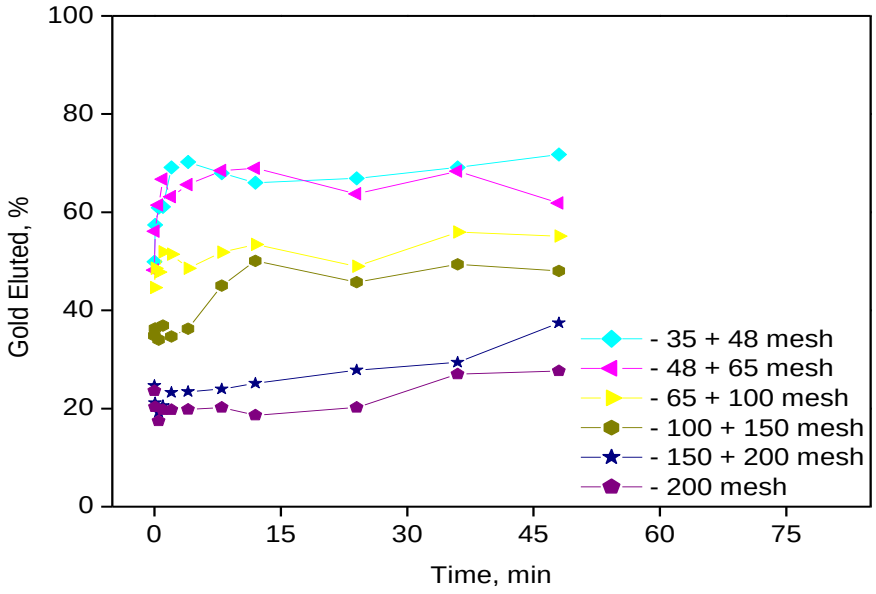

Figure 4.12. Rate of desorption of gold from activated carbon samples of fine particle size fractions (in the range from 35 mesh to 200 mesh) using the Atmospheric ZadraProcedure.

As can be seen from these figures, gold elution increased with a decrease in particle size for size classes greater than 35 mesh size. With further decrease in particle size below 35 mesh, gold elution rate decreased with increase in activated carbon particle size. The overall elution behavior for all the size fractions is illustrated in Figure 4.13.

The results indicate that the stripping reaction favors the coarser carbon particles, that is, the coarser the carbon particles the faster the stripping rate, with the granular carbon eluting on average above 70 % under the stripping conditions considered.

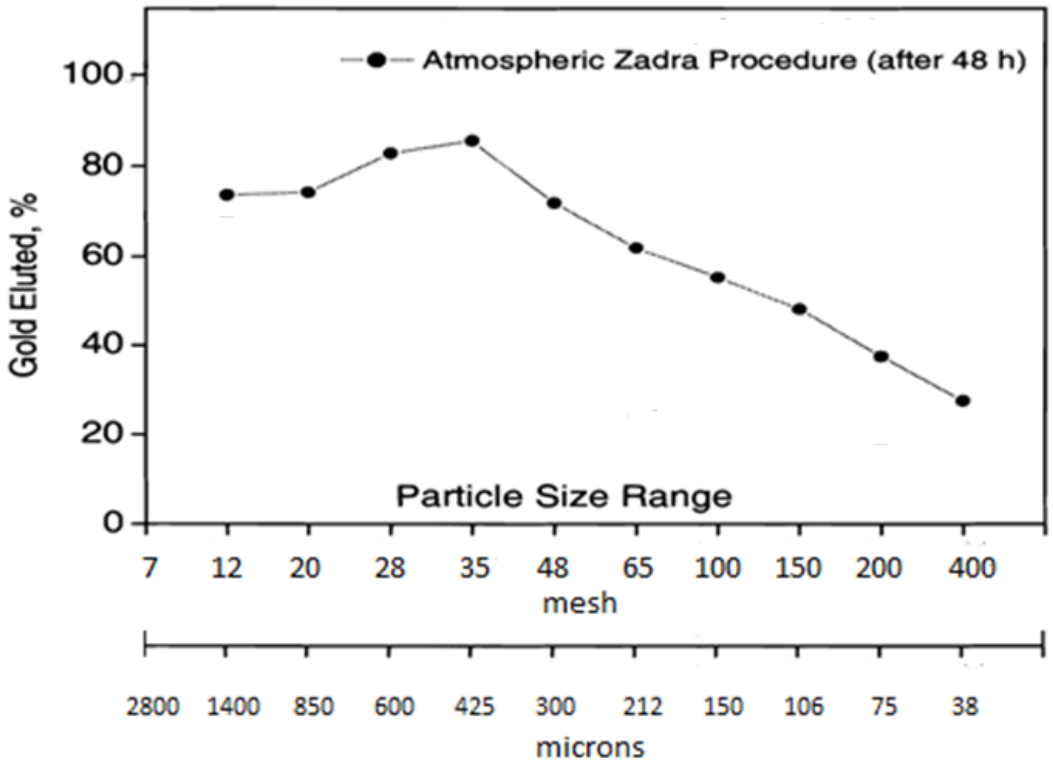

Figure 4.13. The variation of the percent gold eluted as a function of particle size from atmospheric ZadraProcedure, indicating that the percent gold eluted increases initially with decrease in particle size until 35 mesh, and with further decrease in particle size the gold elution decreases.

Unlike the rate of adsorption results presented in the preceding chapter which showed consistency with the inverse dependence of rate on particle size, the results of the stripping reaction by the atmospheric Zadra method are clearly inconsistent with the expectation that rate of reaction is inversely dependent on particle size.

4.2.2.3 Summary of Results from Mintek and Atmospheric Zadra Procedures

The results from the stripping experiments of gold loaded activated carbon of all particle size fractions by Mintek and atmospheric Zadra procedure are illustrated in Figure 4.14. These results give a comprehensive overview of the effect of activated carbon particle size on the desorption of aurodicyanide from activated carbon using traditional elution techniques. Also, this brings to the forefront the reason why it is not economical to use fine activated carbon particles for gold elution even though they exhibit better adsorption kinetics than the coarser ones. For both the procedures, the results were visibly inconsistent with the expectation that rate of reaction is inversely dependent on particle size, as was shown during adsorption kinetics experiments. However, there was an initial inverse dependence of desorption rate on particle size, after 35 mesh, the percent gold eluted dropped dramatically with decrease in particle size for both procedures. A plausible explanation that can be attributed to this phenomenon is the capillary pore effect. It might be possible that gold cyanide elution at atmospheric pressure is difficult from fine activated carbon particles due to the presence of smaller pores as revealed by x-ray micro CT, thereby resulting in higher capillary pressure in fine particles. Thus, this stimulated the research objective to further delve into the desorption phenomena to provide a plausible explanation for this phenomena and develop alternative

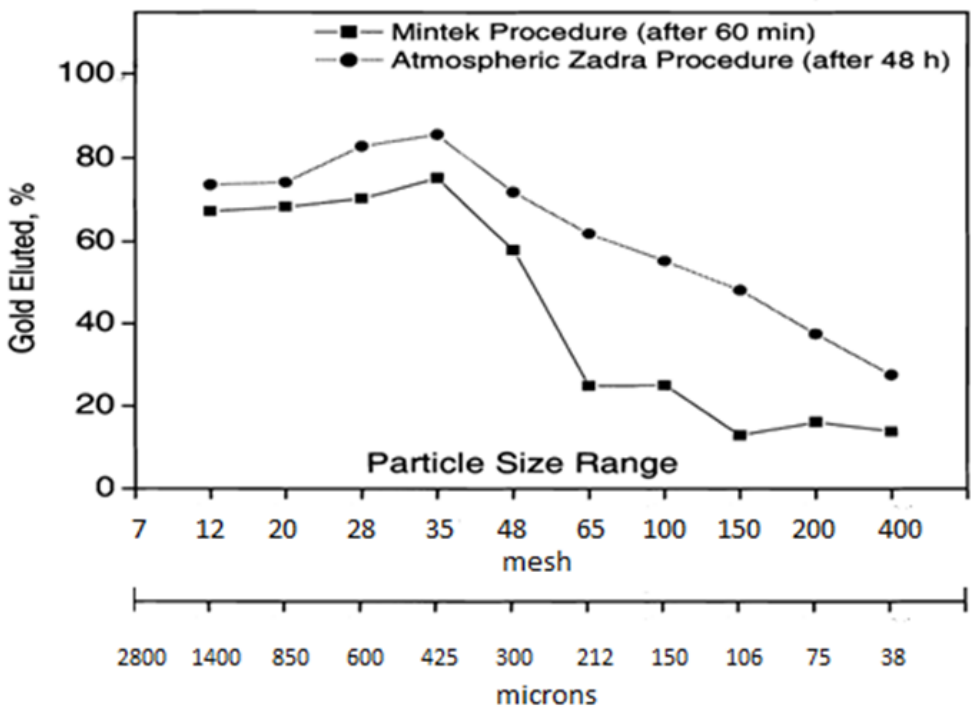

Figure 4.14.Particle size effect on gold elution from Mintek and atmospheric Zadra procedure.

procedures to overcome this phenomena and facilitate improved elution from finer activated carbon particles. It was observed that the percent gold eluted dropped after 35 mesh particle size; hence for all our future stripping experiments, two particle size fractions 7 x 12 mesh and 48 x 65 mesh were selected

4.2.3 Particle Size Effect on Alternative Procedures for Gold Elution

4.2.3.1 Particle Size Effect on Elution Using Hydro-alcoholic Solutions

Hydro-alcoholic solutions of ethanol and isopropanol were used for stripping gold loaded activated carbons. Two different concentrations, 20% and 40%, of alcoholic solution were tried for each of the alcohol components. In addition, these experiments

were conducted at room temperature and 60°C to see the effect of temperature on gold elution using alcohol. The results are illustrated in Figures 4.15 to 4.22.

Further, both ethanol and isopropanol in 20% and 40% concentration each was added to the boiling Zadra solution and then the stripping of loaded activated carbon was carried out.

Elution results with hydro-alcoholic solutions as shown in Figure 4.15, 4.16, 4.17, and 4.18 indicate that on an average, about 30% gold can be eluted in 48 hours at room temperature. Nonetheless, the most encouraging fact from these experimental results is the improved gold elution from the finer particle size fraction as compared to the coarser one.

It is clearly evident from the results, as shown in Figure 4.15and 4.16, that there is no significant effect of the concentration of alcohol in solution. Though 40% alcoholic solution shows a marginally improved gold percentage, for most practical applications 20% concentration is also a safe bet.

From Figure 4.17 and 4.18, it can be concluded that the type of alcohol does not have a prominent impact on the amount of gold eluted. Although isopropanol shows slightly better elution properties in terms of percent gold eluted, any alcohol can be used. These results are well in agreement with the ones reported in literature which states that isopropanol is better than ethanol for gold stripping.

30% elution at room temperature is too low from an economical standpoint. In order to improve percent gold eluted, stripping of loaded activated carbons with hydro-alcoholic solutions was performed at elevated temperature of 60°C. The results are illustrated in Figures 4.19 through 4.22.

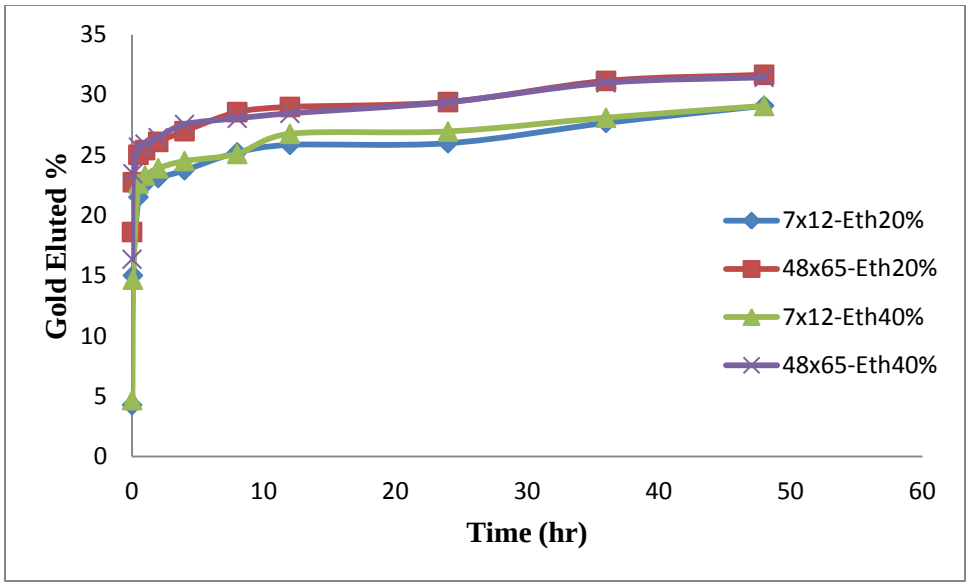

Figure 4.15. Elution of gold loaded activated carbon of two different particle sizes 7x12 mesh and 48x65 mesh using 20% and 40% concentration ethanol solution at room temperature.

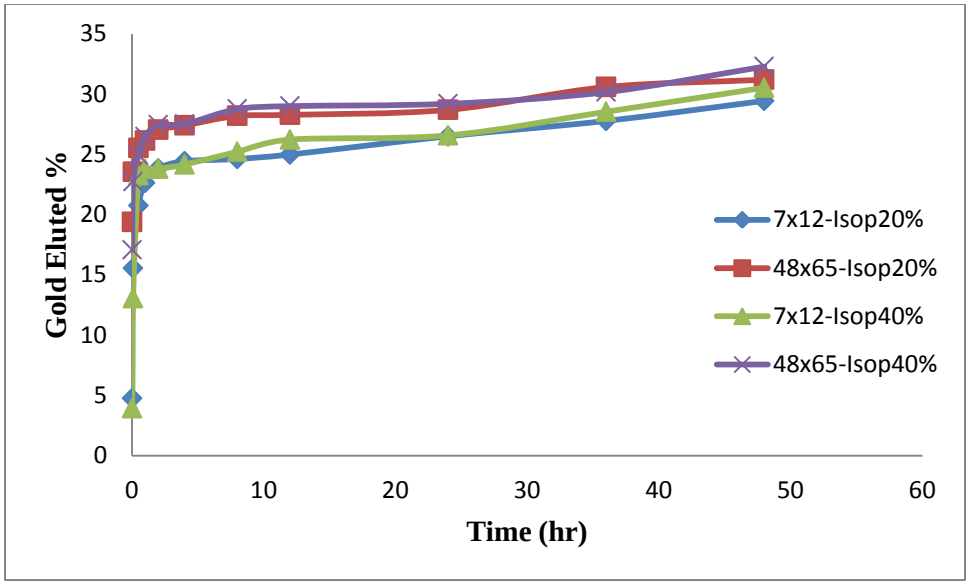

Figure 4.16: Elution of gold loaded activated carbon of two different particle sizes 7x12 mesh and 48x65 mesh using 20% and 40% concentration isopropanol solution at room temperature.

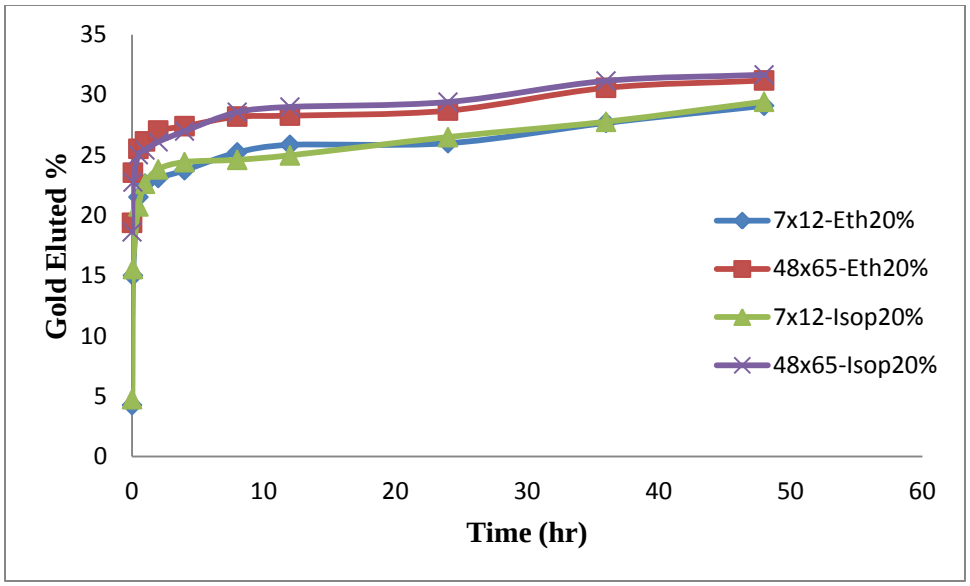

Figure 4.17. Effect of alcohol type on gold elution from activated carbon of two different particle sizes 7x12 mesh and 48x65 mesh using 20% concentration of ethanol and isopropanol, respectively, at room temperature

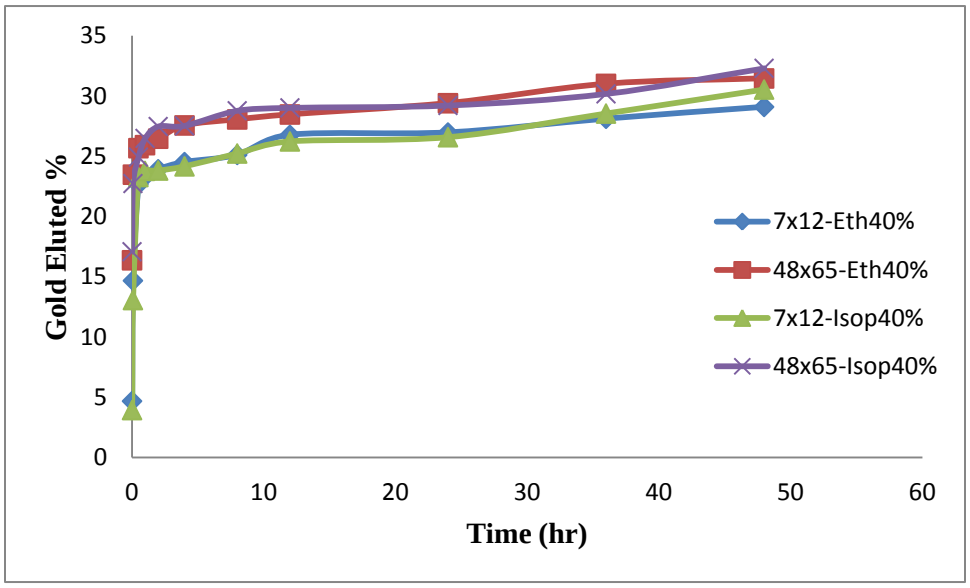

Figure 4.18. Effect of alcohol type on gold elution from activated carbon of two different particle sizes 7x12 mesh and 48x65 mesh using 40% concentration of ethanol and isopropanol, respectively, at room temperature.

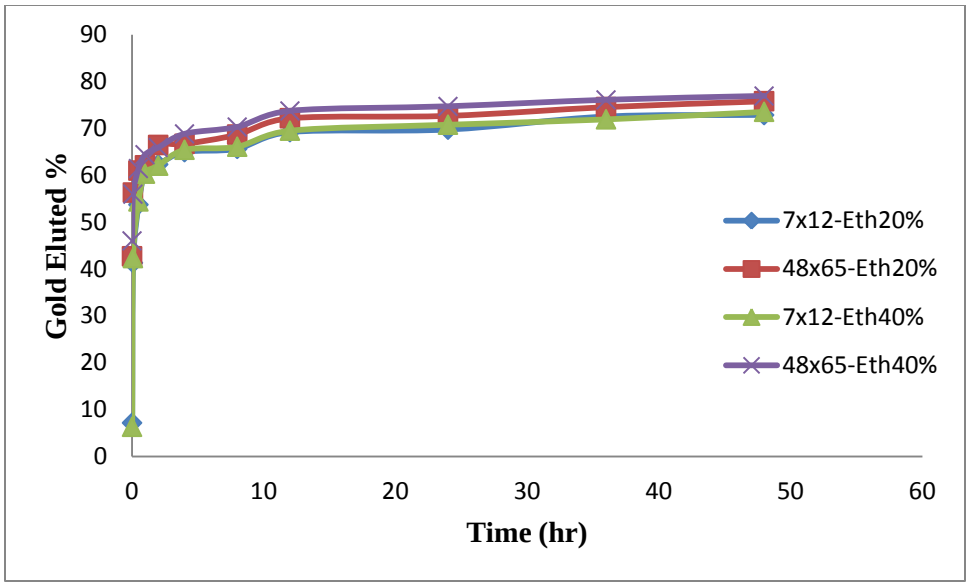

Figure 4.19. Elution of gold loaded activated carbon of two different particle sizes 7x12 mesh and 48x65 mesh using 20% and 40% concentration ethanol solution at 60°C

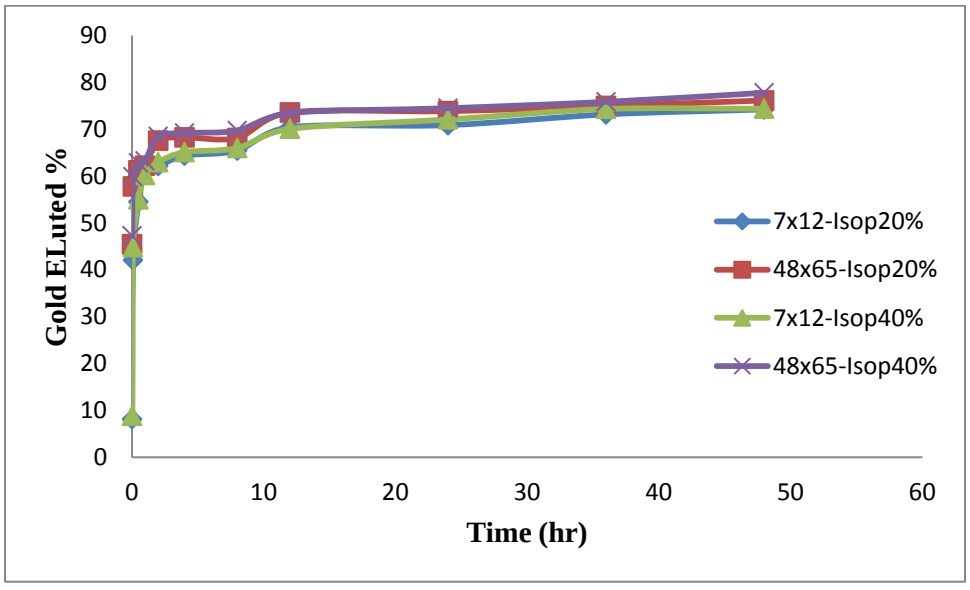

Figure 4.20. Elution of gold loaded activated carbon of two different particle sizes 7x12 mesh and 48x65 mesh using 20% and 40% concentration isopropanol solution at 60°C.

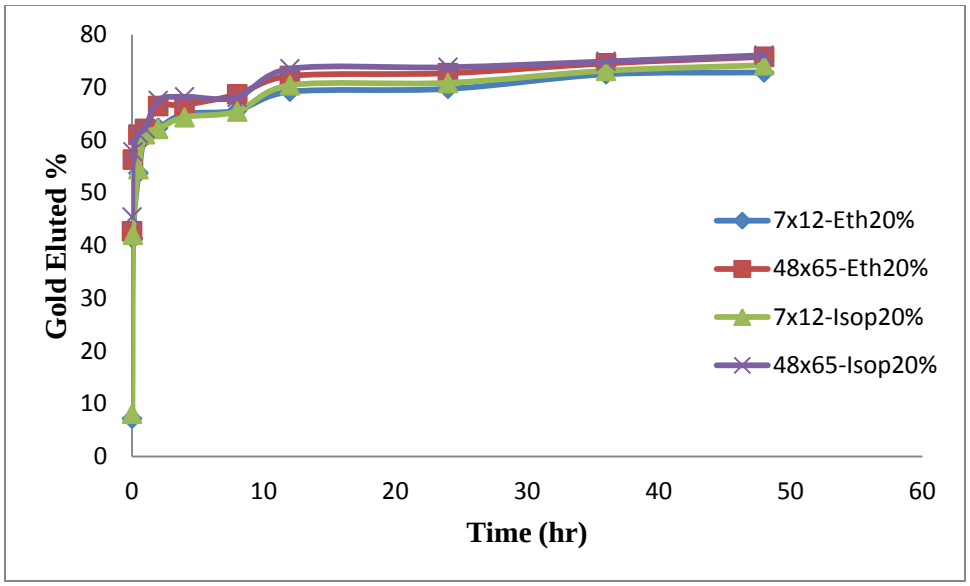

Figure 4.21. Effect of alcohol type on gold elution from activated carbon of two different particle sizes 7x12 mesh and 48x65 mesh using 20% concentration of ethanol and isopropanol, respectively, at 60°C.

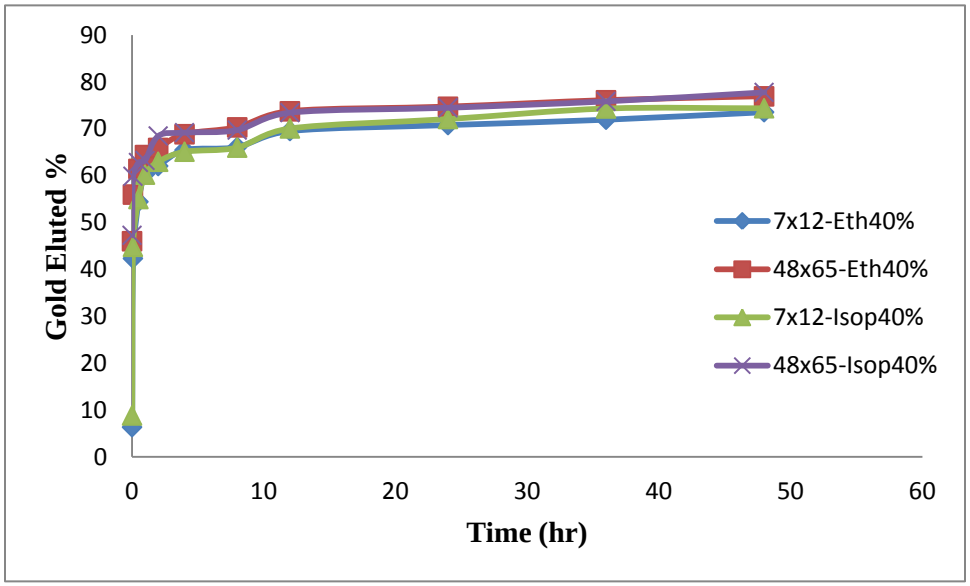

Figure 4.22. Effect of type of alcohol on gold elution from activated carbon of two different particle sizes 7x12 mesh and 48x65 mesh using40% concentration of ethanol and isopropanol, respectively, at 60°C.

It is evident from the results that higher temperature facilitates better stripping, and on an average about 75% gold was eluted. Like in the previous case, the concentration or type of alcohol used did not have a marked impact on the stripping characteristics. On a separate note, isopropanol yielded slightly more gold than ethanol. Here too, the finer activated carbon particles performed better in terms of gold elution than the coarser ones, although the difference was not much. The average percent gold eluted from the coarser particles was approximately 73% while the number was slightly higher at about 77% for the fine particles.

The ability of hydro-alcoholic solutions to cause enhanced gold elution stems from the fact that they have a lower surface tension. This property enables alcohol to penetrate fine pores overcoming the capillary pressures.

Thus, it can be concluded that activated carbon stripping at elevated temperatures dramatically increases gold elution. Also, alcoholic solutions of isopropanol should be used for improved elution properties.

Although 77% gold elution is decent and comparable to the recovery from the atmospheric Zadra procedure for the coarse size fraction, the gold losses considering the unrecovered gold from the activated carbon pores is huge and better processes need to be developed to recover more gold from an economic standpoint.

In this regard, higher temperatures for gold elution could be tried with alcoholic solutions as temperature plays a major role in gold elution. However, higher temperatures with only alcohol pose serious fire hazards due to the high volatility of the alcohol and should be avoided. Hence, to meet the objectives of improved gold elution using higher temperatures, alcohol coupled with Zadra solution was thought of as a potential eluant.

Therefore, in an effort to further improve gold elution, alcohol was coupled with the conventional Zadra stripping procedure. Both ethanol and isopropanol were added separately to the Zadra solution having composition 1% NaOH, 0.5% NaCN, and pH around 12, in 20%, and 40% concentration. The experiments were performed at temperatures near boiling point, i.e., around 98°C. The results are plotted in Figure 4.23 through 4.26. Here too, the results indicate that the concentration of alcohol in the Zadra solution is not a major variable as both 20% and 40% yield similar results. Isopropanol causes a very small increase in percent gold eluted when compared to ethanol.

An average of 81% gold was successfully eluted using this strip solution. The most significant achievement in comparison to conventional Zadra procedure was the improved elution kinetics from fine activated carbon. In the conventional Zadra procedure, about 73% gold was eluted in 48 hours from the coarser 7 x 12 mesh size fraction while almost 62% gold elution was obtained from the finer 48 x 65 mesh size fraction. In contrast, when alcohol coupled Zadra solution was used, almost 80% gold was eluted from the coarser fraction and 81% from the finer fraction for either alcohol, in 48 hours. Although not much for the coarser fraction, a significant improvement was achieved in terms of percent gold eluted from the finer size fraction.

These results seem to satisfy the overall objective of using alcohol for gold elution.

Thus, even though 75% gold elution seemed to be a decent bet, higher gold elution was preferred from an economic feasibility standpoint considering that more than 20% gold losses are huge given the value of the precious metal in the world market.

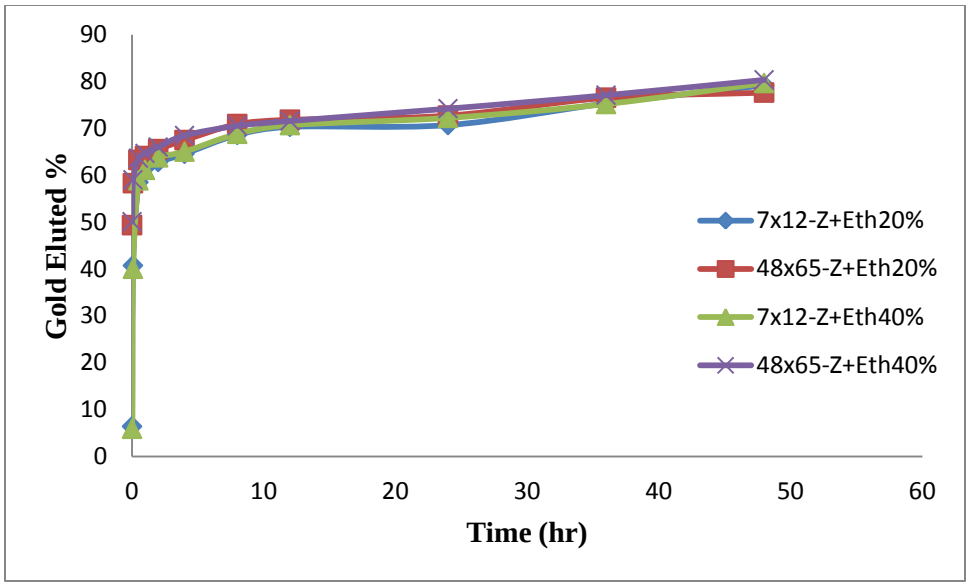

Figure 4.23. Elution of gold loaded activated carbon of two different particle sizes 7x12 mesh and 48x65 mesh using 20% and 40% concentration ethanol + Zadra solution at 98°C.

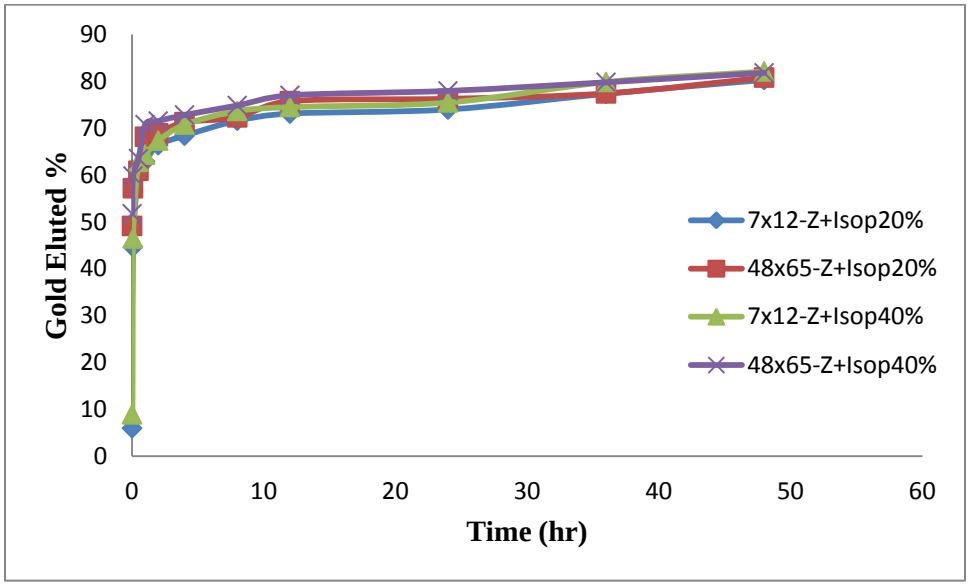

Figure 4.24. Elution of gold loaded activated carbon of two different particle sizes 7x12 mesh and 48x65 mesh using 20% and 40% concentration isopropanol + Zadra solution at 98°C.

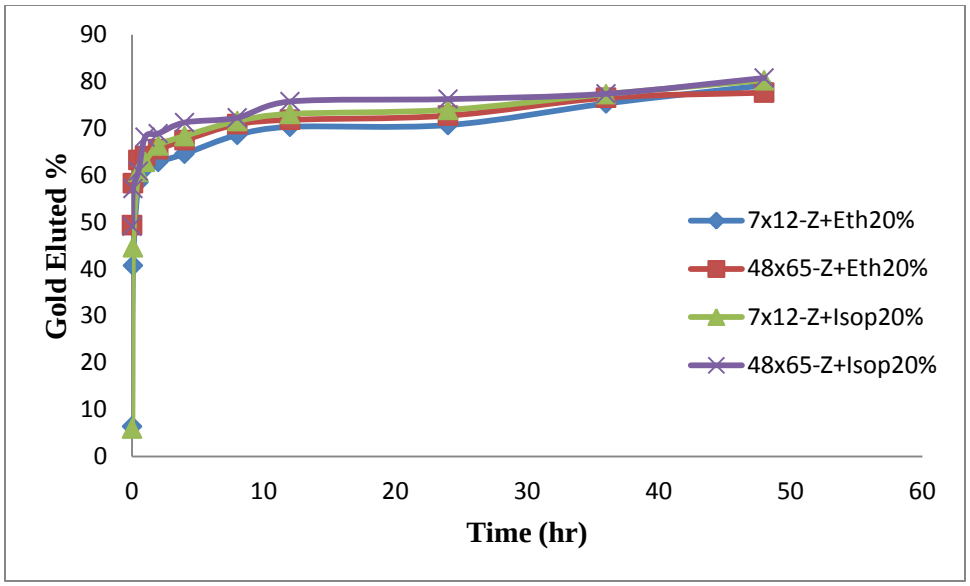

Figure 4.25. Effect of alcohol type on gold elution from activated carbon of two different particle sizes 7x12 mesh and 48x65 mesh using 20% concentration of ethanol + Zadra and isopropanol + Zadra solution, respectively, at 98°C.

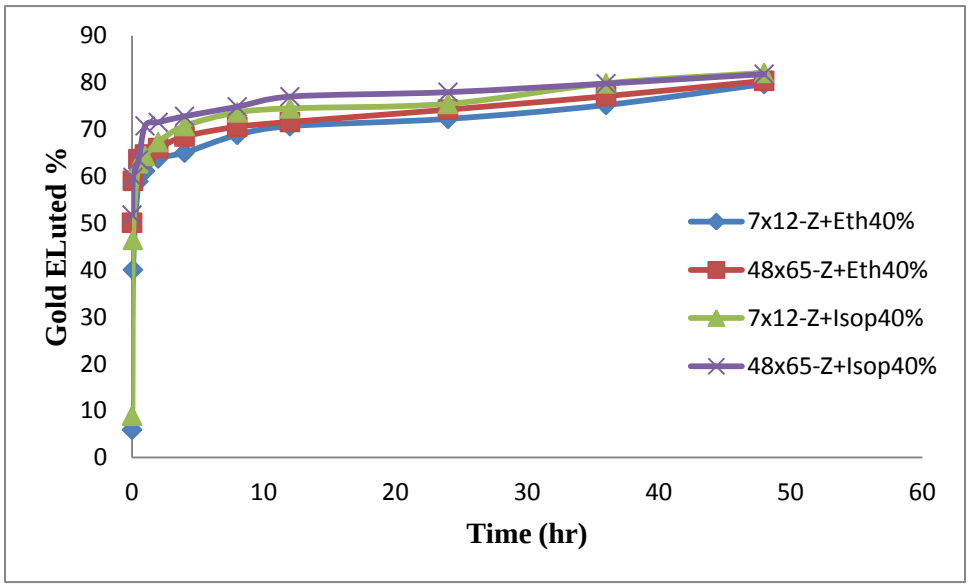

Figure 4.26. Effect of alcohol type on gold elution from activated carbon of two different particle sizes 7x12 mesh and 48x65 mesh using 40% concentration of ethanol + Zadra and isopropanol + Zadra, respectively, at 98°C.

4.2.3.2 Particle Size Effect on Elution Using Vacuum Degassing

Marsden and House (2006) had reported that air or oxygen facilitates gold cyanide adsorption onto activated carbon. Since desorption or stripping is believed to be a reversal of adsorption, vacuum degassing loaded activated carbon prior to stripping should facilitate enhanced elution.

With this belief, loaded activated carbons were vacuum degassed for different exposures of time (0min, 30min, 60min, 90min, 120min, 150min, 180min, 240min, 300min, and 360min) prior to stripping using Zadra solution at 98°C for 48 hours. This was done to optimize the vacuum degassing time required for effective elution. The results from these experiments for the particle size fractions 7 x 12 mesh and 48 x 65 mesh are presented in Figure 4.27 and 4.28, respectively.

The results clearly depict the increase in gold elution with gradual increase in vacuum degassing time for both the size fractions. It is also evident that there is no significant change in percent gold eluted with increase in vacuum degassing time beyond 3 hours (180 minutes). Hence, for all future sets of experiments involving vacuum degassing, the loaded activated carbons were vacuum degassed for 3 hours at -25psi prior to stripping.

Vacuum degassing enables removal of air present in the pores, thereby facilitating gold cyanide elution. Another theory attributed to the increased gold elution due to vacuum degassing the activated carbons is the cavitation effect. Vacuum degassing causes cavitation in the pores of the activated carbon leading to a hot-spot which in turn caused a spike in temperature in the localized region. Higher temperature favors and facilitates enhanced gold elution from the carbon pores.

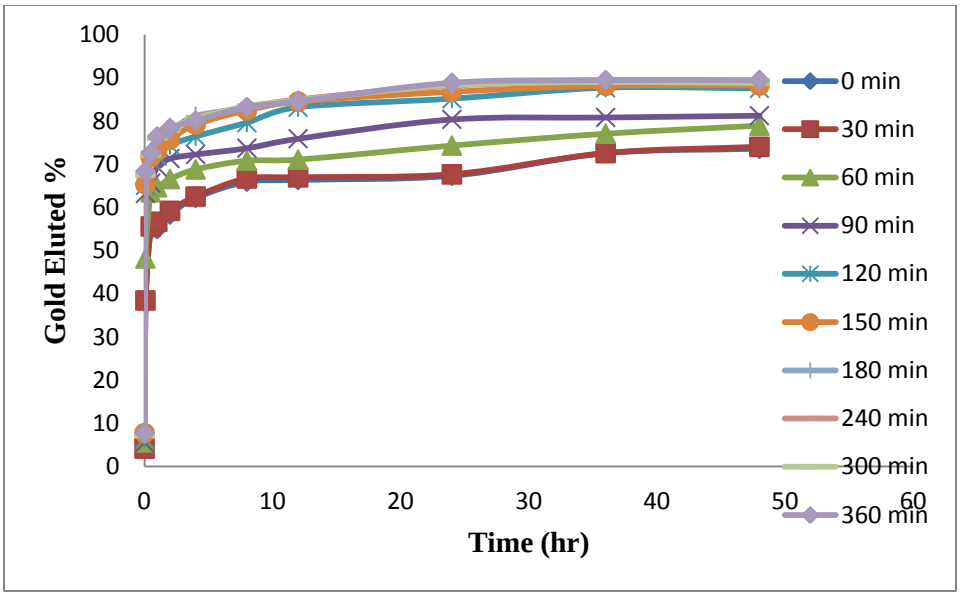

Figure 4.27: Effect of vacuum degassing time on gold elution for 7 x 12 mesh size fraction using Zadra solution at 98°C.

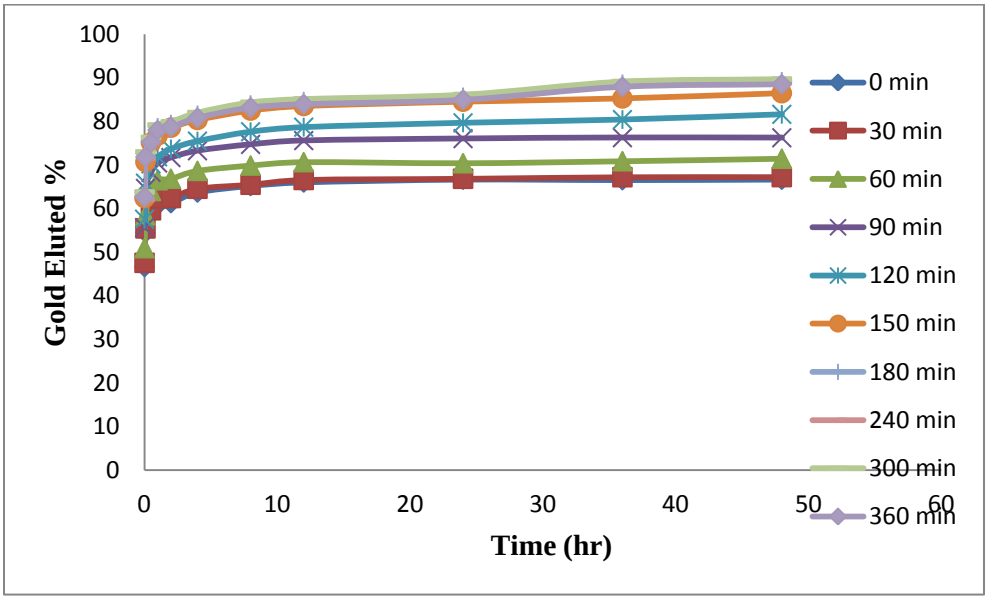

Figure 4.28.Effect of vacuum degassing time on gold elution for 48 x 65 mesh size fraction using Zadra solution at 98°C.

The particle size effect on gold elution involving vacuum degassing is illustrated in Figure 4.29. The stripping results without degassing and with 3 hours of vacuum degassing prior to elution were isolated and plotted separately. In the conventional Zadra procedure, i.e., without degassing, about 73% gold was eluted in 48 hours from the coarser 7 x 12 mesh size fraction while almost 62% gold elution was obtained from the finer 48 x 65 mesh size fraction. In contrast, when the gold loaded activated carbon was vacuum degassed for 3 hours before stripping with Zadra solution for 48 hours, almost 89% gold was eluted from the coarse and fine size fraction alike. This was significant improvement in terms of percent gold eluted for both the size fractions.

These results justify the use of vacuum degassing loaded carbon prior to gold elution.

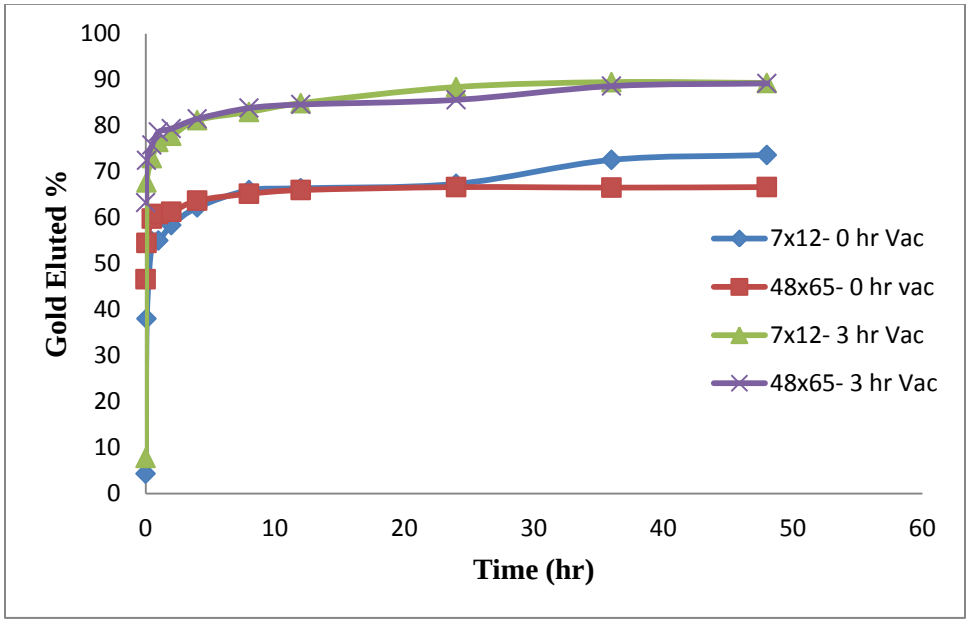

Figure 4.29.Particle size effect on gold elution with 3 hours of vacuum degassing prior to stripping and without degassing using Zadra solution at 98°C.

Hydro-alcoholic solutions of ethanol and isopropanol of 20% concentration were also tried for stripping activated carbon involving vacuum degassing. It was shown in the previous section that the concentration of alcohol did not have a significant effect on amount of gold eluted; hence for economical purposes, 20% alcoholic solution was used. The loaded activated carbons of the two size fractions (-7 +12 mesh) and (-48 +65 mesh) were vacuum degassed for 3 hours prior to stripping. The stripping experiments were carried out at 60°C on the basis of the results shown in the previous section, which showed improved elution over stripping at room temperature. The results as depicted in Figure 4.30 and 4.31, clearly show higher percent gold eluted with 3 hours of vacuum degassing prior to stripping for both particle size fractions. Though isopropanol yielded slightly more gold, an average of 74% gold was eluted without degassing and 84% with vacuum degassing (as shown in Figure 4.32) considering both the size fractions. A closer inspection will reveal slightly higher elution from the fine particle size fraction.

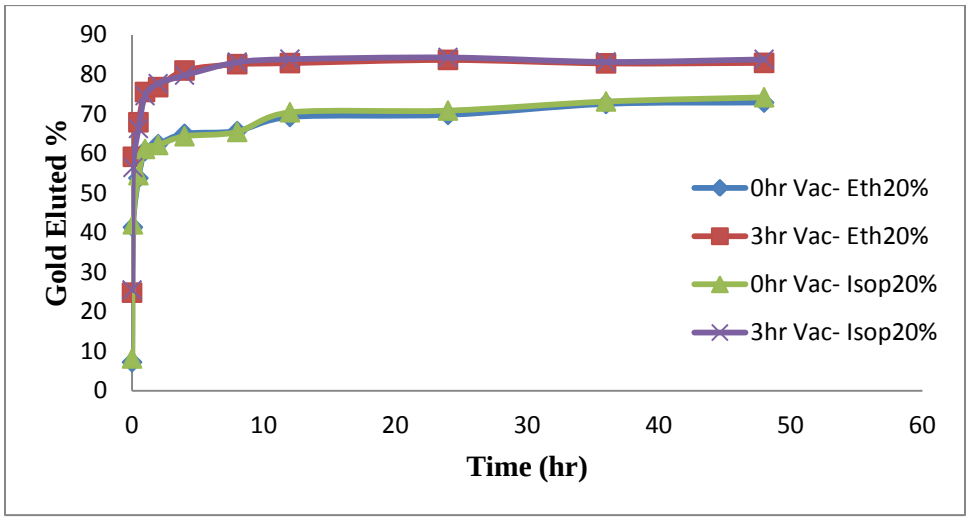

Figure 4.30. Gold elution with 20% alcoholic solution of ethanol and isopropanol at 60°C without and with vacuum degassing for 3 hours for coarser 7 x 12 mesh size fraction

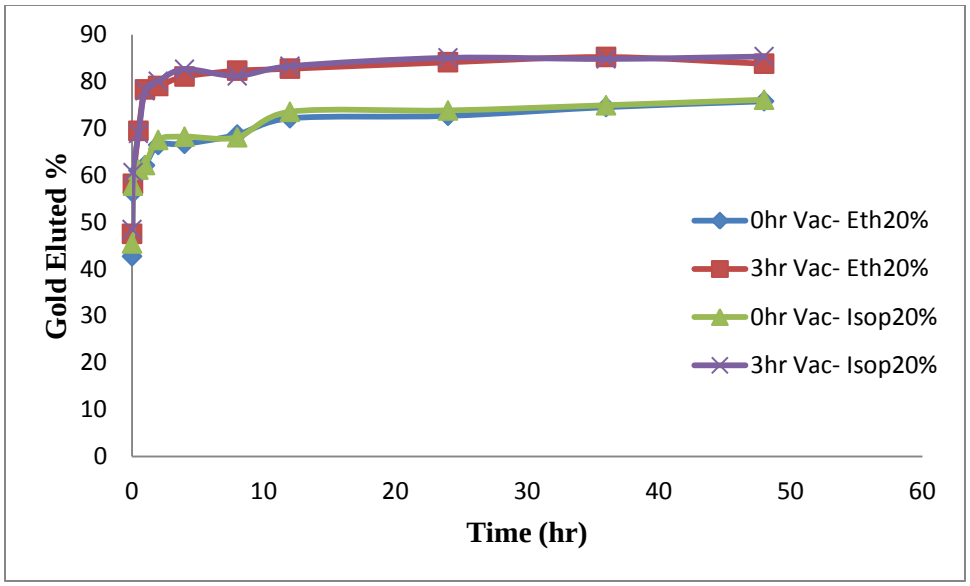

Figure 4.31. Gold elution with 20% alcoholic solution of ethanol and isopropanol at 60°C without and with vacuum degassing for 3 hours for finer 48 x 65 mesh size fraction

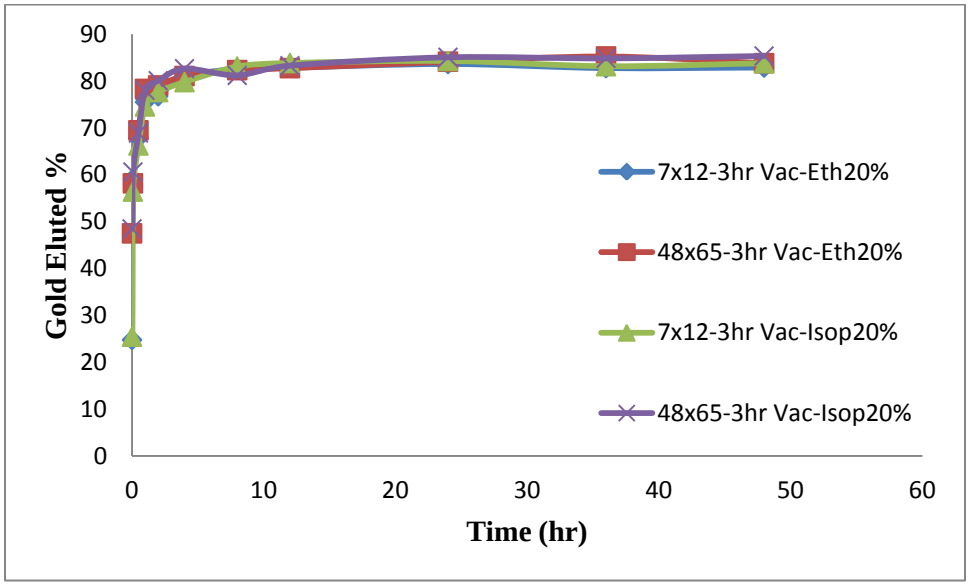

Figure 4.32.Particle size effect on gold elution with 20% alcoholic solution of ethanol and isopropanol at 60°C and 3 hours of vacuum degassing prior to stripping.

Further, in an attempt to try elution at higher temperatures, Zadra coupled with hydro-alcoholic solutions of ethanol and isopropanol of 20% concentration were also tried for stripping activated carbon involving vacuum degassing. 20% alcoholic solution was used in each case based on previous results. The loaded activated carbons of the two size fractions 7 x 12 mesh and 48 x 65 mesh were vacuum degassed for 3 hours prior to stripping. The stripping experiments were carried out at 98°C. The results as depicted in Figure 4.33 and 4.34, clearly show higher percent gold eluted with 3 hours of vacuum degassing prior to stripping for both particle size fractions as compared to without vacuum degassing. Isopropanol resulted in slightly greater gold elution. An average of 79% gold was eluted without degassing, whereas almost 89% gold elution was achieved with vacuum degassing (as shown in Figure 4.35) considering both the size fractions. As in the previous case, a closer inspection will reveal slightly higher elution from the fine particle size fraction in comparison to the coarse one.

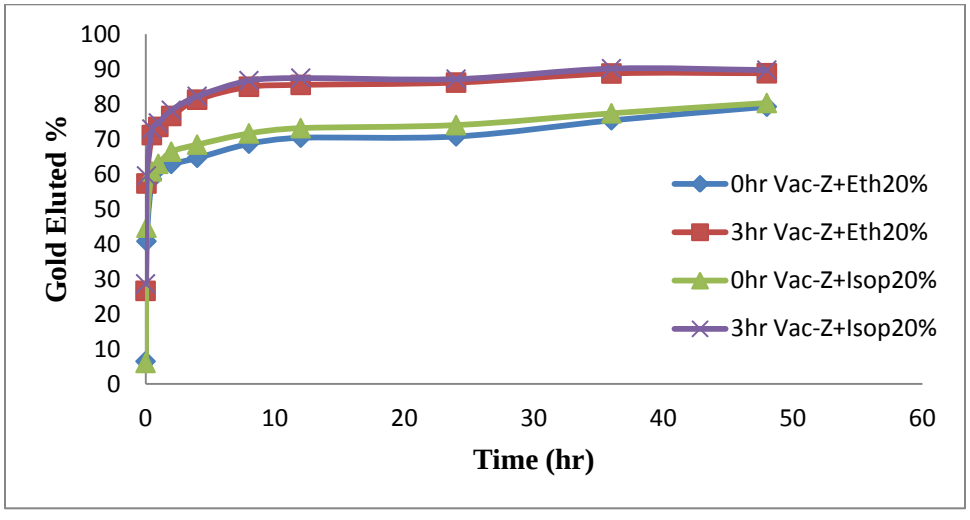

Figure 4.33. Gold elution with Zadra + 20% alcoholic solution of ethanol and isopropanol at 98°C without and with vacuum degassing for 3 hours for coarser 7 x 12 mesh size fraction

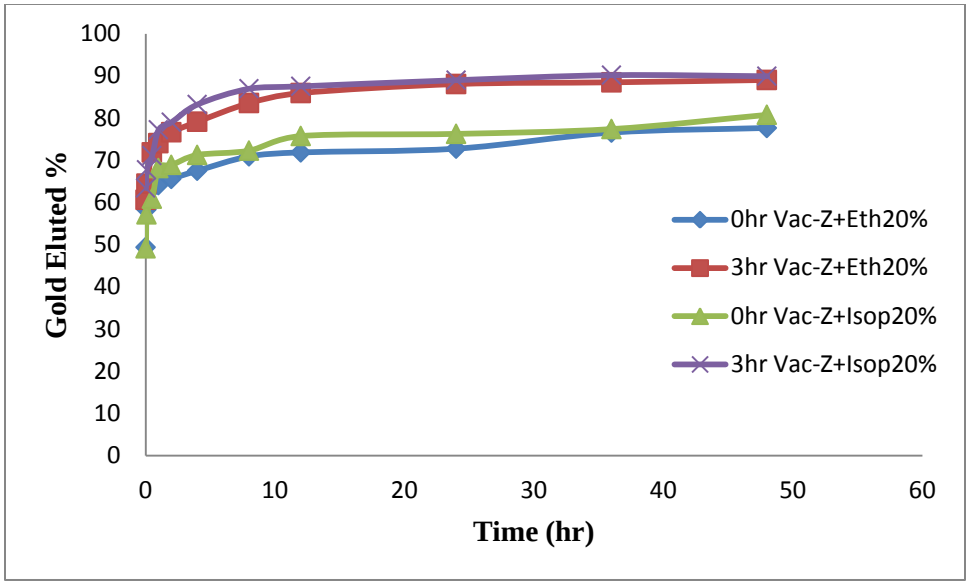

Figure 4.34. Gold elution with Zadra + 20% alcoholic solution of ethanol and isopropanol at 98°C without and with vacuum degassing for 3 hours for finer 48 x 65 mesh size fraction

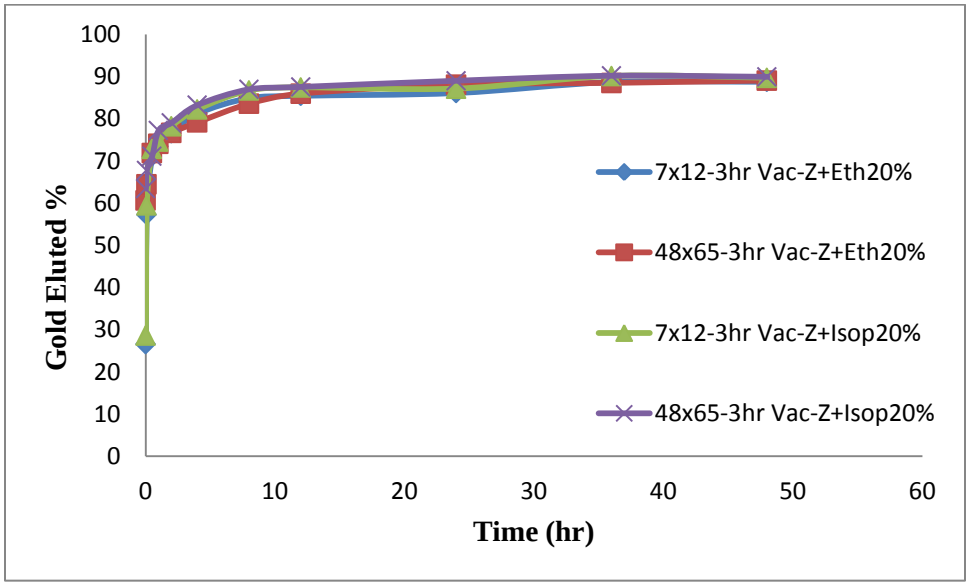

Figure 4.35.Particle size effect on gold elution with Zadra + 20% alcoholic solution of ethanol and isopropanol at 98°C and 3 hours of vacuum degassing prior to stripping.

Table 4.3 summarizes the results of gold elution for the two size fractions with different stripping solutions coupled without and with 3-hour vacuum degassing prior to elution. The values given represent the percent gold eluted after 48-hours stripping.

As can be seen, this is a significant increase over stripping with the same solutions involving vacuum degassing. Clearly, for all the different stripping solutions tried, the percent gold eluted has been enhanced significantly with the application of vacuum degassing for 3 hours prior to gold elution. Also, almost 90% gold was eluted with Zadra solution and Zadra + 20% isopropanol solution coupled with vacuum degassing.

Hence, for most practical applications, if the loaded activated carbon is degassed for 3 hours prior to stripping, only Zadra solution will suffice as an effective eluant. Based on the research findings in this subsection, vacuum degassing the loaded activated carbon prior to stripping can be considered as a major contribution to the gold hydrometallurgy. Also, vacuum degassing is recommended as a potential pretreatment step for the industries involved in gold elution using activated carbon.

Table 4.3. Summary of percent gold eluted in 48 hours with different solutions at the temperatures mentioned, without and with 3 hours of vacuum degassing prior to stripping.

7x12 - 0hr Vac				**48x65 - 0hr vac**		
Isop 20% (60 C)	**Zadra (98 C)**	**Z + Isop 20% (98 C)**		**Isop 20% (60 C)**	**Zadra (98 C)**	**Z + Isop 20% (98 C)**
74.19	73.59	80.26		76.11	66.63	80.77
7x12 - 3hr Vac				**48x65 - 3hr vac**		
Isop 20% (60 C)	**Zadra (98 C)**	**Z + Isop 20% (98 C)**		**Isop 20% (60 C)**	**Zadra (98 C)**	**Z + Isop 20% (98 C)**
83.79	89.25	89.67		85.35	89.17	89.92

4.2.3.3 Particle Size Effect on Elution Using Filter Press

The Zadra stripping solution was used for this method of stripping to investigate the effect of carbon particle size and other procedure variables such as temperature and pressure on the elution rate. Again it was expected that the stripping reaction will be inversely dependent on the carbon particles and directly dependent on the temperature of the strip solution. The Zadra stripping solution was studied at three different temperatures; room temperature, 60^{o}C, and 98^{o}C. A total of 4 bed volumes (a bed volume is taken as 1 L) of strip solution was used for each of the samples stripped at 25, 60, and 98^{o}C, respectively. The stripping occurred at less than a minute per bed volume.

Table 4.4 and Figure 4.36 are results presented for the pressure Zadra stripping solution. The effect of particle size and temperature on the rate of gold elution is shown in Tables 4.4 and Figure4.36,which demonstrate that particle size has an effect on the stripping of gold cyanide from activated carbon. It is apparent from Table 4.4 that as activated carbon particle size decreases, the rate of gold elution increases; reinforcing the expectation that the rate of gold cyanide desorption from activated carbon is inversely dependent on activated carbon particle size.

Table 4.4**.**Effect of particle size and temperature on percent gold eluted by the Filter Press Method using Zadra solution at different temperatures.

	Percent gold eluted after 4 bed volumes	
Temp (°C)	**(7 x12 mesh)**	**(48 x 65 mesh)**
25	0.9	8.9
60	16.7	69.41
98	28.9	98.3

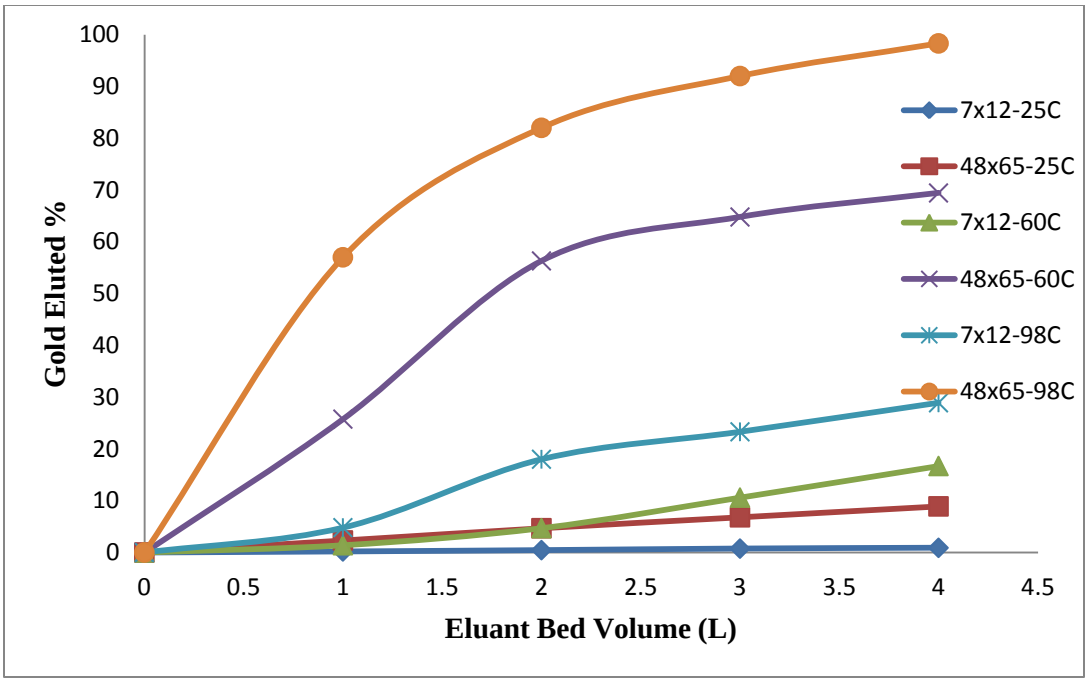

Figure 4.36.Effect of particle size and temperature on elution of activated carbons by the Filter Press Method using Zadra solution at different temperatures.

The effect of temperature on the stripping reaction is also evident in Figure 4.36 and Table 4.4. It is clear from Table 4.4 that the rate of gold cyanide elution is dependent on temperature. It is observed that as the stripping temperature decreases from 98^{o}C to 25^{o}C, the elution reaction rate decreases significantly. These results reinforce the belief that the stripping of gold cyanide from activated carbons is favored by both increasing temperature of the strip solution, application of pressure, and decreasing particle size of the carbon.

It is worth noting that, even though a pressure of 80 psi was applied to the Zadra solution at room temperature, the percent gold eluted was less than 10. This suggests that pressure alone is not sufficient to drive the elution reaction and that temperature plays a prominent role.

4.2.3.4 Particle Size Effect on Elution Using Syringe Pump

The syringe pump was used to force strip solution at flow rates of 1, 2.5, 5, and 15 ml/minute and a calculated minimum pressure of about 2.5 psi (corresponding to 1 ml/min) and a maximum of around 36 psi (corresponding to 15 ml/min) through a bed of loaded carbon samples in a syringe. The expectation will be in lines with the filter press stripping method, i.e., the stripping reaction under this method of stripping will be inversely dependent on particle size. The results for the syringe pump elution are presented in Figure 4.37. Figure 4.37represents the stripping of loaded activated carbon with Zadra solution [1% NaOH and 0.5% NaCN] at 98^{o}C for both the size fractions 7 x 12 mesh and 48 x 65 mesh under different solution flow rates. A 0.45 μm filter membrane attached to the end of the syringe was used for all the stripping experiments in order to prevent all activated carbon particles (especially the fine particles) from falling into the solution.

25 ml bed volume cycle was used to strip the loaded carbon using 1L Zadra solution. 25 ml bed volume cycle was selected as a batch to avoid drastic drop in the solution temperature over the course of the elution procedure. Especially, at lower flow rate, more efforts were taken to ensure that the solution temperature in the syringe does not change much over time during the batch cycle.

The results presented are the percent gold eluted after 40 bed volumes for the four different flow rates tried. Again, as in the preceding section, Figure4.37 shows a trend in the stripping procedure. It is evident from Figure 4.37 that the size of carbon particles does have an effect on the rate of stripping, with the finer activated carbon samples eluting faster

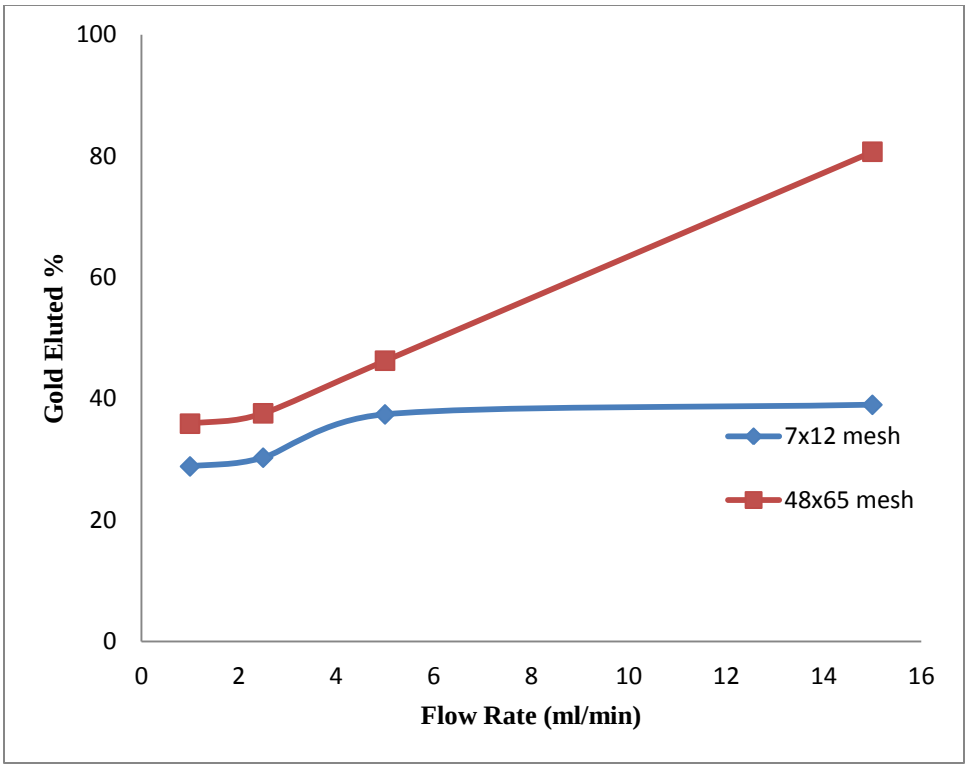

Figure 4.37.Effect of particle size on elution of activated carbons by the Syringe Pump Method using Zadra solution at different flow rates.

than the coarser samples; demonstrating that the rate of elution of gold cyanide from AC is strongly influenced by carbon particle size.

The results clearly indicate that with increase in flow rate or applied pressure, gold elution increases significantly from the finer activated carbon particles. After 40 bed volumes, almost 81% gold is recovered from the finer particles in contrast to 39% from the coarser particles at 15 ml per minute flow rate (or 36 psi pressure) using Zadra solution at 98°C.

Again the results of this section reinforce the results of the preceding section that the stripping reaction is inversely dependent on carbon particle size with the application of external pressure.

4.3 Summary

Several traditional and alternative activated carbon stripping techniques have been experimentally tested and explained in this chapter. This chapter seeks to explain the particle size effect of activated carbon on gold elution and a summary of the stripping of coarse (7x12 mesh) and fine (48x65 mesh) fractions of activated carbon is presented in Table 4.5. Prior to stripping, activated carbons of ten different size fractions were loaded with 250 ppm gold. It was observed that the ultimate gold loading on activated carbon was independent of particle size and these results were in good agreement with the specific surface area and adsorption capacity of activated carbon, as reported in Chapters 2 and 3. The BET surface area was also independent of the particle size and contributes primarily to gold adsorption. It is also very interesting to note that only about 1% of total surface area is used for gold cyanide adsorption. Due to the wide distribution of pore size and expected variation in adsorption site functionality, explaining adsorption and desorption of gold cyanide in micropores is a challenge and needs further research.

Traditional Mintek and atmospheric Zadra elution procedures were performed on the loaded activated carbon for all size fractions. Coarse, granular activated carbon exhibited higher gold elution than the finer size fractions. For both methods, it was observed that the percent gold eluted increased initially with decrease in particle size. With further decrease in particle size beyond 35 mesh, gold elution dropped significantly. For comparison to other elution techniques, elution results for coarse (7x12 mesh) and fine (48x65 mesh) activated carbons are summarized in Table 4.5.

In the case of stripping using hydro-alcoholic solutions of ethanol and isopropanol, the same extent of elution for coarse (7x12 mesh) and fine (48x65 mesh)

Table 4.5.Summary of the extent of elution from various traditional and alternative gold stripping procedures.

Procedure	Extent of Stripping (%)	
	7x12 mesh	48x65 mesh
Traditional Procedures		
Mintek - 98°C - 1 hr	67.29	25.19
Atmospheric Zadra (Z) - 98°C - 48 hr	73.59	66.63
Alternative Procedures		
Ethanol 20% - 25°C - 48 hr	29.11	31.67
Ethanol 40% - 25°C - 48 hr	28.08	31.45
Isopropanol 20% - 25°C - 48 hr	29.43	31.21
Isopropanol 40% - 25°C - 48 hr	30.53	32.29
Ethanol 20% - 60°C - 48 hr	72.84	75.79
Ethanol 40% - 60°C - 48 hr	73.54	76.91
Isopropanol 20% - 60°C - 48 hr	74.19	76.11
Isopropanol 40% - 60°C - 48 hr	74.38	77.77
Zadra+ Ethanol 20% - 98°C - 48 hr	79.21	77.64
Zadra+ Ethanol 40% - 98°C - 48 hr	79.68	80.37
Zadra+ Isopropanol 20% - 98°C - 48 hr	80.26	80.77
Zadra+ Isopropanol 40% - 98°C - 48 hr	82.06	81.79
Vac(3hr) + Zadra - 98°C - 48 hr	89.25	89.17
Vac(3hr) + Ethanol 20% - 60°C - 48 hr	82.88	83.81
Vac(3hr) + Isopropanol 20% - 60°C - 48 hr	83.79	85.35
Vac(3hr) + Zadra+ Ethanol 20% - 60°C - 48 hr	88.75	89.01
Vac(3hr) + Zadra+ Isopropanol 20% - 60°C - 48 hr	89.67	89.92
Filter Press @80psi + Zadra - 98°C - 4 bed volumes	28.91	98.31
Syringe Pump @15 ml/min + Zadra - 98°C - 40 bed volumes	39.11	80.71

activated carbons was achieved. Almost 81% gold was eluted at 98°C using Zadra + alcoholic solution. For all the cases, fine carbon particles yielded slightly more gold than the coarser ones. Although there was not much difference in the type of alcohol or the concentration of the alcohol used, isopropanol at 20% concentration coupled with Zadra solution can be used for most practical reasons.

In the case of stripping using vacuum degassing, both coarse (7x12 mesh) and fine (48x65) activated carbons were well eluted. The extent of elution was independent of activated carbon particle size. 84% gold elution was obtained with vacuum + alcoholic solution while 89% gold was eluted with vacuum + Zadra solution after 3 hours of vacuum degassing prior to elution. Almost 90% gold elution was possible with vacuum + Zadra + alcohol solution.

In the case of pressure stripping (using filter press and syringe pump) using the Zadra solution, excellent elution of the fine activated carbon was achieved, whereas stripping of the coarse activated carbon was not successful, as evident from Table 4.5. The low elution from coarse particles may be due to the small residence time in pressure conditions under which the gold cyanide has to traverse long tortuous paths inside the carbon particles. The pressure experiments were done to simulate conditions in some industries which favor elution under pressure and higher temperatures. Further research in this direction is needed to fully understand the pressure effect on stripping activated carbon particles of various size fractions.

Table 4.5 presents the comprehensive results of the different elution procedures tried in this chapter; it also provides a comparison for the extent of gold elution from traditional and alternative procedures discussed in this chapter.

CHAPTER 5

SIGNIFICANCE OF GRAPHITE SURFACES IN GOLD ADSORPTION

Since the graphitic microstructure of activated carbon has been established and is well reported in literature (Riley, 1947), the adsorption and desorption results are discussed in terms of the surface characteristics of graphite. A separate study of graphite surface chemistry is in progress and current results are used for discussion of the surface state of adsorbed gold cyanide and the adsorption and desorption reaction.

A lot has been said regarding the use of activated carbon for gold recovery from cyanide leach pulps. Over the years, several mechanisms have been proposed and refuted. Mechanisms such as reduction of gold to metallic state during carbon adsorption and partial reduction of gold and formation of gold clusters (McDougall et al., 1980) have fallen out of favor. Although activated carbon adsorption of the gold cyanide complex without chemical change finds some support, the most current accepted theory is the adsorption of ion pairs as the predominant mechanism under high ionic strength alkaline conditions. However, even though the mechanism is somewhat clear, the adsorption site on the carbon surface has intrigued researchers over the years.

It has been established that activated carbon predominantly has a graphitic structure (similar but less ordered structure than that of graphite). X-ray studies of

graphite have revealed small regions of elementary crystallites, composed of roughly parallel layers of hexagonally ordered atoms. These crystallites are disordered, cross-linked, spaced lattice of carbon hexagons. Jones et al. (1989) had proposed that the gold cyanide complex is reversibly adsorbed by the hexagonal carbon ring structure of the face surface of the cryptocrystalline graphite crystallites present in activated carbon. This adsorption was believed to have been facilitated by the bonding between the gold atom and the π electrons of the graphite ring structure. However, based on XPS results, it was analyzed that no interactions had taken place with the oxygen containing functional groups. Overall, this mechanism supported the concept of adsorption of gold cyanide complex without chemical change but did not provide much evidence to support formation of ion pairs. This mechanism of the gold cyanide complex fitting perfectly into the hexagonal ring structure of graphite was criticized by Sibrell and Miller (1992), who said that the ionic radius of cyanide ion (1.92 Å) is much greater than the sum of the covalent radius of carbon and nitrogen. Cashion et al. (1988) proposed on the basis of Mossbauer spectroscopic results that adsorption of the gold cyanide complex occurred via bonding of the nitrogen atoms rather than the gold atoms. In another study, Cook et al. (1989) provided XPS evidence of the presence of AuCN on loaded carbon. This was justified by the low pH of the solution where gold cyanide is formed. Although these evidences attempted to provide a plausible explanation, there was no general consensus on the exact mechanism for gold adsorption on activated carbon.

Miller and Sibrell (1991) did significant work in further emphasizing the importance of graphitic structure of activated carbon on gold adsorption. They found out through experimentation that the gold adsorption densities on graphite, carbon black, and

activated carbon were comparable whereas gold adsorption by diamond could not be detected. From these results, it was inferred that the graphitic structure common to the first three materials played a significant role in gold adsorption.

After establishing the role of graphitic structure in gold adsorption, Miller and Sibrell (1992) focused on the basal planes and edges of the graphite sheets to accurately determine the adsorption sites. It was believed that though graphite, carbon black, and activated carbon had graphitic structure, the arrangement of face and edge surfaces would be random, thereby causing difficulty to analyze the adsorption sites. Hence, highly oriented pyrolytic graphite (HOPG), having almost defect free face and edge surfaces, was used for their analysis. On the basis of experiments performed through counting of radiolabelled samples, autoradiography, and x-ray photoelectron spectroscopy, Sibrell and Miller (1992) determined that adsorption of gold cyanide complex by graphitic carbonaceous material, is much greater at the edges of the graphitic planes than on the planes themselves. They concluded that site-specific adsorption is prevalent in the adsorption of gold by graphitic carbons and most of the favored sites are the edges or edge defects in the graphite crystal structure. Further, they believed that for the ion pair adsorption, van-der-Walls forces were involved and unsymmetrical distribution of charge at the edge defects also played an important role.

Limat et al., (2009) synthesized gold nanoparticles on highly oriented pyrolytic graphite (HOPG) electrodes. They found that most of the particles nucleate at step edges which provide the strongest nucleation sites. They explained that the basal plane of HOPG having all carbon bonds saturated is extremely inert with a small energy barrier

for atom diffusion. Consequently, it is difficult to stabilize nanoparticles on the surface terraces and aggregation takes place at monoatomic step edges.

These evidences suggest that gold cyanide has a tendency to be accommodated at the graphite edge surfaces.

Current research on graphite surface chemistry is in progress and results have been obtained including fundamental wetting characteristics studies accomplished through contact angle measurements of the as-received HOPG single crystal, which was characterized by its distinct face and edge surfaces. To simulate the actual conditions of graphitic layers in activated carbon which contains functional groups, contact angle measurements were repeated on the HOPG face and edge surfaces oxidized with different concentrations of hydrogen peroxide.

Further, Raman spectroscopic studies were performed on the as-received and oxidized HOPG surfaces.

Surface charge is an important property of graphite which dictates several phenomena, including gold adsorption. In this regard, zeta potential measurements of graphite powder in solutions of varying pH were also done to determine its iso-electric point and compare to the values reported in literature for graphitic carbon materials.

From a more realistic approach standpoint, atomic force microscopy (AFM) was used for surface force measurements to determine the iso-electric point (IEP) of the face and edge surface of HOPG as compared to the iep of the amorphous graphite powder.

Finally, molecular dynamics simulations (MDS) was performed to further enhance our understanding of the adsorption of gold cyanide complex on the graphite surfaces.

5.1 Surface Chemistry Experiments

5.1.1 Contact Angle Measurements at Graphite (HOPG) Face and Edge Surfaces

The wettability of HOPG face and edge surfaces before and after oxidation by H_2O_2 has been determined by measuring the contact angle using the captive bubble technique. The effect of pH on contact angle (standard deviation ±2.0°) at the face surface and edge surface of HOPG is displayed in Figure 5.1. The hydrophobicity of the edge surface decreases with increase in pH but there is little change in contact angle with pH for the face surface of HOPG.

Results reported in the literature show that electrokinetic data for nonpolar surfaces change depending on solution pH. The H^+ and OH^- are considered to be the

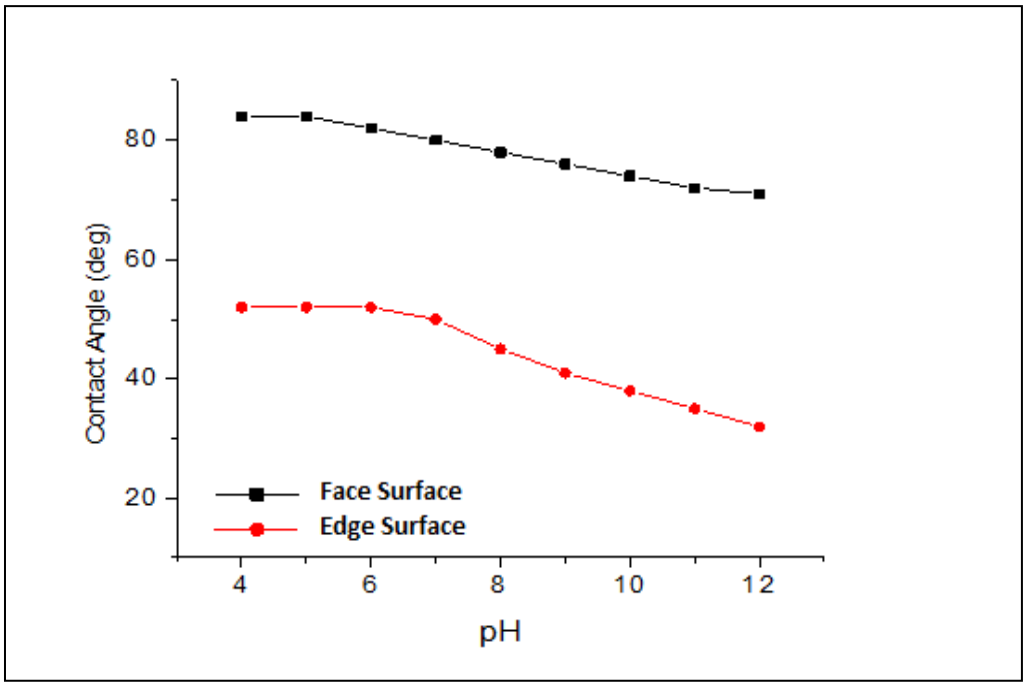

Figure 5.1 - The effect of solution pH on the contact angle at face and edge surfaces of HOPG

potential determining ions for the nonpolar-aqueous interfaces (Healy and Fuerstenau, 1965). In this way, the surface charge density of hydrophobic surfaces changes depending on solution pH. Therefore, decrease in the contact angle with increasing pH suggests that increased adsorption of hydroxide ions facilitates hydrogen bonding at the surface and slightly improved wetting at the face surface.

Quite contrary to the variation in contact angle at the face surface, the contact angle at the edge surface shows a significant decrease with increasing pH (Figure 5.1). This might be attributed to the greater number of hydroxyl functional groups at the edge surface at higher pH. Depending on the pH, the contact angle variation of the graphene edge surface was investigated by Konkena and Vasudevan (2012). Their results show that negative charges form stable dispersion at the edge surface above pH 8. As the pH increases, ionization of the carboxylic acid groups increases on the edge and it is primarily responsible for the presence of these groups together with phenolic and hydroxyl groups. Therefore, superior water dispersibility occurs on the edge. Especially, after pH 9 and above, the value of contact angle decreases much. Also, this can be explained by ketone groups which are found at the edge surface for alkaline pH values. Above pH 9, the OH anion is stabilized by a phenolate to ketone transformation due to the ionization of the phenolic OH which has built up sufficient charge at the edge surface to form stable dispersions (Konkena and Vasudevan, 2012). Briefly, it can be said that the reactivity of water is significantly large at the edge and definitely more than on the face plane and a strong interaction energy occurs between the water and edge (Zhu et al., 2002).

Reaction of oxygen is the key to determine the wetting characteristics of graphite surfaces. Oxidation of carbon brings about a significant change in its physiochemical properties and as a result, the wettability and adsorption properties of such surfaces are affected. The surfaces of edge and face plane of graphite were oxidized using H_2O_2 (at different concentration and for different exposure time). The contact angle values for the face surface and for the edge surface of HOPG untreated and treated with H_2O_2, are given in Table 5.1.

In the absence of H_2O_2, the contact angle measurements show that the face surface is hydrophobic (82°) and the edge surface is less so (54°). It appears that stronger water binding capacity occurs at the edge surface. It is expected that the hydrogen of the terminal C-H bond at the edge surface interacts with the oxygen of the water molecule. On the face surface, hydrogen atoms of water are oriented toward the center of the hexagonal graphite ring structure but water molecules do not remain at the graphite face surface. Table 5.1 shows that on the basis of the contact angle measurement (the standard

Table 5.1. The contact angle values at the face surface and edge surface of untreated HOPG surfaces and surfaces treated with H_2O_2 at natural pH and 22°C.

	face surface			**edge surface**		
	15 min	**30 min**	**1 hr**	**15 min**	**30 min**	**1 hr**
No oxidation	82	82	82	54	54	54
Oxidation with 10% H_2O_2, 22° C	82	78	77	50	44	43
Oxidation with 20% H_2O_2, 22° C	78	77	76	47	43	42
Oxidation with 30% H_2O_2, 22° C	76	76	75	44	41	39

deviation was ±4.0° for the face surface, ± 2.0° for the edge surface), both surfaces oxidize gradually but the edge surface of HOPG seems to be more oxidized than the face surface due to the enhanced activity of the edge surface. The oxidation occurred at the edges of graphitic planes and the carbon edge surface is more hydrophilic due to the presence of acidic groups. Slight difference in the contact angle of the HOPG face surface can be explained by the difference in the extent of oxidation at the step defects on the HOPG face surface (Sorescu et al., 2001). It has been established that the oxygen reacts with carbon surfaces in two major steps: the molecular oxygen is activated on carbon surfaces and subsequently, the stabilized species forms covalent bonds with the carbon atoms. (Schlögl et al., 1990; Schlögl, 1997).

Previous studies by Sorescu et al. (2001) suggest that the interaction of molecular oxygen with carbon is predominantly of van-der-Waals type. The energy difference between the unoccupied states of oxygen and the valence band of graphite is on the order of only a few tenths of an eV and this contributes significantly to the non reactivity of the graphite face surface. A transformation of the unoccupied oxygen state can bring about reaction between oxygen and graphite. However, such a transformation in terms of lowering of the oxygen states is prevented by a kinetic barrier. Such a kinetic barrier can be overcome by physisorption of the oxygen molecules on defect sites, such as defects, kinks or edge planes. It can be said that the hydrophobic properties of face surface is likely to be changed by the effects of edge plane defects.

Aforementioned, the edge surface has high oxidation due to its activity. The oxidation of a carbon surface occurs by only a single step during the direct collision of an oxygen molecule with the reactive edges (armchair or zig-zag) of the graphene sheet and

results in the formation of carbon-oxygen functional groups. In addition, Zhu et al., (2002) studied that water can adsorb on the pure carbon edge sites without the requirement of preexisting hydrophilic functional groups. They mentioned that for water adsorption, functional groups would be helpful but they are not a necessity, since the edge sites are active. It means that the edge surface already has some hydrophilic properties and this hydrophilicity increases due to the oxidation process in which oxygen atoms react with the edge surface and with defects and thereby, different kinds of functional groups (phenolic, carboxylic, and ketonic) can be formed. Therefore, the edge surface shows a less hydrophobic character (Boehm, 2002).

5.1.2 Raman Studies of Graphite (HOPG) Face and Edge Surfaces

To improve our understanding of the nature of graphite surfaces and the effect of oxidation, Raman spectra of face and edge surfaces of as-received and oxidized forms are given in Figure 5.2 through Figure 5.5, respectively. The Raman spectrum consists of mainly two regions, 1100 – 1800 cm-1 (first-order) and 2200 – 3400 cm-1 (second-order) for carbon materials (Tuinstra and Koening, 1970; Cuesta et al., 1994). However, in the literature, face and edge surfaces of HOPG are generally evaluated and compared with each other considering the peaks at 1360 cm^{-1} and 1580 cm^{-1} (Katagiri et al., 1988). In this regard, Tuinstra and Koening (1978) defined these two peaks as the D band for disorder and the G band for ordered graphite structure, respectively.

Figure 5.3 shows that there is no noticeable difference in intensity between the specific Raman bands, 1578 cm^{-1} (G band), 2437 cm^{-1} (2LO band), 2721 cm^{-1} (G` band), and 3246 $cm^{-1}$ (2D` band) belonging to the HOPG face surface. Results reported in the

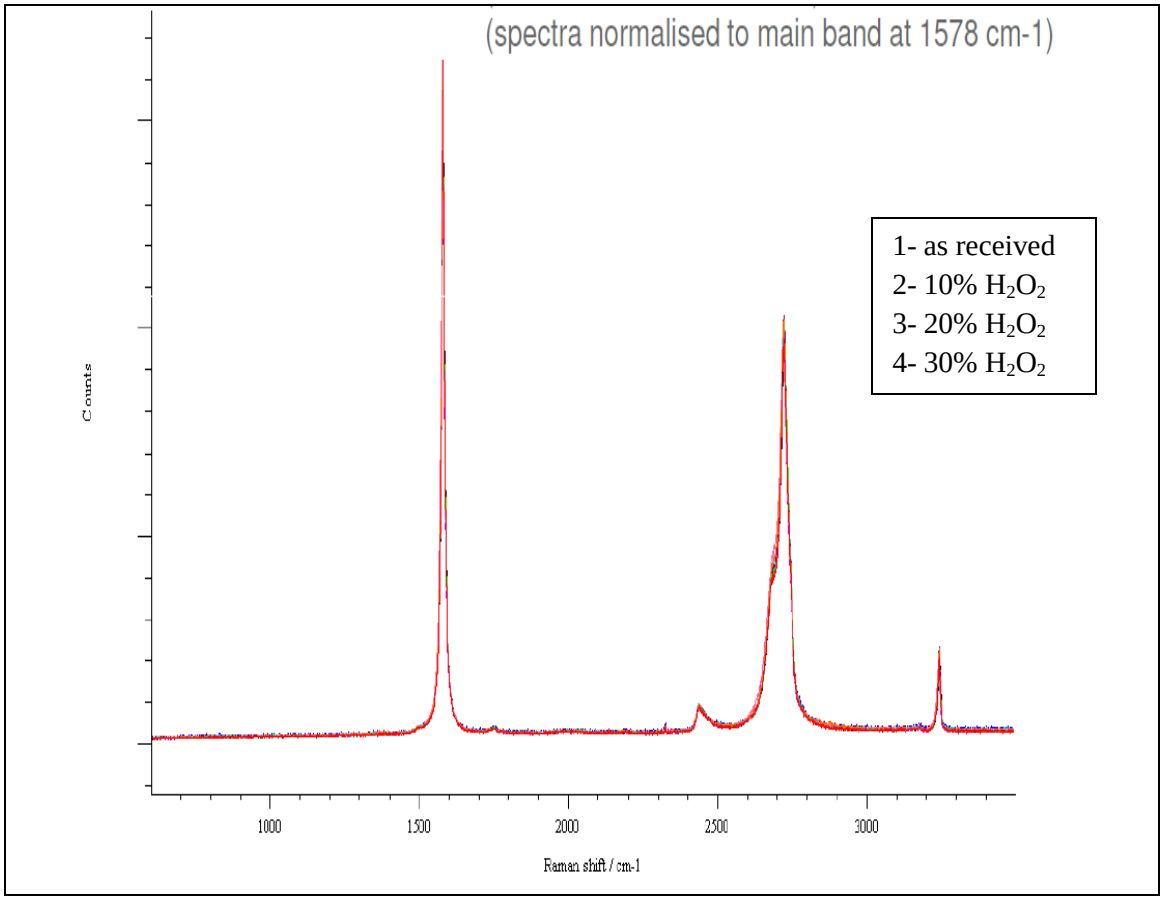

Figure 5.2 – The Raman spectra of the HOPG face surface as-received and treated with different concentration of H_2O_2 showing no significant change in peak position with exposure to different levels of hydrogen peroxide.

literature show that these bands reveal the well-ordered HOPG face surface (Tuinstra and Koening, 1970; Cuesta et al., 1994).

In addition, our results show that there is no shift of the band position depending on H_2O_2 exposure; only the intensity of the G bands decrease a bit. There are no significant changes in the Raman spectra of the HOPG face surface with H_2O_2 exposure. These results are well in agreement with the results from contact angle measurements which also do not reveal much variation at the face surface.

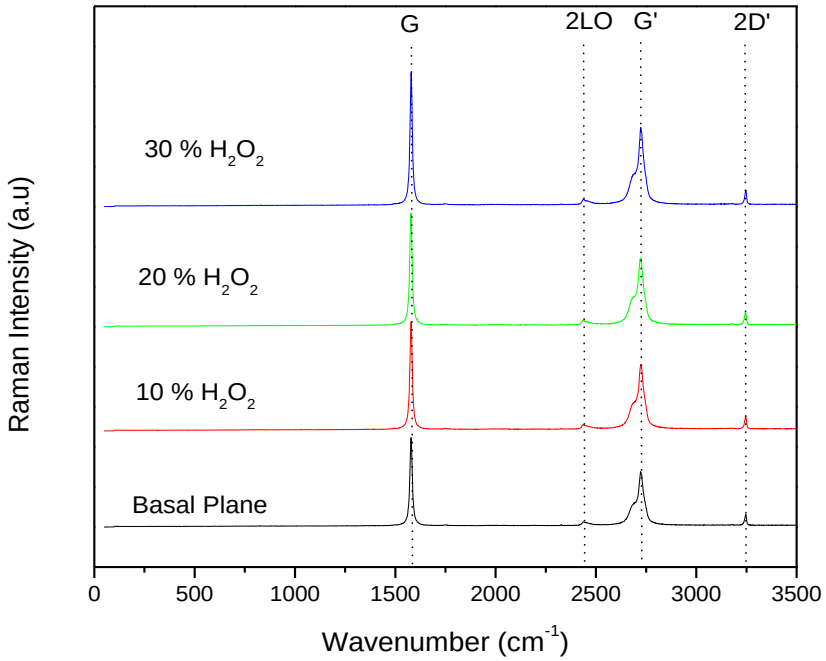

Figure 5.3 – Raman spectra of the face surface as-received and treated with H_2O_2. The average position of each characteristic Raman band is also indicated.

Mernagh et al. (1984) mentioned that there were different explanations for the peak at 1360 cm^{-1} which is observed predominantly on the edge surface and might be due to oxides or C=C groups which are present only at the edge. They declared that the vibration is not directly related to the hexagonal graphite lattice but are analogous to functional groups.

After having analyzed the face surface, the HOPG edge surface was also analyzed using Raman spectroscopic techniques. The as-received edge surface and the edge surface treated with peroxide indicate interesting spectral pattern in Figures 5.4 and 5.5.

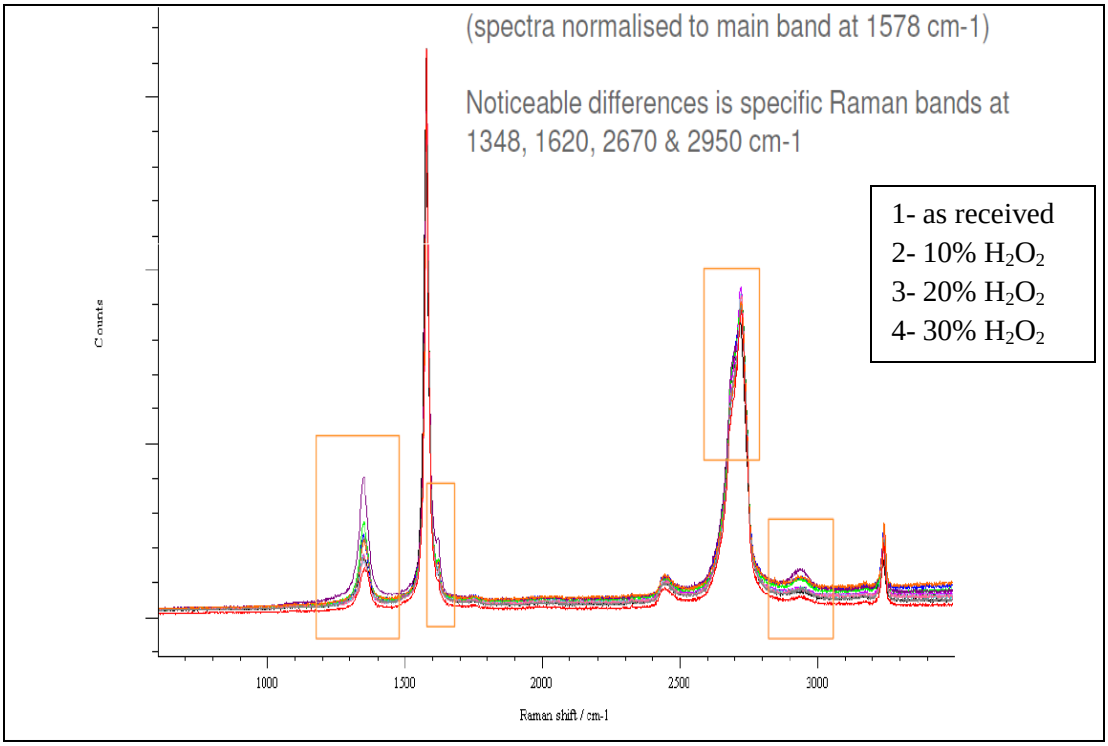

Figure 5.4 – The Raman spectra of the HOPG edge surface as-received and treated with different concentration of H_2O_2

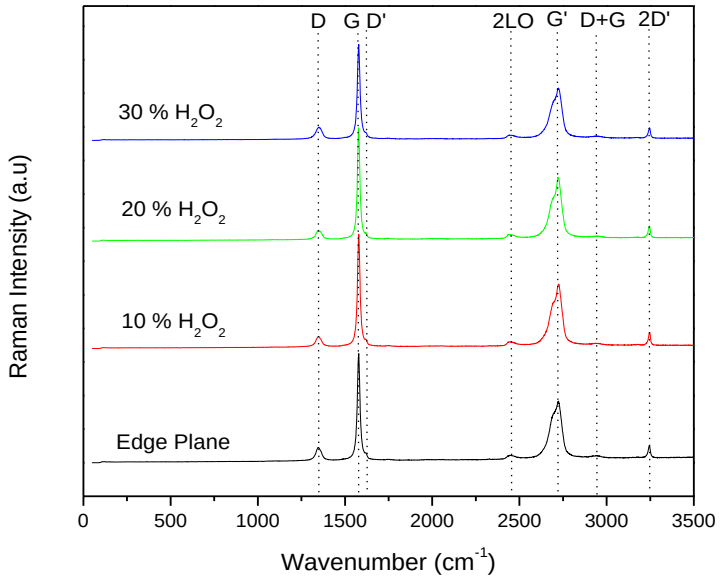

Figure 5.5 – Raman spectra of the edge surface as-received and treated with H_2O_2. The average position of each characteristic Raman band is also indicated.

HOPG has a single dominant G band and any deviation from this well-ordered three-dimensional structure of graphite is reflected in the broadening of the G band and the development of a D band. Raman spectra of the edge surface as-received and treated with H_2O_2 are given in Figure 5.4 and Figure 5.5. The edge surface has a larger peak at 1360cm $^{-1}$ showing the D band. In addition to other bands which are observed from the Raman spectra of the face surface, new bands, 1620 cm^{-1} (D` band) and 2950 cm^{-1} (D+G band), are seen on the Raman spectra of the edge plane surface. These additional bands arise due to the discontinuity of graphite planes at the edge. These values are very close to the values reported in the literature. For the edge surface, the G-band position remains constant at 1578 cm^{-1} and the D-band broadens and displays a shift. The D-band indicates structural defects and partially disordered structures of the sp^2 domains.

With regard to treatment with H_2O_2 solution for oxidation, the oxidation mechanism of highly ordered pyrolytic graphite has been described by the decrease in intensity of peaks and the expansion of the D-band as a less-ordered graphitic (amorphous) structure. Depending on the oxidation agent concentration, a band at 1620 cm^{-1} is clearly observed and the intensity increases with an increase in the oxidation level. This may show that edge surface is more active than the face surface.

Results reported in the literature indicate that oxidation of a carbon surface occurs by the direct collision of an oxygen molecule with the reactive edges of the graphene sheet. The dangling bonds and the unsaturated valencies of the edge carbon atoms further contribute to the oxidation process and lead to the formation of functional groups at the edges. Raman studies have been useful in this direction to understand the ordered structure of the face surface and the disorderness and the functional groups on the edge.

5.1.3 Surface Charge of Graphite

Zeta potential measurements were performed on amorphous graphite powder dispersed in 1mM KCl to determine the pH of its isoelectric point (iep). Graphite powder is nonpolar and hydrophobic in nature. Healy and Fuerstenau (2007) stated that the heat of immersion of graphite in water is low and on this basis, described graphite as a solid of low polarity.

Healy and Fuerstenau (2007) also analyzed that the pH of the iep/pzc of a nonpolar solid, liquid, or gas-aqueous interface should occur at pH 1.0 – 3.0. They also said that for zero field strength materials, i.e., nonpolar, or hydrophobic materials, the pzc will be in the low acidic, pH 1–3 region. Their conclusion was substantiated from careful examination and analysis of the electrokinetic results for nonpolar solids, liquids, and gases in water.

They also established that zero electrostatic field strength materials such as graphite are variously described as being low energy, nonpolar, van der Waals solids, naturally hydrophobic, nonwater wettable, or just simply hydrophobic and all tend to have pzc values at low around pH 1–3 values. They all also have heat of immersion values of around $-0.1\ Jm^{-2}$ ($-100\ ergscm^{-2}$).

The plot of the measured zeta potential of fine graphite powder through electrokinetic measurements with varying pH is given in Figure 5.6.

The plot in Figure 5.6 reveals that the isoelectric point (iep) of nonpolar hydrophobic graphite powder is around pH 2.6. This value is in close agreement to the values reported by Healy and Fuerstenau (2007) for other nonpolar graphitic carbon materials.

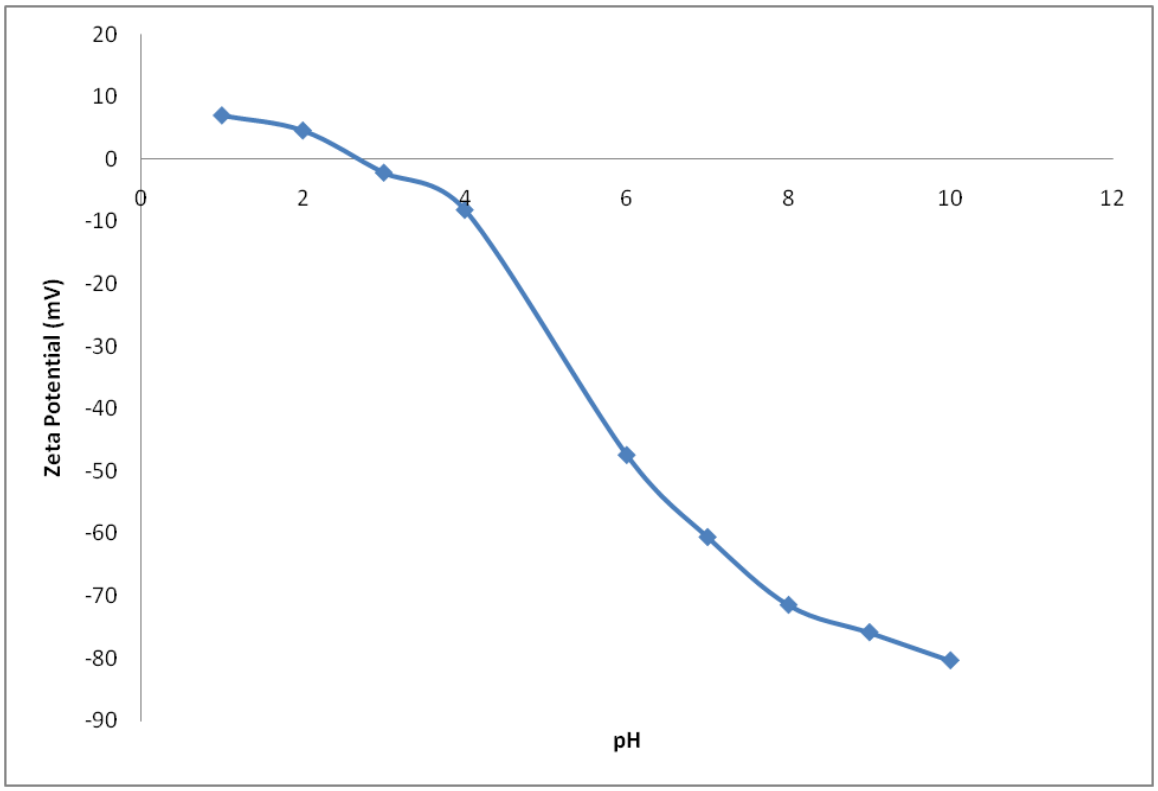

Figure 5.6 – IEP determination of graphite powder (2 – 15 microns) through electrokinetic measurements at varying pH.

They also concluded that the origin of such a low iep/pzc is considered due to exceedingly strong specific adsorption of OH^- or due to a large shift of the interfacial water ionization constant by almost 60 orders of magnitude from that in bulk water.

In addition, to derive more sense in the context of the present investigation with respect to surface charge of HOPG surfaces, in-situ atomic force microscopy (AFM) force measurements at HOPG face and edge surfaces were carried out at different pH solutions prepared from 1mM NaCl solutions. The pH was adjusted using 0.1N and 0.01N NaOH and HCl solutions. Silicon Nitride (Si_3N_4) tip, whose IEP is between pH 6.5 and 6.9 (Gavoille and Takadoum, 2002), was used for making the force curve measurements.

Figure. 5.7illustrates the force curves which were obtained at the face surface of HOPG. As mentioned before, the face surface of HOPG is hydrophobic (nonpolar). The pH of isoelectric point of the nonpolar solid, liquid, or gas-aqueous interface should occur at pH 1.0–3.0. Depending on the value assigned to water molecules or clusters at the interface and nonpolar, or hydrophobic materials, the pzc will be in the low acidic, pH 1–3 region (Healy and Fuerstenau, 2007). Recently, Koestner et al. (2011) determined the IEP of bare HOPG surface in water, through flat plate streaming potential measurements, as pH 2.0 – 2.25. The force curves, as illustrated in Figure 5.7, reveal that at lower pH values, on the basal surface, there is strong attraction between the negatively charged HOPG face surface and the positively charged Si_3N_4 tip. The attraction reduces with increasing pH and finally, the electrostatic repulsion is observed at pH 6.9. Since the tip is hydrophilic and the basal surface is believed to be hydrophobic, the interaction between the tip and the surface is dominated by electrostatic interaction. These results also indicate that the IEP of the Si_3N_4 is between around pH 6.9 which is in close agreement to the values reported in literature (Gavoille and Takadoum, 2002).Similar force measurements were also made for the HOPG edge surface (Figure. 5.8). In order to maintain similar conditions, solution of different pH values was made from 1mM NaCl stock solution. At pH 2 and 3, electrostatic repulsion is noticed as both the HOPG edge surface and the tip are positively charged. The force curves reveal that the IEP of HOPG edge surface is nearly at pH 4 where there is no attraction or repulsion. A slight attraction is observed at pH 5 which is due to the difference in the nature of charges. Again at pH 7.2, which is higher than the IEP of Si_3N_4, we observe significant repulsion as both the edge surface and the tip are negatively charged.

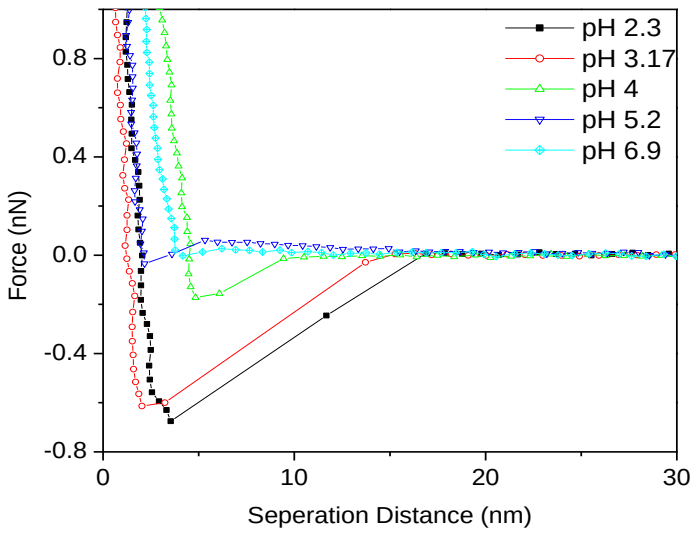

Figure 5.7 – Force vs distance curves obtained at the HOPG face surface with a Si_3N_4 tip at different pH values.

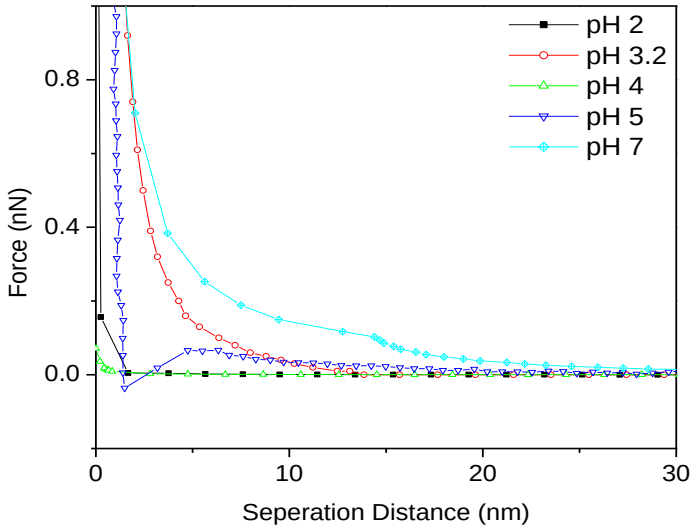

Figure 5.8 – Force vs distance curves obtained at the HOPG edge surface with a Si_3N_4 tip at different pH values.

To summarize the results from AFM surface force measurements, the IEP of the face surface was determined to be around pH 2 - 2.25 (less than pH 2.3) and this value falls well within the range of IEP values for nonpolar and hydrophobic surfaces as determined by Healy and Fuerstenau (2007) and is also in agreement with the value (iep around pH 2.25) reported by Koestner et al. (2011). The IEP of the edge surface was found out to be around pH 4. This value falls outside the pH 1 – 3 range for hydrophobic materials as mentioned by Healy and Fuerstenau, thereby indicating that the edge surface is not hydrophobic; rather it can be termed as less hydrophobic and its IEP is well less than 6, which is common for most carbon and graphitic materials, as determined also by Healy and Fuerstenau (2007).

Alternatively, they also stated that the polarity of solids can be rated on the basis of the contact angle of water on the solid. Healy and Fuerstenau (2007) further said that the graphite face surface can be classified as nonpolar and hydrophobic due to its large contact angle.

They further went on to explain the low pzc of nonpolar materials. They suggested that in low or zero fields provided by the underlying material (graphite in this case), the interfacial water clusters remain stronger acids than in bulk water. However, as the field increases, the loss of the proton is retarded and the acid strength of interfacial water decreases relative to bulk water. This effect can be illustrated more easily for solids where the first adsorbed waters generate surface hydroxyls. At low field strengths, the acidity of the hydroxyl groups exceeds that of bulk water and negative $–O^{-}$ sites dominate to yield a low pzc value. As the field increases to large values, we observe that the water clusters in bulk solution are stronger acids than the surface hydroxyls and $–OH^{+2}$ sites

dominate to yield a high pH pzc. This can further explain the slightly higher iep of the HOPG edge surface due to larger field strengths.

Thus, AFM surface force measurements of the HOPG face and edge surfaces to determine the iep are consistent with the experimental contact angle values, according to the explanation suggested by Healy and Fuerstenau (2007).

5.2 Molecular Dynamics Simulations (MDS)

Current surface chemistry study of graphite includes molecular dynamics simulation and results are discussed in conjunction with gold adsorption by activated carbon. Molecular dynamics simulations (MDS) have been widely used for the analysis of structural and dynamical properties of atoms and molecules, in particular, the interfacial water molecules at solid surfaces. Here, MDS has been adopted to investigate the gold adsorption on graphite surfaces and pores. Also, the wettability of the graphite pores in different solution systems has been investigated and is of relevance to the course of study here. This computation method calculates the time-dependant behavior of a molecular system. Molecular mechanics force fields are built to define forces between the particles and potential energy. This technique has been widely used for analytical purposes, for supporting experimental evidences, and can give us significant insights on the physical movements of atoms and molecules of interest and eventually lead us to a better understanding of interactions between molecules and surfaces.

A free molecular structure simulation program Avogadro (Hanwell et al.) was used to build the graphite crystal and the gold cyanide anion. These molecules were constructed using lattice parameters obtained from the American Mineralogist Crystal

Structure Database. The structures were optimized for their geometry in Avogadro using universal force fields (UFF) and then imported as files having extension .pdb.

Quantum chemistry-based ab initio simulation was performed using a Gaussian 09 simulation package in order to obtain optimized gold cyanide complex structure as well as atomic charges. Ab initio simulation at the PM6 level employing 3-21G basis sets were utilized to create molecular orbitals for C and N, and SDD basis sets were used for Au metal atoms. The gold cyanide complex ion was simulated by structural optimization from which the bond length and bond angle were obtained, and the complex was allowed to fluctuate during the entire simulation until energy was converged. Also, the Mulliken atomic charges of each atom were obtained from ab initio simulation and used for further molecular dynamics simulations.

A molecular dynamics simulation program DL_POLY_214 [Smith & Forester, 1996]was used for the analysis of gold cyanide at graphite surfaces. In the simulations, to examine interactions of the gold cyanide complexes at graphite surfaces, simple cubic cells containing graphitic orientations (face and edge), 1000 water molecules, 8 gold cyanide anions, and potassium counter ions (to maintain charge neutrality) were constructed with periodic boundary conditions. Similar simulations were also performed on face pores and edge pores with a pore width of 25 Å to ensure complete wetting of the pores. In the initial configuration, water molecules and cyanide complexes were randomly distributed in the simulation cell. The charge of the system was balanced by potassium counter ions. The system was simulated for 2 ns, including an equilibration time of 1 ns under NPT ensemble with pressure fixed at 0.1 MPa and the temperature fixed at 298 K. The results were analyzed based on the last 1 ns in the simulation under

NVT ensemble using Hoover's thermostat (Melchionna et al., 1993). The Leap-frog method with a time step of 1fs was used to integrate the particle motion. The Ewald sum was used to account for the electrostatic interactions.

Similar simulations were also performed on graphitic face pores to investigate the effect of pore width on water accommodation. In addition to water, isopropanol was added to the system to observe if alcohol could preferentially wet the hydrophobic pore. The isopropanol molecules were built using Avogadro and optimized by ab inito simulations using Gaussian 09 software. 200 isopropanol molecules were then added to the system and the simulation was run under NVT ensemble for 2ns, including an equilibration time of 1 ns.

The equilibrated results for each case are presented in the subsequent sections.

5.2.1 MDS of Gold Cyanide at Graphite Surfaces and Pores

Molecular dynamics (MD) simulations of gold cyanide with potassium counter ions at graphite face surface and edge surface have been performed. After equilibration, snapshots are presented in Figure 5.13 (a) and (b), respectively.

Although gold cyanide adsorption and elution experiments are conducted in very alkaline solutions of pH around 10.5 -12, incorporating the pH effect in molecular dynamics simulation is a challenge in itself. For instance, to obtain a solution of pH 12 in MDS, one hydrogen atom for every 10^{12} water molecules will have to be incorporated in the system. Hence, a huge number of water molecules will have to be simulated in the water box and such large numbers of molecules are beyond the scope of simulation capabilities even with a super-computer. Hence, the pH effect is neglected in MDS.

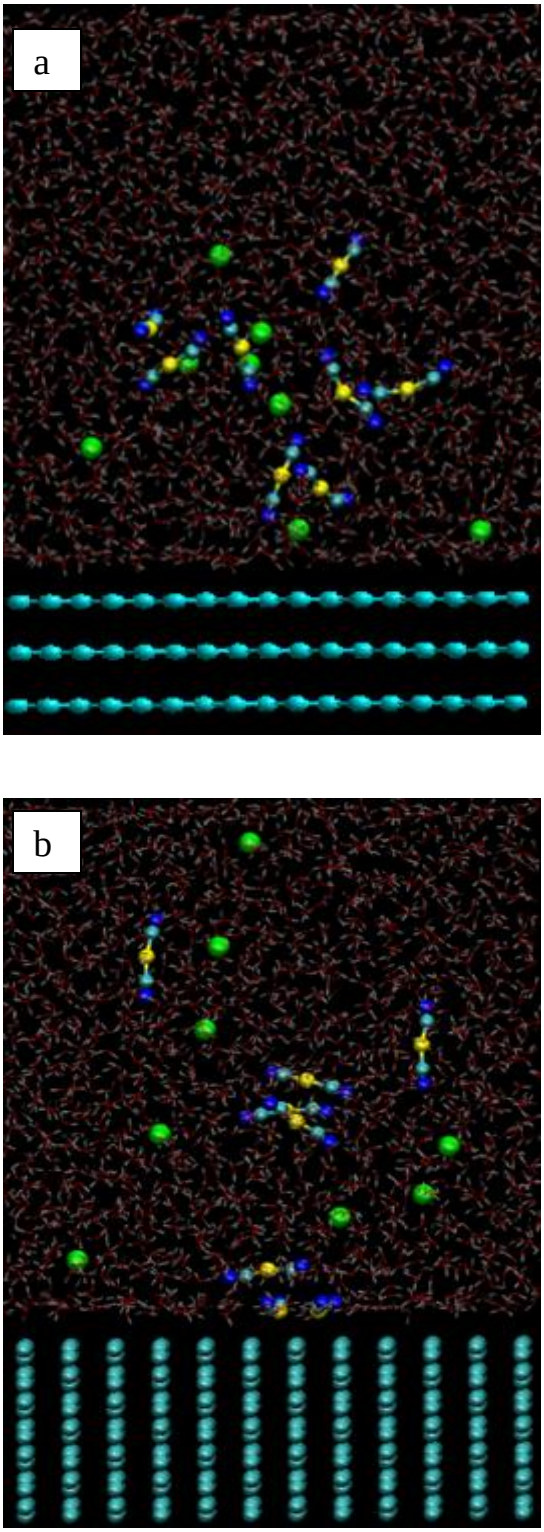

Figure 5.13 The equilibrium positions of gold cyanide at graphite face surface (a) and edge surface (b) as revealed from MDS.

It is clearly evident from the simulation results that gold cyanide has a favorable tendency to get accommodated at the graphite edge surface. In Figure 5.13 (a) the aurodicyanide ions tend to form clusters, as has been observed before by other researchers (Yin et al., 2012), but do not get oriented along the graphite face surface. On the contrary, the aurodicyanide anions exhibit favorable tendency to adsorb on the graphite edge surface in clusters. These MD simulation results of gold cyanide at graphite surfaces support the evidences and hypothesis put forward by Sibrell and Miller (1992) that gold cyanide is adsorbed at the graphite edge surface with almost negligible or no adsorption at the face surface.

As has been seen throughout the study, activated carbons present a variety of advantages over other gold recovery methods. Therefore, the mechanism of adsorption and the reason for selective adsorption from cyanide solutions are of interest. A better understanding of the adsorption reaction would lead to advances in activated carbon preparation and would enable an improved basis for the selection of the most suitable carbons.

In this regard, it has been established that the order of carbon adsorption for the metal-cyanide complexes is as follows (Marsden and House, 2006):

$Au(CN)^{2-} > Hg(CN)_2^{0} > Ag(CN)^{2-} > Cu(CN)_3^{2-} > Zn(CN)_4^{2-}$

The only species directly competing with gold and silver cyanides for adsorption sites is the neutral mercury cyanide molecule $Hg(CN)_2^{0}$. One of the theories of activated carbon adsorption is based upon ionic size and hydration. It is assumed that aurocyanide ions are larger and have a smaller hydration shell than other metal-cyanide ions and thus are selectively adsorbed by activated carbon. The MDS results on hydration have shown that

$Au(CN)_2^-$ ions have a lower hydration state than many other metal-cyanide complexes and thus, the low hydration state may be an important reason for gold selectivity over, for instance, silver in activated carbon adsorption from cyanide solution. This further supports the conclusion that the lower the hydration number of a metal-cyanide complex, the higher the chances of carbon adsorption.

Moreover, the strong tendency of $Au(CN)_2^-$ to form stable clusters may increase the possibility of adsorption. The hydrophobic tendency of aurocyanide anions and their corresponding cluster formation probably contribute to the selectivity exhibited in ion pair adsorption by activated carbon. The phenomenon of aggregation may be of importance in the adsorption reaction and cluster formation may account for stabilization at the activated carbon surface.

TEM analysis of activated carbon has revealed the presence of slit pores, which are responsible for gold adsorption. To simulate such slit pores, molecular dynamics simulations were performed in 25 Å graphite slit pores, i.e., face pore and edge pore. Snapshots of the equilibrium positions are illustrated in Figure 5.14 (a) and (b).

The simulation results again clearly show that gold cyanide tend to form clusters, as seen in previous simulations too, and are well accommodated at the edge surface of a graphite edge pore. There is no favorable adsorption of the gold cyanide at the graphite face surface of the face pore although the tendency to form clusters is still evident. These simulation results help us to provide a plausible explanation to determine the sites of gold cyanide adsorption in activated carbon.

The color code as used in the simulation is as follows: red – oxygen, white – hydrogen, cyan – carbon, yellow – gold, blue – nitrogen, and green – potassium.

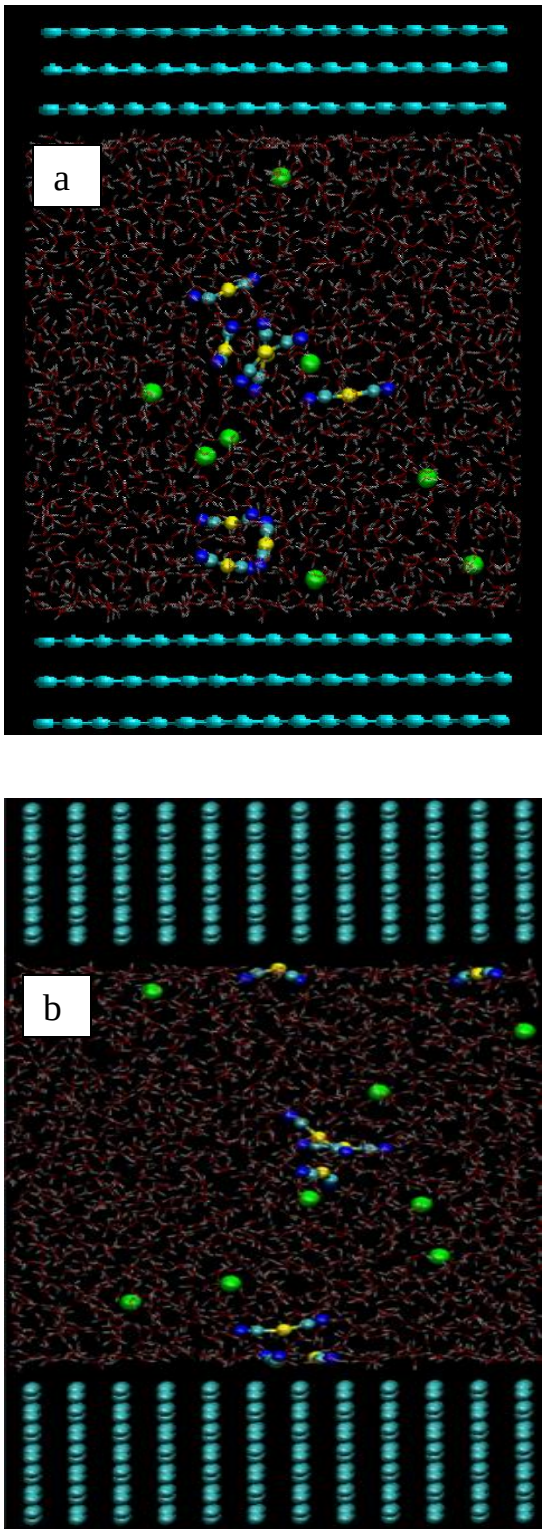

Figure 5.14. The equilibrium positions of gold cyanide at graphite face pore (a) and edge pore (b) as revealed from MDS.

5.2.2 MDS for the Effect of Pore Size on Wetting

The effect of graphitic pore size on wetting was studied with the help of molecular dynamics simulations. Water and isopropanol mixed with water were the two solvents tried on a 10 Å face pore.

With the aid of MD simulation, behavior of water molecules and isopropanol molecules in the vicinity of hydrophobic graphite surfaces was observed (Figure 5.15). The color code used for this simulation was similar to the one in the previous section with red color corresponding to oxygen atoms, white spheres describing hydrogen, and cyan-colored spheres for carbon atoms. At a typical graphite hydrophobic surface, due to the absence of hydrogen bonding sites, water molecules are excluded from the surface and the distance of this exclusion zone has been found out to be 3.52 Å.

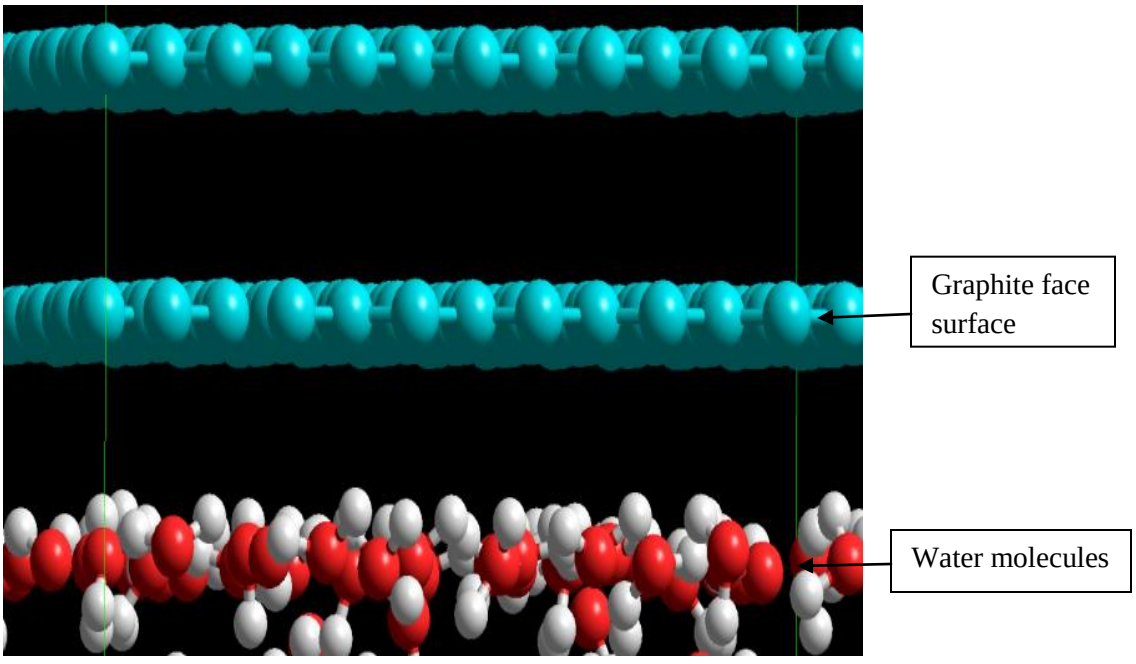

Figure 5.15. Snapshot of the equilibrium position showing an exclusion zone of 3.52 Å (color code: cyan – carbon, white – hydrogen, red – oxygen)

The presence of the exclusion zone between the carbons of the graphite surface and the layer of water molecules closest to the surface indicate that the maximum distance of approach for the water molecules is almost 3.5 Å away from the hydrophobic graphite surface.

When two graphite surfaces are separated at a distance of less than 10 Å, water repellency is observed, i.e., water is unable to penetrate the pore, as seen in Figure 5.16. Moreover, if the water molecules are already present near the hydrophobic graphite surface, the water molecules are removed from the pore when another hydrophobic graphite surface is approached from the opposite side. The exclusion of water molecules between the two graphite surfaces produces significant liquid drainage and is an important phenomenon of interest in the context of activated carbon pores.

On the other hand, the MDS results suggest that the presence of isopropanol molecules significantly alters the interaction between the hydrophobic graphite surfaces. It appears that the isopropanol molecules are accommodated at the hydrophobic graphite pore of 10 Å width, to minimize hydrophobic interactions. From Figure 5.17, it seems that the isopropanol molecules arrange themselves in such a way that the hydrogen atoms are in the nearest vicinity of graphite surface. Consequently, when the two surfaces are close to each other, no hydrophobic attraction is expected due to substitution of the interfacial water with isopropanol. This can also be explained on the basis of capillary pressure. Use of alcohol reduces the surface tension and hence, the capillary pressure required for the isopropanol molecules to enter and the wet the pore is also less.

These simulation results are also helpful in explaining the increased gold elution with the use of hydro-alcoholic solutions as presented in Chapter 4.

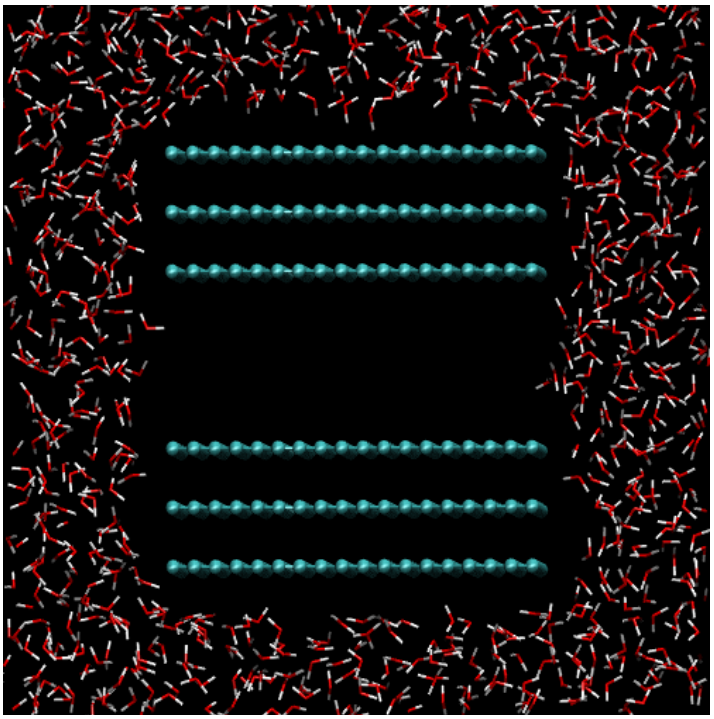

Figure 5.16. MDS snapshot of two hydrophobic graphite surfaces interacting in water with water excluded from the pore of 10 Å width.

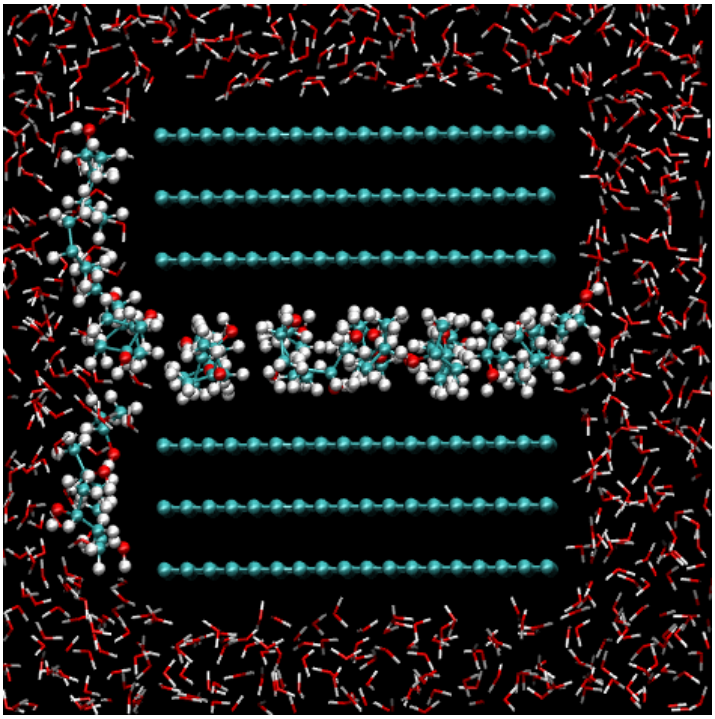

Figure 5.17.MDS snapshot of two hydrophobic graphite surfaces interacting in water/isopropanol mixture with Isopropanol molecules accommodated in a graphite pore of 10 Å width, indicating wetting of the pore.

5.3 Summary

This chapter essentially provides results from surface chemistry studies of graphite (HOPG) surfaces - face and edge in the context of gold adsorption. Several techniques including contact angle measurements, Raman spectroscopic studies, electrokinetic measurements, and AFM surface force measurements were adopted to study the HOPG surfaces.

Contact angle measurements of the as-received HOPG face and edge surfaces reveal that there is little change in contact angle with pH at the face surface, whereas there is significant change at the edge surface. Results indicate that the contact angle decreases by only a few degrees at the face surface with increase in pH, whereas the decrease is more prominent at the edge surface with increase in pH. HOPG surfaces oxidized with different concentration of H_2O_2 and for various exposure times also showed similar trend. There was not much decrease in contact angle at the face surface even after an hour of exposure with 30% H_2O_2. On the other hand, contact angle decreased significantly with increase in oxidation level and exposure time. It can be concluded from these results the HOPG face surface is definitely hydrophobic, whereas the edge surface is less hydrophobic.

Raman spectroscopic studies also reveal the presence of characteristic G band (graphite) and the D band (disorderness) on the graphite surfaces. The locations of these bands are consistent with the ones reported in literature. The HOPG face surface clearly shows the G band and the G' band and from this the highly ordered structure of the face surface can be inferred. Also, the intensity of the peaks at the face surface does not change with the level of oxidation. On the other hand, characteristic D band, D' band and

2D' band are visible on the HOPG edge surface. These peaks indicate the highly disordered nature of the edge surface. Also, quite contrary to the Raman spectra of the face surface, the spectra at the edge surface reveal that the intensity of the G band decreases while that of the D band increases with increase in oxidation level.

Thus, from the Raman spectra of the face and edge surfaces, it can be concluded that the edge surface is much disordered in nature and has a higher tendency to get oxidized than the face surface. These results are also consistent with the contact angle measurements.

Zeta potential studies of fine graphite powder through electrokinetic measurements give us an idea of the surface charge with variation in pH. The isoelectric point (iep) of graphite powder was determined to be around pH 2.6 which is very close to the values reported by Healy and Fuerstenau for graphitic carbon materials.

Further, the iep of the HOPG face and edge surface was investigated using AFM surface force measurements. The results (Table 5.2) show that the iep of the face surface is less than pH 2.3. This value supports the result by Koestner et al., who claimed that the iep of the face surface is around pH 2.25 using flat plate streaming potential measurements. The iep of the edge surface was determined to be around pH 4. This is a new contribution to the scientific literature as it has never been reported before.

Also in this chapter, theories related to the gold cyanide adsorption mechanism on activated carbon and the adsorption sites on activated carbon have been reviewed in relation to the significance of graphitic structure in gold adsorption. After much discussion, it can be concluded that gold cyanide adsorbs as ion pairs on the graphitic edge surfaces.

Table 5.2 – IEP of graphite (HOPG) surfaces.

HOPG Surface	**IEP as determined from AFM surface force measurement**	**Reference**
face	< pH 2.3	pH 2- 2.5 (Koestner et al.2011)
edge	around pH 4	Not yet reported

Previous evidences of autoradiographs of radiolabelled gold cyanide adsorbed on the HOPG edge surface and subsequent confirmation by XPS studies had provided some basis to confirm the adsorption sites on activated carbon. In this study, molecular dynamics simulations studies have further confirmed that indeed gold cyanide is favorably adsorbed on the graphite edge surface.

Molecular dynamics simulation studies have also revealed the effect of pore width on wetting. It is clearly illustrated that water is unable to penetrate the slit pore of 10 Å widths, whereas isopropanol from a water/isopropanol mixture is accommodated in the pore of the same dimension.

This further explains the ability of hydro-alcoholic solutions to facilitate better gold elution due its ability to penetrate tiny pores. MDS of alcohol pore wetting thereby supports the gold elution experiments using alcoholic solutions as presented in Chapter 4.

CHAPTER 6

SUMMARY AND CONCLUSIONS

An attempt has been made to justify the use of fine activated carbon particles as a potential substitute for coarse granular activated carbon primarily for its high adsorption rate and improved desorption behavior using alternative elution techniques. The results from this thesis research confirm previous findings on the effect of particle size on equilibrium loading and rate of gold adsorption from alkaline solution by activated carbon. In contrast, the effect of particle size on desorption using conventional Mintek and atmospheric Zadra techniques is not as might be expected where the gold elution increased initially and then dramatically decreased with decrease in particle size below 35 mesh. Such strange desorption behavior originally shown in the Elnathan thesis (Elnathan, 2007) was confirmed and studied further with a range of particle sizes. Also, this unusual particle size effect motivated research in the direction of developing alternative techniques for improved gold elution from fine particles.

To gain a thorough understanding of the particle size effect of activated carbon on gold adsorption and desorption, the carbon particles of different size fractions were characterized for their BET surface area and pore volume distribution. BET surface area analyses indicate that the specific surface area of activated carbon is independent of particle size with an average area of approximately 920 m^2/g. The average pore diameter

was found to be 2.18 nm. According to BET results, micropore surface area contributes most to the overall surface area for both coarse and fine particles. SEM and CT images do not reveal much about the internal pore network. Hence, for practical reasons, the BET results have been used to explain the adsorption and elution behavior.

Adsorption experiments carried out with different size fractions of activated carbon reveal that the adsorption capacity is independent of the particle size and the results relate well to the invariant specific surface area of different size fractions of activated carbon. The equilibrium loading capacity of activated carbon was reported to be around 26 to 28 mg Au/g C and is well in agreement with the values reported for industrial operations. Kinetic experiments clearly showed the dependence of adsorption rate on the activated carbon particle size. As expected, finer activated carbon exhibited enhanced kinetics with close to 90% of the gold adsorbed within the first hour as compared to only 40 – 50% gold being adsorbed in the first hour by coarse activated carbon particles. The initial rate of gold adsorption and the calculated reaction rate constants depict faster adsorption kinetics in fine particles in comparison to the coarse ones.

Based on current understanding of the adsorption process, several traditional and alternative elution processes were examined. Traditional Mintek and Atmospheric Zadra elution processes were performed for all size fractions. For both methods, it was observed that the percent gold eluted increased initially with decrease in particle size but dropped significantly with further decrease in particle size below 35 mesh. Based on these results, two size fractions (7x12 mesh and 48x65 mesh) were selected for study of alternative elution processes.

The particle size effect was almost eliminated by elution with hydro-alcoholic solutions as a similar extent of gold elution was obtained using ethanol and isopropanol. Also, isopropanol at 20% concentration coupled with Zadra solution yielded almost 81% gold and can be used for most practical operations.

Further, vacuum degassing loaded activated carbon prior to stripping raised the bar a bit as almost 90% gold elution was possible with vacuum + Zadra + alcohol solution for both size fractions.

The significance of pressure in gold elution from activated carbon was demonstrated by the use of filter press and syringe pump procedures. Fine carbon particles showed significantly higher gold elution than the coarser size fraction (7x12 mesh) using Zadra solution and with the application of pressure.

Thus, it can be concluded from these experiments that vacuum degassing the loaded activated carbon particles for 3 hours and then stripping with Zadra + 20% isopropanol solution yielded best results. This method is suitable to be implemented for industrial operations.

Current surface chemistry studies of face and edge surfaces of graphite throw a lot of light on its significance in gold adsorption. Contact angle measurements at these surfaces have revealed that the face surface is hydrophobic whereas the edge surface is less hydrophobic. Also, oxidation of these surfaces with H_2O_2 caused significant decrease in contact angle on the edge surface while not much change in contact angle was observed on the face surface. This somewhat indicated that the functional groups tend to form at edge sites and renders the edge surface less hydrophobic. Results from the Raman spectra illustrated that the face surface was highly ordered while the edge surface was

disordered and has a greater tendency to oxidize. These results were consistent with the contact angle measurements.

The isoelectric point (iep) of graphite powder was determined to be around pH 2.6 through zeta potential measurements. Further, the isoelectric points of HOPG face and edge surfaces were investigated through AFM surface force measurements. The results show that the iep of the face surface is less than pH 2.3 and these results compliment results reported in literature which report an iep of pH 2.0 – 2.5 from flat pate streaming potential measurements. The iep of the edge surface was found to be around pH 4 and can be considered as an unique contribution to the scientific literature.

In addition, molecular dynamics simulations (MDS) were performed to explain the significance of graphitic sites in gold adsorption. MDS reveal and also support previous findings that gold cyanide is favorably adsorbed at the graphite edge surface. MDS has also revealed the inability of water molecules to penetrate a slit pore of 10Å in dimension whereas isopropanol is able to enter a slit pore of the same dimensions. This further explains the efficacy of alcohol for better gold elution.

Overall it can be inferred that fine activated carbon particles present better gold adsorption rates but are difficult to strip with traditional Zadra or Mintek solutions. Hence, the carbon particles can be vacuum degassed prior to stripping with Zadra + alcohol solution to yield elution values of close to 90% of the adsorbed gold.

.

REFERENCES

Marsden, J., House, I., 2006. The chemistry of gold extraction, 2nd Edition. Society for Mining, Metallurgy, and Exploration, Inc. (SME), Colorado.

Miller, J. D., Munoz, G. A., Duyvesteyn, S., 2001. Magnetic activated carbon particles for adsorption of solutes from solution. Provisional Patent No U2975.IP.

Munoz, G. A., Duvyvestyn, S., Miller, J. D., 2002.Gold recovery from cyanide leaching solutions by magnetic activated carbons. 26th International Precious Metals Conference, 3-5.

Miller, J. D., Munoz, G. A.,Duyvesteyn, S., 2004.Design and synthesis of powdered magnetic activated carbon for aurodicyanide anion adsorption from alkaline cyanide leaching solutions. Fundamentals and Applications of Anion Separations, 277-283.

Munoz, G. A., 2006. Magnetic activated carbons for gold adsorption from alkaline cyanide solutions, PhD Thesis, University of Utah, Salt Lake City.

Adams, M. D., 1989. The chemistry of the carbon-in-pulp process, PhD Thesis. University of Witwatersrand, Johannesburg.

Bansal, R. C.,Donnet, J. B.; Stoekli, F., 1988.Active carbon. Marcel Dekker Inc., New York.

Depci, T., Kul, A. R., Onal, Y., 2012.Competitive adsorption of lead and zinc from aqueous solution on activated carbon prepared from Van apple pulp: Study in single- and multi-solute systems. Chemical Engineering Journal 200-202, 224-236

Muller, B. R.,2010. Effect of particle size and surface area on the adsorption of albumin-bonded bilirubin on activated carbon. Carbon 48(12), 3607-3615.

Jankowska, H.; Swiatkoski, A.; Choma, J., 1991.Active carbon; Ellis Horwood, West Sussex, England.

McDougall, G. J., and Fleming, C. A., 1987. Extraction of precious metals on activated carbon, ion exchange and sorption processes in hydrometallurgy. M. Streat and D.Naden

eds., 74-76.

Dubinin, M.M., 1979. Microporous structures of carbonaceous adsorbents. Characterization of Porous Solids, Society of Chemical Industry, London.

Rodriguez-Reinoso, F., Molina Sabio, M., 1998.Textural and chemical characterization of microporous carbons. Advances in Colloid and and Interface Science 76-77, 271-294.

de Andrade Lima, L.R.P., and Hodouin, D.,2006. Analysis of the gold recovery profile through a cyanidation plant. International Journal of Mineral processing 80(1), 15-26.

Davidson, R.J., 1974. The mechanism of gold adsorption on activated charcoal. Journal of the South African Institute of Mining and Metallurgy, 67-76.

Adams, M. D., Fleming, C.A., 1989.The Mechanism of Gold Adsorption of Aurocyanide onto Activated Carbon. Metall. Trans. 208, 315-325.

Ibrado, A. S., Fuerstenau, D. W., 1995. Infrared and X-ray photoelectron spectroscopy studies on the adsorption of gold cyanide on activated carbon. Minerals Engineering, 441-458.

Jones, W.G., and Linge, H.G.,1989.Effect of ore pulp on the adsorption rate of gold cyanide on activated carbon. Hydrometallurgy 22, 231-238.

McDougall, G.J., Hancook, R.D., Nicol, M.J., Welington, O.L., Copperthwaite, R.G., 1980.The mechanism of the adsorption of gold cyanide on activated carbon. Journal of the South African Institute of Mining and Metallurgy80(9), 334-356.

Rees, K. L., and van Deventer, J. S. J., 2000.The mechanism of enhanced gold extraction from ores in the presence of activated carbon. Hydrometallurgy 58(1), 61-80.

Fleming, C. A., and Nicol, M. J., 1984.The absorption of gold cyanide onto activated carbon. Factors influencing the rate of loading and the equilibrium capacity. Journal of the South African Institute of Mining and Metallurgy 84(9), 85-89.

Coetzee, J.W., and Gray, D.E., 1999. Counter-current vs co-current flow in carbon-in-pulp adsorption circuits. Minerals Engineering 12(4), 415-422.

Zadra, J.B., 1950. A process for the recovery of gold from activated carbon by leaching and electrolysis. Report of Investigations No. 4672. Washington, DC: U.S. Bureau of Mines

Zadra, J.B., Engel, A.L., and Heinen, H.J., 1952. Process for recovering gold and silver from activated carbon by leaching and electrolysis. Report of Investigations No. 4843. Washington, DC: U.S. Bureau of Mines.

Davidson, R.J., and Duncanson, D., 1977. The elution of gold from activated carbon using deionized water. Journal of South African Institute of Mining and Metallurgy 77, 254-261.

Davidson, R.J., Veronese, V., and Nkosi, M.V., 1979.The use of activated carbon for the recovery of gold and silver from gold-plant solutions. Journal of the Southern African Institute of Mining and Metallurgy 79(10), 281–297.

McArthur, D., Schmidt, C. G., Tumilty, J. A., 1987. Optimizing carbon properties for use inCIP. Edited by Salter, R. S., Wyslouzil, D. M., McDonald, G. W. Proceeding of the International Symposium on Gold Metallurgy, Pergamon Press, 26, 35-38.

Muir, D.M., Hinchliffe, W., Tsuchida, N., Ruane, M., 1985.Solvent elution of gold from C.I.P. carbon**.** Hydrometallurgy 14, 47-65.

Espiell, F., Roca, A., Cruells, M., Nunez, C., 1988.Gold desorption from activated carbon with dilute NaOH/organic solvent mixtures. Hydrometallurgy 19, 321-333.

Ubaldini, S., Fornari, P., Massidda, R., and Abbruzzese, C., 1998. An innovative thiourea gold leaching process. Hydrometallurgy 48, 113-124.

Cashion, J. D., McGrath, A.C., Volz, P., Hall, J. S., 1988.Directanalysisofgoldspecies on activated carbon by Mössbauer spectroscopy. Inst. Mining Metall. 97, C129–C133.

Klauber, C., 1991. X-ray photoelectron spectroscopic study of the adsorption mechanism of aurucyanide onto activated carbon. Langmuir 7, 2153–2159.

Sibrell, P. L.; Miller, J. D., 1992.The significance of graphitic structural features in gold adsorption by carbon. Minerals and Metallurgical Processing 9, 189-195.

Sibrell, P. L., 1991. The characterization and treatment of Carlin trend carbonaceous gold ores. PhD Thesis, University of Utah, Salt Lake City.

Sibrell, P. L., Miller, J. D., 1991. The search for adsorbed gold cyanide on carbon surface. The Australasian Institute of Mining & Metallurgy, Melbourne, 21-25.

Mooiman, M. B. and Miller, J. D., 1984.Selectivity Considerations in the Amine Extractions of Gold from Alkaline Cyanide Solution. Minerals and Metallurgical Processing, 153-157.

Lagerge, S., Zajac, J., Partyka, S., Groszek, A.J., Chesneau, M., 1997. Adsorption of cyanide gold complexes inferred from various experimental studies. Langmuir 13, 4683–4692.

Lagerge, S., Zajac, J., Partyka, S., Groszek, A.J., Chesneau, M., 1999. Comparative study on adsorption of cyanide gold complexes onto different carbonaceous samples:

measurement of the reversibility of the process and assessment of the active surface inferred by flow microcalorimetry. Langmuir 15, 4803–4811.

Poinen, G., Thurgate, S.M., Kirton, G., Ritchie, I.M., 1998. Adsorption of dicyanoaurate (I) ions on highly oriented pyrolytic graphite. Appl. Surf. Sci. 134, 73-77.

Zhu, Y., McBride, J.D., Hansen, T.A., Beebe Jr., T.P., 2001. Controlled production of molecule corrals using cesium ion bombardment: a TOF-SIMS, XPS, and STM study. J. Phys. Chem. B: Conden. Matter, Mater., Surf., Interf. Biophys. 105(10), 2010-2018.

Paruchuri, V., Nalaskowski, J., Beebe Jr., T.P., Miller, J.D., 2003. Organization of surface micelles confined in molecule corrals at a graphite surface: direct evidence for the surface templating effect. 225th ACS National Meeting, March 23-27, New Orleans, LA. American Chemical Society, Washington, DC.

Papier, E., Li, S., Donnet, J., 1987. Contribution to the study of basic surface groups on carbons. Carbon 25, 243-247.

Papirer, E., Dentzer, J., Li, S., Donnet, J. B., 1991. Surface groups on nitric acid oxidized carbon black samples determined by chemical and thermo desorption analyses. Carbon 29, 69-72.

Papirer, E., Polania-Leon, A., Donnet, J. B., Montagnon, P., 1995.Fixation of potassium aurocyanide on active carbons. Carbon 33(9), 1331-1337.

Polonia-Leon, A., Papirer, E., Donnet, J. B., Dagois, G., 1993. Modification et interaction des fonctions oxygenees en surface des charbons actifs. Carbon 31(3), 473-479.

Ofori-Sarpong, G., Tien, M., Osseo-Asare,K., 2010.Myco-hydrometallurgy: Coal model for potential reduction of preg-robbing capacity of carbonaceous gold ores using the fungus, Phanerochaetechrysosporium. Hydrometallurgy102, 1-4

Van deventer, J.S.J., and Van der Merwe, P.F., 1994. Factors affecting the elution of gold cyanide from activated carbon. Minerals Engineering 7(I), 71–86.

Davies, T. J., Moore, R. R., Banks, C. E. and Compton, R. G., 2004.The cyclic voltammetric response of electrochemically heterogenous surfaces. J. Electroanal. Chem. 574, 123–152.

Davies, T. J., Hyde, M. E., and Compton R. G., 2005.Nanotrench arrays reveal insight into graphite electrochemistry. Angew. Chem., Int. Ed. 44, 5121–5126.

Banks, C.E., Compton, R.G., 2006. New electrodes for old: from carbon nanotubes to edge plane pyrolytic graphite. Analyst 131(1), 15-21.

McCreery, C.L., 1991. Carbon electrodes: structural effects on electron transfer kinetics. Electroanalytical Chemistry 17, 221-374.

McCreery, R. L., 2008. Advanced carbon electrode materials for molecular electrochemistry. Chemical Reviews 108, 2646-2687.

Dale, A., Brownson C., Kampouris, D.K., and Banks, C.E., 2012.Graphene electrochemistry: fundamental concepts through to prominent applications. Chem. Soc. Rev. 41, 6944–6976.

Robinson, R. S., Sternitzke, K., McDermott, M. T., McCreery, R. L., 1991. Morphology and electrochemical effects of defects on highly oriented pyrolytic graphite. J. Electrochem. Soc.138, 2412-2418

Rice, R. J., McCreery, R. L., 1989. Quantitative relationship between electron transfer rate and surface microstructure of laser-modified graphite electrodes. Anal. Chem. 61, 1637-1641.

Morcos, I., Yeager, E., 1970. Kinetic studies of the oxygen—peroxide couple on pyrolytic graphite. Electrochim.Acta 15, 953-975.

Randin, J. P., Yeager, E., 1971. Differential capacitance study of stress-annealed pyrolytic graphite electrodes. J.Electrochem. Soc. 118, 711-714.

Wightman, R. M., Paik E. C., Borman, S., Dayton, M. A., 1978. Evaluation of the basal plane of pyrolytic graphite as an electrochemical detector for liquid chromatography. Anal. Chem. 50, 1410-4414.

Wightman, R. M., Deakin, M. R., Kovach, P. M., Kuhr, P. M., Stutts, K. J., 1984. Methods to improve electrochemical reversibility at carbon electrodes. J. Electrochem.Soc.131,1578-1583

McDermott, M.T., Kneten, K., and. McCreery, R.L., 1992. Anthraquinonedisulfonate adsorption, electron-transfer kinetics, and capacitance on ordered graphite electrodes: the important role of surface defects. J. Phys. Chem. 96, 3124-3130.

Müller E. A., Gubbins, K.E., 1998. Molecular simulation study of hydrophilic and hydrophobic behavior of activated carbon surfaces. Carbon36, 1433.

Müller, E. A., Vega, L. F., Rull, L. F., Gubbins, K. E., 1996. Adsorption of water on activated carbons: A molecular simulation study. J. Phys. Chem.100, 1189.

Kwon, S., Vidic, R., Borguet, E., 2002. Enhancement of adsorption on graphite (HOPG) by modification of surface chemical functionality and morphology. Carbon 40, 2351–2358

Jensen, P., Clement, A., Lewis, L. J., 2004. Diffusion of nanoclusters. Computational Materials Science 30, 137–142

Wildgoose, G. G., Banks, C. E., Leventis, H. C., & Compton, R. G., 2006. Chemically modified carbon nanotubes for use in electroanalysis. MicrochimicaActa.152(3-4), 187-214.

Domi, Y., Ochida, M., Tsubouchi, S., Nakagawa, H., Yamanaka, T., Doi, T., Abe, T., and Ogumi, Z., 2012. Electrochemical AFM observation of the HOPG edge plane in ethylene carbonate-based electrolytes containing film-forming additives. J. Electrochem. Soc. 159, A1292-A1297.

Miller, J. D., and Lin, C. L., 2004. Three-dimensional analysis of particulates in mineral processing systems by cone beam x-ray microtomography. Mineral & Metallurgical Processing 21(3), 113-124.

Shipman, A. J., Jativa, F., 1987.Mintek manual on testing of activated carbons. Council for Mineral Technology, Johannesburg, South Africa, 1-11.

La Brooy, S.R., Bax, A.R., Muir, D.M., Hosking, J.W., Hughes, H.C. and Parentich, A., 1986. Fouling of Activated Carbon by Circuit Organics, Gold 100. Proceeding of the International Conference on Gold, Volume 2, Extractive Metallurgy of Gold, Johannesburg, SAIMM.

Urbanic, J. E., Jula, R. J., Faulkner, W. D., 1985.Regeneration of activated carbon used for recovery of gold. Miner. Metall. Process., 193-198.

Elnathan, F., 2007.The effect of activated carbon particle size on gold cyanide adsorption and elution.PhD Thesis, University of Utah, Salt Lake City.

Riley, H. L., 1947.Amorphous carbon and graphite. Quarterly Reviews-Chemical Society 1, 59-72.

Cook, R., Crathorne, E.A., Monhemius, A.J., Perry, D.L., 1989. An XPS study of the adsorption of gold (I) cyanide by carbons. Hydrometallurgy 22, 171-182.

Limat, M., Foti, G., Hugentobler, M., Stephan, R. and Harbich, W., 2009 Electrochemically stable gold nanoclusters in HOPG nanopits. Catal. Today146**,** 378-385

Healy, T. W., Fuerstenau, D. W., 2007. The isoelectric point/point-of zero-charge of interfaces formed by aqueous solutions and nonpolar solids, liquids, and gases. Journal of Colloid and Interface Science 309, 183–188

Konkena, B., Vasudevan, S., 2012.Covalently linked, water-dispersible, cyclodextrin: reduced-graphene oxide sheets. Langmuir 28(34), 12432.

Sorescu, D. C., Jordan, K. D., Avouris, P., 2001. Theoretical study of oxygen adsorption on graphite and the single-walled carbon nanotube. J. Phys. Chem. B 105, 11227-11232.

Zhu, H. W., Jiang, B., Xu, C. L., Wu, D. H., 2002. Long super-bundles of single walled carbon nanotubes. Chemical Communications 17, 1858-1859.

Tunistra, F., Koening, J. L., 1970. Raman spectrum of graphite. J. Chem. Phys. 53, 1126-1130.

Cuesta, A., Dhamelincourt, P., Laureyns, J., 1994. Raman microprobe studies on carbon materials. Carbon 32, 1523-1532.

Katagiri, G., Ishida, H., Ishitani, A. 1988. Raman spectra of graphite edge planes. Carbon26(4), 565–571.

Mernagh, T. P., Cooney, R. P., Johnson, R. A., 1984. Raman spectra of graphon carbon black, Carbon22(1), 39–42.

Gavoille,J., and Takadoum, J., 2002.Study of surface forces dependence on ph by atomic force microscopy. Journal of Colloid and Interface Science 250**,** 104–107.

Koestner, R., Roiter, Y., Kozhinova, I., Minko, S., 2011. Effect of local charge distribution on graphite surface on nafion polymer adsorption as visualized at the molecular level. J. Phys. Chem. C 115, 16019–16026.

Hanwell, M.D., Curtis D.E.,Lonie, D.C., Vandermeersch, T., Zurek,E., and Hutchison, G.R.,2012.Avogadro: an advanced semantic chemical editor, visualization, and analysis platform. Journal of Cheminformatics,4-17.

Smith, W., Forester, T. R., 1996.DL_POLY_2.0: A general-purpose parallel molecular dynamics simulation package. Journal of Molecular Graphics14(3), 136-141.

Melchionna, S., Ciccotti, G., and Holian, B. L., 1993. Hoover NPT dynamics for systems varying in shape and size. Molecular Physics78, 533-544.

Yin, X., Opara, A., Du, H., Miller, J. D., 2011.Molecular dynamics simulations of metal–cyanide complexes: Fundamental considerations in gold hydrometallurgy. Hydrometallurgy106(1–2), 64-70.